2019

# PATTERN-PROCESS LINKAGES IN FORESTED ECOSYSTEMS

Eryn Elizabeth Schneider

# PATTERN-PROCESS LINKAGES IN FORESTED ECOSYSTEMS

By

Eryn Elizabeth Schneider

Bachelor of Science, St. Catherine University, St. Paul, Minnesota, 2008
Master of Science, Northern Arizona University, Flagstaff, Arizona, 2012

Dissertation

presented in partial fulfillment of the requirements
for the degree of

Doctor of Philosophy
in Forest and Conservation Science

The University of Montana
Missoula, MT

May 2019

Approved by:

Scott Whittenburg, Dean of The Graduate School
Graduate School

Dr. Andrew J. Larson, Chair
Department of Forest Management

Dr. Jon Graham
Department of Mathematical Sciences

Dr. Kelsey Jencso
Department of Forest Management

Dr. Cara Nelson
Department of Ecosystem and Conservation Sciences

Dr. Carl Seielstad
Department of Forest Management

Schneider, Eryn, Ph.D., Spring 2019 Forest Ecology and Management

# Pattern-process linkages in forested ecosystems

Chairperson: Dr. Andrew Larson

## ABSTRACT

Ecological pattern-process linkages have been called the Rosetta's stone of ecology. The pattern-process linkage is a feedback whereby ecosystem processes drive structural patterns, and vegetation patterns also strongly influence vital ecosystem processes. The role of competition and gap dynamics in creating spatial heterogeneity was assessed in Sitka-spruce western hemlock forests. Results indicated that despite low species richness, these forests are structurally diverse with the spatial imprint of competition obscured by gap dynamics through stand development. The influence of forest structural and spatial heterogeneity on snow accumulation and persistence was examined in a mixed-conifer forest. Tree neighborhood type (open, clump, individual) and winter leaf habit (deciduousness) had a significant effect on snow processes, likely driven by interception and the spatial variation of longwave radiation. Random forest models relied on forest canopy metrics associated with the amount, location, and type of forest vegetation to predicting peak snow water equivalent (SWE) and snow disappearance. Variation of peak snow density was not explained with canopy or terrain metrics. Models parameterized with ground and LiDAR based canopy metrics performed equally well for SWE and snow disappearance. The results of this research provide managers with new tools for objectively quantifying forest heterogeneity, informing treatments that seek to create structural and spatial complexity, and a method for estimating the distribution of snow accumulation and melt in complex forests. These studies provide a clear links between forest spatial patterns and important ecosystem processes including competition, gap dynamics, and snow accumulation and disappearance.

# Table of Contents

## ACKNOWLEDGEMENTS

"No one who achieves success does so without the help of others. The wise and confident acknowledge this help with gratitude." -Alfred North Whitehead

Many people have endured, encouraged, and celebrated with me through this journey. My deepest gratitude goes out to the man who decided I was worthy of higher academic pursuits, my adviser, Dr. Andrew Larson. This research would not have happened without your unrelenting support, trust, and encouragement. I could not have been luckier in an adviser. I am humbled by your unwavering example of what an academic can be, your commitment and love for what you do, and for your ability to raise the bar to push me when I didn't believe in myself. Your example of an effective work life balance is invaluable. In the dark depths of this process your willingness to listen, your compassion and your confidence in me inspired me to pick it up and to finish. Thank you isn't enough for being treated not only as a student, but as a colleague and friend.

To my committee, thank you for joining and enduring this ride. Your individual expertise improved the rigor of this research and pushed my levels of understanding. To Dr. Kelsey Jencso, thank you for showing me how to teach, I often found myself watching how you taught rather than focusing on the content. Your excitement and engagement with my research, your wealth of ideas, and suggestions of alternative approaches make me want to do more. Taking on a new area of research, hydrology, was daunting but you supported me through it and have allowed me to become an expert. Dr. Cara Nelson, I am grateful for your strong female perspective and for being committed to my success without compromising expectations of academic rigor. It was comforting and motivating knowing I had a cheerleader in my corner. Thank you, Dr. Jon Graham for seeing, fostering, and pushing my statistical understanding. Your constant calm, expansive expertise, and approach made space for me to work out the process and to be confident in my knowledge. Dr. Carl Seilestad, our conversations about teaching pedagogies and aspirations illuminated a common footing creating a connection that is invaluable. You helped me understand remote sensing with a patient approach, point clouds are a little less intimidating. Your thoughtful questions push me to slow down, pull back and look for

other big picture perspectives, making me a better scientist. You all have supported me, pushed me, and continue to inspire me. I am grateful.

Through this process there has been no one more constant and supportive than my husband, Matt. Words will always fail to express what you mean to me and my gratitude for all you have done. It is crazy to look back and know we started at the same time I started this research. Thank you for enduring all the plane flights and the many miles apart. I appreciate all the time you spent listening to my frustrations and triumphs through this process and for letting my work process be messy and all consuming. Thank you for believing in me and being proud of me. Thank you for loving me on this crazy rollercoaster.

A special thank you needs to go out to two very important people in my life, Dr. Brooke Vetter and Dr. Valerie Keffala. Brooke, we have been doing this academic thing together since our first semester of undergrad. I am grateful for your friendship and knowing I wasn't alone in the struggling, yelling at the computer screen, telling the story from the results, and fighting the imposter thoughts. Thank you for the long phone calls to celebrate and the longer calls to vent. Not many people are lucky enough to have a friend that is, and has been, a solid work and life support system to share it all with. Thank you for being there and understanding. To Valerie, in the darkest moments you made the space for me to remember what I love about what I do, to pick it back up and to finish stronger than I started. You encouraged me to live my me, to be the badass I know I am. You provided compassion in the struggles and gave me the knowledge on how to keep going. You are my favorite example of how boundaries, compassion, and vulnerability foster connections and gratitude for the little things. You helped me find joy and value in this research.

To my family, you have all shaped parts of who I am. We are rarely given opportunities that show us how much our family has our backs, I was given an obvious chance during this research. When I was face down, unable to do it on my own you were all there to carry me, support me, and challenge me. To my sister, thank you for letting me be your first student and teaching me how to read, it has been the foundation of my academic successes. To my brother, thank you for being my silent warrior. Thank you for listening to me cry in the pain, for seeing me, and for your unique form of compassion and motivation. To my mom, thank you for reading drafts and offering encouragement. Because we are fiercely similar, you gave me the gift of voice and understanding the value of a well supported argument even if we couldn't see it then;

thank you. To my dad, no one has even seen me and understood me more. My many hours in “the jungle” have paid off. Thank you for your example of determination and perseverance; I am the doctor and teacher I always told you I was going to be! Thank you all for having my back, for making me better, and for making me smile in your explanations of what I do.

Lastly, there are countless field volunteers who quite literally made this research happen. There are too many to list, but you know who you are. Thank you for letting me teach you about snow in the forest and how to sample it. Thank you for your time, your curiosity, and your reassurance that I was doing something really cool.

With a grateful heart, THANK YOU!

## INTRODUCTION

The intrinsic pattern-process linkage has been called the Rosetta's stone of ecology, and remains a challenge for ecologists (Levin 1992, McIntire and Fajardo 2009, O'Sullivan and Perry 2013). All natural ecosystems are patterned, whether as patches or as gradients, creating heterogeneity across an ecosystem (Legendre and Fortin 1989). Even within a heterogeneous landscape, vegetation is organized in spatially recognizable patterns that have been used as surrogates for processes such as competition, disturbance, succession, and invasion dynamics for decades (*sensu* Watt 1947, Legendre and Fortin 1989). Modern advances in spatial analysis techniques that incorporate "space as a surrogate" for more difficult, and often impossible, direct experimental manipulation, have maximized the inferential power of the pattern-process linkage (McIntire and Fajardo 2009). Extensive and detailed spatial datasets, at scales relevant to many ecosystems processes, are still rare. As such, identification of strong links between the patterns of vegetation and their mechanistic influence on important ecosystem processes remains an important goal (Schroder 2006).

The pattern-process linkage is a feedback whereby ecosystem processes drive structural patterns, but vegetation patterns also strongly influence vital ecosystem processes such as disturbance regime or soil moisture availability (O'Sullivan and Perry 2013). My dissertation research has been designed to investigate both directions of this relationship in forested ecosystems. Forests with heterogeneous horizontal and vertical structures offer ideal systems to test hypotheses of this linkage because trees are dominant organisms that strongly influence physical and biological processes in their local neighborhoods (Franklin and Van Pelt 2004). Both the processes that create structural heterogeneity in forests, such as competition and disturbance, and the influence of that heterogeneous structure on ecosystem processes, such as below-canopy snow dynamics, provide ecosystem services that are important for maintaining ecological, social, and economic health.

The studies included here examine two different forest types, which are governed by different external forces, but the ecological theories and mechanisms remain constant and transferable to other forest types.

Chapter 1 examines the forward pattern-process relationship, where I test hypotheses of competition and gap dynamics on the creation of structural heterogeneity in old-growth forests.

Deriving this form of pattern-process relationship utilizes a top-down approach, whereby processes that are driving pattern creation are inferred from repeated observations of similar or recurring patterns (O'Sullivan and Perry 2013). Using stem-maps in Sitka-spruce western hemlock forests of Southeast Alaska, I sought to:

(1) Quantify and analyze the spatial patterns of spruce-hemlock forests to examine the roles of competition and gap dynamics;

(2) Test the applicability of a newly proposed gap delineation method based on surrounding tree shadow lengths compared to traditional canopy tree death methods for higher latitude forests.

This study presents the first quantitative analysis of spatial aspects of structural complexity in this forest type for the region. Evaluating the processes of competition and gap dynamics from tree spatial patterns yields insights into the timing and strength of each of these processes during forest stand development. I offer the first evaluation of a new tree shadow based method for objectively delineating gap structure.

The reciprocal pattern-process relationship is explored in chapters 2 and 3, where I examine the influence of forest vegetation patterns on the processes of snow accumulation and disappearance. A bottom up approach guides the remaining chapters (O'Sullivan and Perry 2013). I studied the fine-scale processes and interactions in order to elucidate emergent behaviors at the forest stand scale. In chapter 2, I was interested in determining if spatial heterogeneity within the forest canopy induces heterogeneity in snow accumulation and persistence. In this study a stem-mapped and intensively snow sampled mixed-conifer forest in western Montana allowed me to:

(1) Quantify tree spatial patterns in a mixed-conifer forest, identifying different local tree neighborhoods—individual trees, dense tree clumps, and openings.

(2) Test the hypothesis that differences in snow accumulation and disappearance processes arise from the patterns of overlying vegetation, particularly their control on interception and interactions with energy budget. I used a set of linear contrasts to test the predictions that peak snow accumulation and snow persistence differ between:

1. Openings and clumps;
2. Openings and individuals;
3. Deciduous conifer and evergreen conifer individuals; and
4. Evergreen individuals of different species.

The purpose of this research was to improve our basic understanding of the functional consequences of within-stand structural and spatial heterogeneity for underlying snow processes. Such results can support management approaches that mediate forest structural complexity and tree spatial patterns, and seek to balance multiple management objectives.

Chapter 3 increases in scale, from point values to plot scale patterns of snow accumulation and disappearance. Aided by a stem-mapped forest and an extensive snow dataset spanning four winters (2014-2017) I was able to:
(1) Quantify the temporal and spatial variation in snow parameters (i.e., snow density, snow water equivalent, snow disappearance date) beneath a heterogeneous mixed-conifer canopy; (2) Model the distribution of snow parameters using detailed forest canopy metrics derived from ground and LiDAR measurements; (3) Compare the performance of LiDAR metrics relative to ground based measurements.

This study provides the first, temporally and spatially extensive dataset of snow properties beneath a forest canopy and allowed for the quantification of variations in snow attributes due to vegetation. Characteristics of the vegetation canopy and stem distribution were used to parameterize a random forest model to estimate the distributional patterns of snow accumulation and disappearance. High resolution, high frequency snow data allowed me to explicitly test the linkage between vegetation patterns and the spatial variability of snow accumulation and melt at the point and plot scales. The introduction of LiDAR metrics into a regression tree modeling framework has not been tested in the field of snow hydrology and offers a cost effective management tool for quantifying the distribution of snow parameters over large extents and for forecasting the timing and quantity of available water supplies.

These studies clearly demonstrated the strong link between forest vegetation patterns and important ecosystem processes. Pattern analysis provides an important approach for gaining insight into the mechanisms driving the creation and consequences of forest spatial patterns. My results illustrate a shift in the controlling processes that shape forest structural complexity from lower to upper latitudes within the same forest type. This study is a reminder that we should not naïvely assume that an ecological theory uniformly applies across the range of a forest type.

The processes of snow accumulation and disappearance were significantly influenced by the presence and patterns of forest vegetation. Forest structural complexity characterized by tree arrangement, size and type were important variables driving snow dynamics. Chapters 2 and 3

uniquely captured the influence of *Larix*, a deciduous conifer, on snow accumulation and disappearance. Capturing and accounting for detailed forest structure in estimating peak SWE and snow disappearance were more important than the source of the data, as random forest models parameterized with ground or LiDAR derived canopy measures performed equally well. This work offers researchers and managers new tools for quantifying, understanding, and managing structurally complex forests.

**References**


Franklin, J.F., and Van Pelt, R. 2004. Spatial aspects of structural complexity in old-growth forests. Journal of Forestry, 102(3): 22-28.

Legendre, P., and Fortin, M.J. 1989. Spatial pattern and ecological analysis. Vegetatio, 80(2): 107-138.

Levin, S.A. 1992. The problem of pattern and scale in ecology: the Robert H. MacArthur award lecture. Ecology, 73(6): 1943-1967.

McIntire, E.J., and Fajardo, A. 2009. Beyond description: the active and effective way to infer processes from spatial patterns. Ecology, 90(1): 46-56.

O'Sullivan, D., and Perry, G.L. 2013. Spatial simulation: exploring pattern and process. John Wiley & Sons.

Schröder, B., 2006. Pattern, process, and function in landscape ecology and catchment hydrology? how can quantitative landscape ecology support predictions in ungauged basins? Hydrology and Earth System Sciences Discussions, 10(6): 967-979.

Watt, A.S. 1947. Pattern and process in the plant community. Journal of Ecology, 35(1-2): 1-22.

# **CHAPTER 1.** Spatial aspects of structural complexity in Sitka spruce – western hemlock forests, including evaluation of a new canopy gap delineation method


## Abstract

Structural complexity in long-lived forests where stand-replacing disturbances are rare is thought to emerge from chronic small scale disturbances and competitive interactions between trees. We analyzed tree size distributions, tree spatial patterns, and canopy gap attributes in ten, 1.42 ha stem mapped plots in old-growth Sitka spruce-western hemlock forests in southeast Alaska. Most plots had rotated sigmoid or reverse J-shaped diameter distributions. Overstory tree patterns were uniform at short distance (<5 m) and random or aggregated at larger distances (>5 m); understory trees were spatially random or aggregated at most scales. Tree patterns were highly variable across plots. Overstory and understory tree populations were spatially independent in most medium canopy cover (40%-70%) plots, but spatially repelled in most high canopy cover (>70%) plots. Canopy gap delineation using a traditional geometric approach identified more gaps and greater forest area in gaps compared to a new method based on canopy tree shadow lengths. We recommend defining the lower limit of canopy gap size using overstory tree crown diameter; gap delineation based on overstory tree shadow length is overly conservative at higher latitude sites. Our analyses show that, despite their low species richness, the temperate rainforests of southeast Alaska are highly structurally diverse.


## Introduction

Old-growth forests provide important ecosystem functions including wildlife habitat, regulation of energy and nutrient cycles, and long-term carbon sequestration unmet by younger forests (Spies 2004). Horizontal and vertical heterogeneity—structural complexity—are emergent properties of old-growth stands that directly influence their functional characteristics (Franklin and Van Pelt 2004). Structural complexity is the long-term result of disturbance history, competitive interactions, tree mortality and recruitment, and the edaphic mosaic (Lertzman et al. 1996; Franklin et al. 2002; Franklin and Van Pelt 2004, Larson et al. 2015).

In forests where stand replacing disturbances are rare, conceptual models of stand dynamics assume that small scale disturbances (i.e., wind, snow and ice, insects, disease) drive the development of structural and spatial heterogeneity in maturing forests (Nowacki and Kramer 1998, Franklin et al. 2002). As stands transition from mature to old-growth, the structural and compositional consequences of canopy gap formation obscure the imprint of earlier competition-

driven self-thinning mortality (Lertzman et al. 1996; Franklin et al. 2002). Overstory tree mortality creates localized canopy gaps allowing light to reach the forest floor (Lertzman and Krebs 1991). Gap size and the architecture of surrounding canopy trees directly influence and alter the patterns of light, moisture, and nutrients available to the understory (Canham et al. 1990, Van Pelt and Franklin 1999, Van Pelt and Franklin 2000). Gap-associated microenvironments influence seedling performance, regeneration response, community composition, and productivity (Lertzman and Krebs 1991; McCarthy 2001, Coates 2002).

Gap patterns and dynamics have been investigated in the coastal temperate rainforests of southeast Alaska (Alaback 1988; Ott 1997; Ott and Juday 2002). However, it is not clear how well the canopy gap concept applies at higher latitudes, because light that penetrates the forest canopy is increasingly displaced away (because of low sun angles) from the structural gap and associated soil resources with increasing latitude (Canham et al. 1990; Zhu et al. 2015, Kramer et al. 2001). An additional challenge is how to detect and classify canopy gaps in an objective, repeatable manner that is linked to ecosystem function and forest dynamics. Zhu et al. (2015) recently introduced a method to objectively define minimum gap size based on the shortest shadow length of canopy trees surrounding a gap and canopy tree crown diameter, which directly accounts for the influence of surrounding canopy trees to moderate the light regime and modify the within gap microclimate and associated processes. The applicability of this new method to other forest types, especially higher latitude forests requires evaluation.

Tree spatial patterns reflect both the disturbance regime and past species interactions. Distinct structural patterns can be detected from within a structurally complex forested matrix, which provide insight into the underlying ecological processes (McIntire and Fajardo 2009).

Competitive interactions are an additional mechanism driving structural change in long-lived and old-growth forests, and past competition may be detected in tree spatial patterns (Franklin et al. 2002; Parish and Antos 2004, Lutz et al. 2014, Larson et al. 2015). In temperate forests of the Pacific Northwest, the very shade-tolerant tree *Tsuga heterophylla* (western hemlock) is a strong competitor that may directly influence forest dynamics (Lutz et al. 2014). Competition theory predicts that large canopy trees will outcompete smaller understory trees for resources in their immediate environment, leading to a spatial segregation of the two populations at local scales (i.e., up to about 10 m) and a tendency towards a uniform distribution of overstory trees (Moeur 1997; Larson and Churchill 2008). Previous work has found spatial segregation between large overstory trees, particularly hemlock, and understory trees (i.e., ingrowth; Getzin et al. 2006; Lutz et al. 2014). If present, strong competitive interaction suggests that the large overstory trees are strongly influencing the forest dynamics.

Northern coastal Sitka spruce (*Picea sitchensis*) – western hemlock (*Tsuga heterophylla*) forests form the largest expanse of intact old-growth temperate rainforest worldwide, providing a natural observatory in which to examine the structure and stand development of long-lived forests (Alaback 1988; McCarthy 2001). The objectives of this study were to characterize the structural and spatial attributes of unmanaged northern coastal spruce-hemlock forests, and to interpret this analysis of forest stand structure and spatial pattern in terms of past developmental processes, especially gap dynamics and competitive interactions between trees. We first report species composition and forest structure, including tree diameter distributions, providing context for our spatial analyses and interpretation of forest dynamics. Second, we investigate canopy gap attributes, including gap size distributions, total open space unoccupied by overstory tree crowns, and an assessment of the new Zhu et al. (2015) gap

detection method. Third, we use spatial point pattern analysis to investigate past competitive interactions between tree populations, and to test the hypothesis of spatial segregation between overstory and understory tree populations (Lutz et al. 2014). These objectives require large plots (>1 ha) in which the locations of individual trees are mapped, a field sampling approach that complements traditional forest sampling with small (<1 ha) fixed area plots, but are better suited for different objectives (Lutz 2015).

## Methods

*Study Area and Sampling Design*

The data analyzed here were collected in 1964 as part of a forest inventory study designed, "To determine which basal area factor and point cluster pattern combinations would provide acceptably accurate measurements of basal area per acre." (LaBau 1967). The original study was motivated by a directive from the U.S. Forest Service Washington Office that instructed USFS Regional Offices to convert forest inventory field sampling from fixed radius plots to point (i.e., prism) sampling. The scope of the original study was old-growth spruce-hemlock forests (LaBau 1967).

Study sites were located in old-growth Sitka spruce-western hemlock forests within the Tongass National Forest around Juneau and Petersburg, Alaska in the summer of 1964 (Figure 1). Using a stratified random sampling design, plots were located using aerial photographs (1:15,840 scale; LaBau 1967). Plots were required to be: (1) accessible—less than a mile from a road or beach; (2) commercial forest land capable of producing at least 8,000 board feet per acre (actual gross Scribner board foot volume for sampled plots: 26,764 - 110,947 bd ft); (3) at least 150 years old; (4) a spruce and/or hemlock forest in which at least 50% of timber volume was either spruce or hemlock; and (5) covering at least 2.02 ha (5 acres). Twenty-six potential plot

locations were identified and classified as medium density (canopy closure of 40-70%) or full density (70-100% canopy closure) stocking based on aerial photo interpretation. All five locations falling into the medium density category were selected for sampling. The remaining sites were in high density areas, of which five were randomly selected for sampling. A total of 10, 1.42 hectare (100.6 × 140.8 m; 5 × 7 chains) plots were located and sampled. Because the old-growth near Juneau tends to have lower timber volumes, two plots were located near Petersburg, Alaska. Plot elevations ranged between 10 m and 500 m above sea level. The climate of southeast Alaska is mild and maritime with summer and winter mean temperatures of 8$^{o}$C and 1$^{o}$C respectively; and mean annual precipitation is 145 cm and 266 cm for Juneau and Petersburg, respectively, occurring year-round, making prolonged drought rare (WRCC 2016).

*Data Collection*

Plot locations identified in aerial photographs were navigated to in the field and used as plot centers. Plot boundaries were laid out and corners staked using a staff compass, topographic chain, and relascope (LaBau 1967). Closure requirements for the primary plot boundary control traverse specified an allowable error of 1 in 300 (LaBau 1967). All live trees greater than 7.6 cm (3.0 in) in diameter at breast height (DBH, 1.37 m) were mapped in 20.12 m (66.0 ft) wide parallel columns within each 1.42 ha plot by making perpendicular side shots from a staked steel tape located in the center of each column. Each column was subdivided into 404.9 m$^2$ subplots (1/10$^{th}$ acre) to facilitate tree measurement and data recording. Within subplots, each tree was assigned a unique identifying number and species, DBH, and height in number of 4.9 m (16 ft) logs, as well as tree spatial coordinates were measured and recorded (LaBau 1967). Dead trees were not sampled.

To facilitate our study of gap attributes and tree spatial patterns, we designated three canopy strata based on tree height; overstory, midstory and understory (Larson and Franklin 2006). We designated trees ≥25 m tall as overstory trees, approximating the 75$^{th}$ percentile of tree heights which had a lower DBH limit of 38.5 cm, and consistent with past usage in this forest type (Hennon and McClellan 2003). Trees 10-25 m tall were termed midstory, and ≤ 10 m were designated as understory trees. To fully explore the analytical consequences of this definition of overstory trees we conducted a sensitivity analysis using overstory tree heights of 20, 25, and 30 m on gap parameters (*see* Table S2, S3).

*Spatial Analysis*

*Gap analysis*

Canopy openings are regions of the forest canopy unoccupied by overstory tree crowns. For this analysis, we define open areas as regions with no direct overhead overstory canopy cover, with no lower size limit. Canopy gaps (Figure 2) are defined as contiguous open areas of sufficient size to create forest understory conditions that are functionally different from smaller canopy openings, in terms of, for example, increased available light, nutrients, or soil moisture (Zhu et al. 2015). The classical definition of a canopy gap is an opening created by the death of a dominant overstory tree (Runkle 1982).

Open area and canopy gaps were identified and quantified using mapped tree locations, modeled tree heights, maximum crown dimensions, and tree shadow lengths. Tree heights were determined using estimated crown ratio values and a regionally parameterized height to diameter relationship (Keyser 2015). We used modeled total tree heights for gap delineation because the field-measured height in merchantable logs will always underestimate, sometimes severely, total tree height. Crown ratio values were determined using a set of Wiebull-distribution based

equations (Keyser 2015). Species specific maximum crown diameter estimates were determined using regionally parameterized relationships between tree diameter and maximum crown dimensions (Bechtold 2004; Keyser 2015).

We used a canopy opening detection algorithm developed by Churchill et al. (2017) for point pattern datasets. The opening algorithm determines the location and area of unoccupied space in a point pattern (i.e., a tree stem map) based on a user designated threshold distance from a fixed grid of points to the nearest tree. Polygons are then drawn in all unoccupied areas larger than the threshold distance from each of the surrounding tree boles. A tree crown buffer with a length equal to the average overstory tree crown radius is subtracted from the polygon so gaps extend from overstory tree crown edge to crown edge. All overlapping polygons are merged, and the area of each merged opening is calculated. This calculated gap area is the open area devoid of any overstory foliage, which is analytically equivalent to a canopy gap as defined by Runkle (1982). Eliminating the tree crown buffer is analytically equivalent to Runkle's (1982) expanded gap, where displaced light due to the canopy gap is still highly influential extending to the base of the boles of gap bordering trees (Runkle 1982). An edge correction buffer equal to the threshold distance was applied to the perimeter of each plot to ensure only complete canopy gaps would be calculated. Without this buffer, partial gaps on the plot edge would be calculated, potentially inflating total gap area since no information is available for trees beyond the sampling window.

*Geometric gaps*

We used the classic definition of a canopy gap (Runkle 1982) as a benchmark against which to evaluate the new method proposed by Zhu et al. (2015). Developmental canopy gaps result from the death of one or more canopy trees (Runkle 1982). The smallest functional gap

would then be the open area caused by the death of a single overstory tree. We used this to define the lower limit of a functional "geometric gap" with a lower limit equal to the crown diameter of a single overstory tree (Figure 2B). A functional gap using this definition had a threshold distance of 8.88 m and tree crown buffer of 4.44 m. This value is consistent with the average size of a single tree canopy gap across forest types (Canham et al. 1990).

*Shadow gaps*

Using the methods of Zhu et al. (2015), we determined the lower limit of functional gap size using the shortest shadow length of an average overstory tree; gaps greater than or equal to this area are termed "shadow gaps". Shadow length was calculated using an overstory tree height of 25 meters, average plot latitude, and the solar angle at noon (1200 hrs) averaged over the growing season (Figure 2A; Zhu et al. 2015). The average crown diameter of an overstory tree was subtracted from the shadow length to determine the lower limit of a functional shadow gap. Shadow gaps were quantified using the algorithm described above with a threshold distance of 11.78 m and tree crown buffer of 4.44 m.

*Open area*

Total open area in the plot devoid of overstory foliage was calculated using the same opening algorithm with a threshold distance of 4.44 m and tree crown buffer of 4.44 m. These values determined open area extending from the edge of all non-overlapping overstory tree crowns—the total area with no direct overhead overstory canopy coverage. Non-gap open area was calculated as the difference between total open area and functional gap area.

*Stand level spatial analysis*

We analyzed tree spatial patterns and interactions at the stand and within-stand scales using the statistical program R version 3.2.1 (R Core Team 2016) and functions in the spatstat

library (Baddeley and Turner 2005). Stand level spatial patterns were evaluated using the pair correlation function with an isotropic edge correction and default distance range. The pair correlation function ($g$) is a normalized, non-cumulative density function that calculates the probability of finding the observed density of neighboring trees in a ring centered around each point in a given point pattern across a range of distances (Wiegand and Moloney 2004). Significance is assessed by comparing the empirical result to the density generated through a random point process at those same distances (Wiegand and Moloney 2004). The advantage of using a non-cumulative function is that spatial patterns can be detected at given inter-tree distances rather than up to a given distance. Observed values less than 1 indicated a uniform pattern and greater than 1 suggest aggregation. Significance was evaluated using a Monte Carlo simulated 95% confidence envelope. A goodness of fit test was unnecessary since spatial analysis was exploratory. The pair correlation function was used to evaluate the spatial patterns of: (1) overstory trees of all species, (2) only western hemlock (i.e., *Tsuga*) overstory, and (3) understory trees of all species. Spatial patterns of overstory spruce only were not evaluated due to low sample size.

*Within-stand level spatial analysis*

By reducing the scale of observation to within the stand, patches of trees and individuals can be identified. These local spatial patterns were evaluated using a clustering algorithm that assigns each tree to a patch or as a widely spaced individual using an analytically determined fixed inter-tree distance (Plotkin et al. 2002; Larson and Churchill 2008). Inter-tree distance is measured from stem center to stem center. Trees are a member of the same patch if the inter-tree distance is less than the inter-tree distance from at least one other patch member. Individual trees have no neighbors within at least the inter-tree distance. Inter-tree distance was determined using

percolation analysis, where the inflection point in distribution is used as the inter-tree distance (Plotkin et al. 2002). Analysis was conducted on all overstory trees.

*Competition analysis*

The bivariate pair correlation function ($g_{i,j}$) was used to examine competitive spatial relationships between overstory (*i*) and understory (*j*) populations. A null model of population independence was used to test the prediction of overstory-understory segregation, especially that driven by *Tsuga* (hemlock; Goreaud and Pelissier 2003). If overstory trees suppress ingrowth, then the observed $g_{over,under}(r) < 1$ where the sub-populations are repelled from each other. Competitive interactions between *Tsuga* overstory—all species understory and all species overstory—all species understory were evaluated.

To evaluate overall spatial patterns and relationships by canopy density type, all spatial analysis methods were also conducted using the pool function in the spatstat library in R paired with a Monte Carlo simulation envelope utilizing the respective null models (Baddeley et al. 2016). When overstory *Tsuga* populations were evaluated in a pooled framework, plot 104 was removed from the analysis in the medium density class due to an insufficient sample size of overstory *Tsuga* stems.

## Results

*Forest structure and composition*

Western hemlock (*Tsuga heterophylla)* dominated overstory and understory species composition, accounting for over 90% of stems in medium density plots and 75% in full density plots (Table 1). However, the largest trees in terms of diameter were Sitka spruce (*Picea sitchensis*). Plot 104, a full density plot located in a riparian area, was a compositional outlier with Sitka spruce making up 75% of the species composition, and the only plot to have black

cottonwood (*Populus trichocarpa*) (Table S1). Red alder (*Alnus rubra*) and yellow cedar (*Cupressus nootkatensis*) accounted for only 0.25% and 1.2% of total stems, respectively. When present, all non-dominant species were mostly confined to the midstory and understory positions.

Stem density ranged from 315-666 trees $ha^{-1}$ in medium and 246-664 trees $ha^{-1}$ in full density plots. Twenty-five percent and 46% of the trees were tall enough to be considered overstory trees, but accounted for 76% and 83% of the total plot basal area in medium and full density plots respectively. The two plots located near Petersberg (plots 143, 161) were not structurally different from the plots located near Juneau in any of our analysis.

Forests in the medium and full density strata exhibited different, recognizable patterns in their size distributions. Medium density plots exhibited reverse J-shaped diameter distributions, except for plot 104 which had a rotated sigmoid distribution (Figure 3). Conversely, most full density plots exhibited rotated sigmoid distributions, with the exception of plot 76 which had a reverse J distribution, and plot 32 which exhibits a distribution transitional between unimodal and rotated sigmoid (Figure 4).

*Gaps*

Stand stem maps indicate that old-growth tree structure consists of varying sizes and numbers of canopy gaps, widely spaced individual trees, and tree patches (Figure 5, S1, S2). Medium density plots consistently had greater numbers of gaps accounting for more of the total open area in each plot (Table 2, Figure S3). The classical geometric gap definition (Runkle 1982) produced two to six times more area in functional gaps than gaps delineated using the Zhu et al. (2015) shadow method, and this difference held over a range of overstory tree heights (Figure S3, Table S2-S3). In both plot density strata, the distribution of geometric gaps followed a right skewed normal distribution covering the full range of gap size classes, while shadow derived

gaps exhibited a flat distribution with a more restricted range of size classes, especially in full density plots (Figure 6, S4).

*Spatial Patterns*

*Stand level*

Stand level overstory tree spatial patterns exhibited a spatially random tree distribution across most distances, with significant aggregation observed across most distances for understory trees (Table 3). All full density overstory trees tended to exhibit significant uniformity, mostly at short distances (1-3 m), with medium density plots tending towards more random distributions across all distances (Figure S5, S6). *Tsuga* overstory trees in medium density plots were randomly arranged, but one plot indicated significant aggregation around 10 m and one plot exhibited significant uniformity around 4 m (Figure S7). Full density overstory *Tsuga* was uniformly distributed at short distances (1-4 m) in four of the five plots and aggregated at three different ranges (6-7 m, 13 m, and 17 m; Figure S8) in the other plot. Understory trees in all but one plot (plot 104) exhibited significant aggregation across most distances in both density classes, but was much stronger in full density plots (Figure S9, S10). Stand-level tree spatial patterns were random across all distances when plots were pooled by density class for all univariate overstory and understory tree analyses: the pooled analysis masked the substantial inter-plot variation.

*Within stand spatial patterns*

Within stand spatial patterns consisted of widely spaced individuals, tree patches with two or more individuals, and inter-tree percolation distances consistent with average tree crown diameter. Percolation analysis identified overstory, midstory, and understory inter-tree distances around 8, 6, and 4 m respectively which are consistent with the average maximum crown

diameter for each subpopulation (Figure 7). Medium density overstory trees were evenly distributed among patch sizes in terms of percent density and basal area, while overstory trees in full density plots occurred mainly as two very large patches that accounted for 85% and 83% of the density and basal area (pooled by density) respectively, with little variation in patch distribution between plots (Table 4, Table S4).

*Competition*

Overstory hemlock and understory populations were spatially independent across most distances regardless of density class except two full density plots which indicated significant repulsion between the two populations across nearly all distances (Figure 8, 9). Medium density plots exhibit some small scale attraction (1-3 and 10 m), with one plot also indicating repulsion around 11 m (Figure 8). Two of the full density plots indicate repulsion across all distances (1-25 m), with significant repulsion detected in the other three (Figure 9). Pooled analysis indicated that overstory hemlock and understory populations are spatially independent, again obscuring the between plot variation.

An examination of the spatial relationship between all overstory and all understory trees indicated significant repulsion, attraction, and independence across various differences between plots and within in density class. Most medium density plots showed significant attraction at short and middle distances, one plot indicating only independence, and one plot with repulsion around 11 m (Figure S11). High between plot variation was also apparent for full density plots, where one plot showed independence, three plots had significant repulsion anywhere from 3-25 m, and the last plot overstory and understory trees were spatially attracted from 2-12 m (Figure S12).

## Discussion

Our analyses quantify for the first time spatial aspects of structural complexity in Sitka spruce-western hemlock forests, and provide a new line of evidence supporting a role for gap dynamics in this forest type. Large, stem mapped plots offer a means to investigate attributes of forest structure and dynamics that cannot be studied with traditional small fixed area plots (e.g., Lutz et al. 2014), an approach that has not previously been used in the temperate rainforests of southeast Alaska (but see Deal et al. 1991). Our analyses of tree spatial patterns, gap size distributions, and spatial relationships between overstory and understory trees show that, despite their low species richness, the temperate rainforests of southeast Alaska are highly structurally diverse.

The original sampling design for this study targeted old-growth forests, which at the time of sampling in 1964 were defined as sites with no evidence of past timber harvest in which at least 150 years had passed since stand-initiating disturbance (LaBau 1967). Previous work in old-growth spruce-hemlock forests of southeast Alaska showed that old-growth structural features do not become apparent until about 160-200 years after stand-initiating disturbance (Alaback 1984). Thus, our study sites likely include both true old-growth stands, as well as younger stands that might be better described as transitional (*sensu* Zenner 2005) or early old-growth (*sensu* Freund et al. 2015).

*Forest structure*

Tree diameter distributions provide insights into past forest development and vary predictably along a forest age and structural development gradient (Alaback 1984, Zenner 2005). In wind-disturbed spruce-hemlock forests of southeast Alaska, young forests originating from stand-replacement disturbance characteristically exhibit a unimodal diameter distribution up to

about stand age 160 years; at greater ages a reverse-J diameter distribution was most common (Alaback 1984). A rotated sigmoid diameter distribution is generally associated with stands that are transitional between the mature and old-growth structural stages (Zenner 2005, Freund et al. 2015). Sites with disturbance histories that include intermediate non-stand replacing disturbances typically exhibit more complex DBH distributions, including rotated sigmoid (Ott and Juday 2002, Zenner 2005) and bi- or multi-modal distributions (Deal et al. 1991, Kramer et al. 2001, Ott and Juday 2002, DeGayner et al. 2005).

All plots included trees >100 cm DBH (Table S1), and nine of 10 plots had either rotated sigmoid or reverse J-shaped diameter distributions (Figure 3, 4), evidence that these are late-successional stands that have either attained old-growth structure or are transitional between mature and old-growth (c.f., Ott and Juday 2002). Plot 32 had a skewed normal distribution (Figure 4), indicating that this site may be just beginning to transition to old-growth structure (Alaback 1984). Reverse-J shaped DBH distributions were most common and most pronounced in the medium canopy density stratum (Figure 3), suggesting that these sites may have more highly developed old-growth attributes, and have developed for a longer time since the last stand-replacing disturbance than the full canopy density plots (Figure 4). However, a complete population age structures would be needed to definitively assess stand age and developmental histories (Deal et al. 1991).

*Gap delineation, area, and size distributions*

Two types of canopy gaps occur in the temperate rainforests of southeast Alaska: developmental gaps and edaphic gaps. Developmental canopy gaps are the result of individual tree mortality and small-scale, chronic disturbance. Most trees die standing or from bole breakage in temperate old-growth conifer forests of the Pacific Northwest, with only about 20 to

25% of trees uprooted (Spies et al. 1990, Hennon and McClellan 2003, Larson and Franklin2010). Tree death and gap formation due to bole breakage is often associated with preexisting decay and prior wounding, which compromise tree structural integrity and predispose mortality (Hennon 1995, Hennon and McClellan 2003, Larson and Franklin 2010). Edaphic gaps are persistent canopy openings within the forest matrix associated with sites unsuitable for development of a closed canopy, such as stream courses, rock outcrops, or wetlands (Lertzman et al. 1996). Extreme structural variants of edaphic gaps also occur that prevent the development of a closed canopy. For example, low-productivity palustrine forested wetlands—sites that support development of spruce-hemlock forests but where a shallow depth to the water table limits productivity (Bisbing et al. 2015), sometimes preventing development of a closed canopy. Another example is "priority" gaps (*sensu* Schmidt et al. 1998) where patches of dense mats of hardwood or shrub stems establish early in stand development and exclude conifer regeneration, preventing canopy closure. A strength of our analysis is that it provides an unbiased sample of forest gap structure and tree spatial patterns in coastal spruce-hemlock forests. However, we are not able to distinguish developmental gaps from edaphic gaps. Thus, our analysis of forest canopy gap structure represents the combined effects of site conditions (edaphic and priority gaps) and past tree mortality (developmental gaps).

Gap structure was present in both canopy density classes with an average of 34% and 20% of total medium and full density plot areas influenced to some degree by canopy openings (Table 2). These values are similar to the average of 30.2% found by Lertzman et al. (1996) for combined developmental and edaphic gap area in forests of coastal British Columbia. On average, 23.2% and 6.0% of plot area was in functional canopy gaps for medium and full density categories, respectively, using the geometric (Runkle 1982) gap delineation method. This range

is consistent with previous estimates of the area in developmental canopy gaps, which range from 3.8% to 33.7% in old-growth Alaskan temperate forests (Nowacki and Kramer 1998, Ott and Juday 2002). We used mapped tree locations and modeled tree heights and crown widths to estimate area in canopy openings and gaps, while previous studies directly measured canopy gaps in the field. Although modeled tree crowns do not represent actual crown geometry with perfect fidelity, our results for gap size distributions and total area in openings or gaps agree with previous field-based gap delineation studies.

Our estimates of the functional gap size distribution using the geometric delineation approach are slightly different from previous studies, but our range of gap size values are consistent with other studies. Geometric gaps exhibited an approximately normal, right skewed distribution, while canopy gap distributions in old-growth temperate forests in southeast Alaska and British Columbia consistently exhibit right skewed or negative exponential distributions suggesting the prevalence of many smaller gaps (Lertzman and Krebs 1991; Ott 1997; Nowacki and Kramer 1998, Bartemucci et al. 2002; Ott and Juday 2002). Our geometrically derived gaps spanned the range of size classes (1-600+ $m^2$), with many mid-sized gaps (100-300 $m^2$) and some large gaps (>600 $m^2$) apparent in both density classes (Figure 6). In temperate forests in southeast Alaska canopy gaps have been found to range from 6-264 $m^2$ (Nowacki and Kramer 1998, Ott and Juday 2002), from 5-525 $m^2$ in southwest British Columbia (Lertzman and Krebs 1991), up to1,253 $m^2$ on rare occasions in northern British Columbia (Bartemucci et al. 2002, and from 25.5-366 $m^2$ in more southern temperature forests (Van Pelt and Franklin 2000). Using field based methods, gaps >600 $m^2$ are rare usually only detected using Runkle's (1982) expanded gap definition, where the gap extends from tree bole to bole rather than the canopy edges (Bartemucci et al. 2002). However, in Chilean temperate rainforest average canopy gap

size was 425 $m^2$ (Veblen 1985) and gaps as large as 739 $m^2$ were measured in the southern Sierra Nevada (Van Pelt and Franklin 2000).

We do not recommend using the Zhu et al. (2015) gap delineation method (i.e., shadow gaps, Figure 2A) in tall, higher latitude forests, such as the coastal spruce-hemlock forests studied here. At our study sites, the Zhu et al. (2015) method underestimated the number of and total area in canopy gaps (Figure 6, S3, Table 3, S2-S3) relative to the classical Runkle (1982) method because the Zhu et al. (2015) definition of a minimum functional gap size increases with decreasing sun angle. The Zhu et al. (2015) method is much more appropriate for lower latitude tropical and subtropical forests where the understory light regime is more directly regulated by overhead canopy cover and gaps (Canham et al. 1990). Canopy gaps regulate other environmental variables in addition to light, such as precipitation throughfall rates and snow accumulation and persistence on the forest floor (Dickerson-Lange et al. 2017), and soil moisture (Gray et al. 2002). These important gap-influenced processes and environmental features are closely related to the actual geometry of canopy gaps, which is better represented using the Runkle (1982) geometric gap method.

*Tree spatial patterns and evidence of past competition*

Competitive interactions produced a much stronger spatial signal in full density than medium density plots. However, we did not observe what we expected in terms of spatial patterns and competitive interactions in the pooled analyses. Significant spatial patterns consistent with past competitive mortality were evident only in individual plot analyses. The pooled analyses masked significant spatial patterns due to alternate scales of significant patterns between plots within a density class, which may be due to a high degree of variation in edaphic and biophysical conditions in the region. The overall random distribution of canopy trees, and

those in medium density stands was not consistent with our prediction of uniformity, but is consistent with the findings for canopy tree patterns in old-growth of similar forest types (Larson and Churchill 2008, Lutz et al. 2014). In contrast, most of the individual full density plots indicated significant uniform spatial patterns from 1-3 m suggesting that earlier self-thinning mortality was an important developmental process in those stands (Larson et al. 2015).

Site and species-specific factors may explain why we did not find the predicted spatial signature of strong competitive interactions between overstory and understory trees. First, the sampling design did not capture the smallest diameter trees (>7.6 cm DBH). The lack of significant aggregation in the understory trees may also be partially attributed to the missing smallest size classes, which typically show the strongest signal of spatial aggregation, with midstory trees tending towards random distributions (Van Pelt and Franklin 2000, Parish et al. 1999, Lutz et al. 2014). In addition, the low solar angles in latitudes above $50^{o}$ N displaces the available light in canopy gaps away from the gap into the forest matrix creating a spatial disconnect between the location of the gap and the regeneration response (Canham et al. 1990; Coates and Burton 1997; Kneeshaw and Bergeron 1998; Van Pelt and Franklin 2000). This displacement may contribute to the apparent attraction between overstory and understory trees at some sites, as seedlings and saplings have been found to be more or equally abundant on edges of gaps and into the forest matrix, where the competitive interactions with the overstory is inconsequential compared to the availability of light or the presence of suitable establishment sites (Ban et al. 1998, Van Pelt and Franklin 2000, Coates 2002).

*Conclusions*

This study provides two novel contributions towards objectively quantifying structural complexity in tall, higher latitude forests. We provide the first quantification of spatial aspects of

structural complexity for higher latitude Sitka spruce-hemlock forests. Despite their low species richness, forest structure was highly heterogeneous, characterized by a forest mosaic of canopy gaps, tree patches, and a diverse range of tree sizes. These distinctive structural features contribute to the unique ecological functions of old-growth forests that are unmet by younger stands (Spies 2004; Franklin and Van Pelt 2004). However, the strong competition and spatial segregation signals observed in more southern temperate conifer forests were much weaker and only occasionally apparent in our data, likely due to low sun angles, lower site productivity, and greater edaphic heterogeneity in our higher latitude rainforest study sites

This study is the first to test Zhu et al.'s (2015) shadow gap delineation method in tall, higher latitude forests. We consider it an excellent method at lower latitudes, but because of the singular emphasis on noon solar angles to define canopy gaps, the Zhu et al. (2015) approach underestimates total area and number of canopy gaps in higher latitude forests. Thus, we do not recommend using the Zhu et al. (2015) method at higher latitude sites. Objectively delineating canopy gaps using the traditional geometric gap (Runkle 1982) is more appropriate for higher latitude forests, including coastal Sitka spruce-western hemlock forests.

## References


Alaback, P.B. 1984. A comparison of old-growth forest structure in the western hemlock–Sitka spruce forests of southeast Alaska. *In*: Proceedings of the Symposium: Fish and Wildlife Relationships in Old-Growth Forests, Juneau, AK, 12–15 April 1982. *Edited by* W.R. Meehan, T.R. Merrell Jr., and T.A. Hanley. American Institute of Fishery Research Biologists, Morehead City, NC. pp. 219–226.

Alaback, P. B. 1988. Dynamics of old-growth temperate rainforests in southeast Alaska. *In* Proceedings of the 2nd Glacier Bay Science Symposium. *Edited by* A.M. Milner and J.D. Wood. Gustavus, AK. pp. 150-153.

Alaback, P.B., and Juday, G.P. 1989. Structure and composition of low elevation old-growth forests in research natural areas of southeast Alaska. Nat. Area J. **9**(1): 27-39.

Baddeley, A., Rubak, E., and Turner, R. 2016. Spatial point patterns: methodology and applications with R. CRC Press, Boca Raton, FL.

Baddeley, A., and Turner, R. 2005. Spatstat: an R package for analyzing spatial point patterns. J. Stat. Softw. **12**(6):1–42.

Ban, Y., Xu, H., Bergeron, Y., and Kneeshaw, D.D. 1998. Gap regeneration of shade intolerant *Larix gmelini* in old growth boreal forests of northeastern China. J. Veg. Sci. **9**(4): 529-536.

Bisbing, S.M., Cooper, D.J., D'amore, D.V., and Marshall, K.N. 2015. Determinants of conifer distributions across peatland to forest gradients in the coastal temperate rainforest of Southeast Alaska. Ecohydrology. **9**(2): 354-367.

Bartemucci, P., Coates, K.D., Harper, K.A., and Wright, E.F. 2002. Gap disturbance in northern old-growth forests of British Columbia, Canada. J. Veg. Sci. **13**(5): 685-696.

Bechtold, W.A. 2004. Largest-crown-width prediction models for 53 species in the Western United States. West. J. Appl. For. **19**(4): 245-251.

Canham, C.D., Denslow, J.S., Platt, W.J., Runkle, J.R., Spies, T.A., and White, P.S.1990. Light regimes beneath closed canopies and tree-fall gaps in temperate and tropical forests. Can. J. For. Res. **20**(5): 620-631.

Churchill, D.J., Carnwath, G.C., Larson, A.J., and Jeronimo, S.A. 2017. Historical forest structure, composition, and spatial pattern in dry conifer forests of the western Blue Mountains, Oregon. USDA For. Serv. Gen. Tech. Report PNW-GTR. *In press*.

Coates, K.D. 2002. Tree recruitment in gaps of various size, clearcuts, and undisturbed mixed forest of interior British Columbia, Canada. For. Ecol. Manag. **115**(1): 387-398.

Coates, K.D., and Burton, P.J. 1997. A gap-based approach for development of silvicultural systems to address ecosystem management objectives. For. Ecol. Manag. **99**(3): 337-354.

Deal, R.L., Oliver, C.D., and Bormann, B.T. 1991. Reconstruction of mixed hemlock-spruce stands in coastal southeast Alaska. Can. J. For. Res. **21**(5): 643-654.

DeGayner, E.J., Kramer M.G., Doerr, J.G., and Robertsen, M.J. 2005. Windstorm disturbance effects on forest structure and black bear dens in southeast Alaska. Ecol. Appl. **15**(4): 1306-1316.

Dickerson-Lange, S.E., Gersonde, R.F., Hubbart, J.A., Link, T.E., Nolin, A.W., Perry, G.H., Roth, T.R., Wayand, N.E. and Lundquist, J.D. 2017. Snow disappearance timing is

dominated by forest effects on snow accumulation in warm winter climates of the Pacific Northwest, USA. Hydrological Processes. DOI: 10.1002/hyp.11144
Franklin, J.F., Spies, T.A., Van Pelt, R., Carey, A.B., Thornburgh, D.A., Berg, D.R., Lindenmayer, D.B., Harmon, M.E., Keeton, W.S., Shaw, D.C. and Bible, K. 2002. Disturbances and structural development of natural forest ecosystems with silvicultural implications, using Douglas-fir forests as an example. For. Ecol. Manag. **155**(1): 399-423.
Franklin, J.F., and Van Pelt, R. 2004. Spatial aspects of structural complexity in old-growth forests. J. Forest. **102**(3): 22-28.
Freund, J.A., Franklin, J.F., and Lutz, J.A. 2015. Structure of early old-growth Douglas-fir forests in the Pacific Northwest. For. Ecol. Manag. **335**: 11-25.
Getzin, S., Dean, C., He, F., Trofymow, J.A., Wiegand,K., and Wiegand, T. 2006. Spatial patterns and competition of tree species in a Douglas-fir chronosequence on Vancouver Island. Ecography **29**(5): 671–682.
Goreaud, F. and Pélissier, R. 2003. Avoiding misinterpretation of biotic interactions with the intertype $K_{12}$-function: population independence vs. random labelling hypotheses. J. Veg. Sci. **14**(5): 681-692.
Gray, A.N., Spies, T.A., and Easter, M.J. 2002. Microclimatic and soil moisture responses to gap formation in coastal Douglas-fir forests. Can. J. For. Res. **32**(2): 332-343.
Hennon, P.E. 1995. Are heart rot fungi major factors of disturbance in gap-dynamic forests? Northwest Sci. **69**(4): 284-293.
Hennon, P.E., and McClellan M.H. 2003. Tree mortality and forest structure in the temperate rain forests of southeast Alaska. Can. J. For. Res. **33**(9): 1621-1634.
Keyser, C. E. 2015. Southeast Alaska and Coastal British Columbia (AK) Variant Overview–Forest Vegetation Simulator. USDA For. Serv., Forest Management Service Center Internal Rep. Fort Collins, CO.
Kneeshaw, D.D., and Bergeron, Y. 1998. Canopy gap characteristics and tree replacement in the southeastern boreal forest. Ecology **79**(3): 783-794.
Kramer, M.G., Hansen, A.J., Taper, M.L., and Kissinger, E.J. 2001. Abiotic controls on long-term windthrow disturbance and temperate rain forest dynamics in southeast Alaska. Ecology **82**(10): 2749-2768.
LaBau, V.J. 1967. An analysis of design and technique of cluster point sampling in coastal Alaska old-growth forests. Thesis. Oregon State University.
Larson, A. J., and Churchill, D. 2008. Spatial patterns of overstory trees in late-successional conifer forests. Can. J. For. Res. **38**(11): 2814–2825.
Larson, J.A., and Franklin, F.J. 2006. Structural segregation and scales of spatial dependency in *Abies amabilis* forests. J. Veg. Sci. **17**(4): 489-498.
Larson, J.A., and Franklin, F.J. 2010. The tree mortality regimen in temperate old-growth coniferous forests: the role of physical damage. Can. J. For. Res. **40**(11): 2091-2103.
Larson, A.J., Lutz, J.A., Donato, D.C., Freund, J.A., Swanson, M.E., HilleRisLambers, J., Sprugel, D.G., and Franklin, J.F. 2015. Spatial aspects of tree mortality strongly differ between young and old-growth forests. Ecology **96**(11): 2855-2861.
Lertzman, K.P., and Krebs, C.J. 1991. Gap-phase structure of a subalpine old-growth forest. Can. J. For. Res. **21**(12): 1730-1741.
Lertzman, K.P., Sutherland, G.D., Inselberg, A., and Saunders, S.C. 1996. Canopy gaps and the landscape mosaic in a coastal temperate rain forest. Ecology **77**(4): 1254-1270.

Lutz, J.A., Larson, A.J., Furniss, T.J., Donato, D.C., Freund, J.A., Swanson, M.E., Bible, K.J., Chen, J., and Franklin, J.F. 2014. Spatially nonrandom tree mortality and ingrowth maintain equilibrium pattern in an old-growth *Pseudotsuga-Tsuga* forest. Ecology **95**(8): 2047-2054.

Lutz, J.A. 2015. The evolution of long-term data for forestry: large temperate research plots in an era of global change. Northwest Sci. **89**(3): 255-269.

McCarthy, J. 2001. Gap dynamics of forest trees: a review with particular attention to boreal forests. Environ. Rev. **9**(1): 1-59.

McIntire, E.J.B., and Fajardo, A. 2009. Beyond description: the active and effective way to infer processes from spatial patterns. Ecology **90**(1): 46-56.

Moeur, M., 1997. Spatial models of competition and gap dynamics in old-growth *Tsuga heterophylla/Thuja plicata* forests. For. Ecol. Manag. **94**(1): 175-186.

Nowacki, G.J., and Kramer, M.G. 1998. The effects of wind disturbance on temperate rain forest structure and dynamics of southeast Alaska. USDA For. Serv. Pacific Northwest Research Station General Technical Report PNW-GTR-421.

Ott, R.A. 1997. Natural disturbance at the site and landscape levels in temperate rainforest of southeast Alaska. PhD Thesis. University of Alaska, Fairbanks, AK.

Ott, R.A., and Juday, G.P. 2002. Canopy gap characteristics and their implications for management in the temperate rainforests of southeast Alaska. For. Ecol. Manag. **159**(3): 271-291.

Parish, R., and Antos, J.A. 2004. Structure and dynamics of an ancient montane forest in coastal British Columbia. Oecologia **141**(4): 562-576.

Parish, R., Antos, J.A., and Fortin, M.J. 1999. Stand development in an old-growth subalpine forest in southern interior British Columbia. Can. J. For. Res. **29**(9): 1347-1356.

Plotkin, J.B., Chave, J., and Ashton, P.S. 2002. Cluster analysis of spatial patterns in Malaysian tree species. Am. Nat. **160**(5): 629-644.

R Core Team. 2016. R: A language and environment for statistical computing. R Foundation for Statistical Computing, Vienna, Austria. Available from http://www.R-project.org.

Runkle, J.R. 1982. Patterns of disturbance in some old-growth mesic forests of eastern North America. Ecology **63**(5): 1533-1546.

Schmidt, M.G., Ogden, A.E., and Lertzman, K.P. 1998. Seasonal comparison of soil temperature and moisture in pits and mounds under vine maple gaps and conifer canopy in a coastal western hemlock forest. Can. J. Soil Sci. **78**(2): 291-300.

Spies, T.A. 2004. Ecological concepts and diversity of old-growth forests. J. For. **102**(3): 14-20.

Spies, T.A., Franklin, J.F., and Klopsch, M. 1990. Canopy gaps in Douglas-fir forests of the Cascade Mountains. Can. J. For. Res. **20**(5): 649-658.

Van Pelt, R., and Franklin, J.F. 1999. Response of understory trees to experimental gaps in old-growth Douglas-fir forests. Eco. Apps. **9**(2): 504-512.

Van Pelt, R., and Franklin, J.F. 2000. Influence of canopy structure on the understory environment in tall, old-growth, conifer forests. Can. J. For. Res. **30**(8): 1231-1245.

Veblen, T.T. 1985. Forest development in tree-fall gaps in the temperate rainforests of Chile. Natl. Geogr. Res. **1**(2): 162-183.

Wiegand, T., and Moloney, K.A. 2004. Rings, circles, and null-models for point pattern analysis in ecology. Oikos **104**(2): 209-229.

Western Regional Climate Center (WRCC). 2016. Period of record general climate summary: Juneau, AK [online]. Available from http://www.wrcc.dri.edu/cgi-bin/cliMAIN.pl?akjune. [accessed 12 December 2016].

Zenner, E.K. 2005. Development of tree size distributions in Douglas-fir forests under differing disturbance regimes. Eco. Apps. **15**(2): 701-714.

Zhu, J., Zhang, G., Wang, G.G., Yan, Q., Lu, D., Li, X. and Zheng, X. 2015. On the size of forest gaps: Can their lower and upper limits be objectively defined? Arg. Forest Meteorol. **213**: 64-76.

## Tables

**Table 1.** Stand structure and compositional attributes for old-growth Sitka spruce-western hemlock forest stands in southeast Alaska. Medium density represents forests with 40-60% canopy closure and full density is 70-100% canopy closure. Plus minus values are the standard error of the mean. Overstory trees are ≥ 25 m in height, mid-story is trees with heights of 10-25 m, and understory trees are all trees < 10 m tall.

| | All | | | | Overstory | | Mid-story | | Understory | |
|---|---|---|---|---|---|---|---|---|---|---|
| **Species** | **Density (TPH)** | **Basal area ($m^2$/ha)** | **DBH range (cm)** | **QMD (cm)** | **Density (TPH)** | **Basal area ($m^2$/ha)** | **Density (TPH)** | **Basal area ($m^2$/ha)** | **Density (TPH)** | **Basal area ($m^2$/ha)** |
| **Medium density** | | | | | | | | | | |
| PISI | 89 ± 37 | 18.38 ± 9.37 | 7.6 - 177.5 | 41.9 ± 4.4 | 34 ± 9 | 16.05 ± 3.76 | 51 ± 8 | 2.30 ± 0.44 | 4 ± 1 | 0.07 ± 0.02 |
| TSHE | 425 ± 95 | 46.01 ± 10.85 | 7.6 - 132.6 | 30.2 ± 2.7 | 70 ± 7 | 33.23 ± 4.00 | 220 ± 20 | 11.36 ± 0.98 | 135 ± 16 | 1.40 ± 0.16 |
| POTR | 6 ± 6 | 0.80 ± 0.80 | 15.2 - 44.5 | 6.7 ± 6.7 | 2 ± 0 | 0.42 ± 0.00 | 3 ± 0 | 0.37 ± 0.00 | 1 ± 0 | 0.02 ± 0.00 |
| ALRU | 6 ± 5 | 0.44 ± 0.37 | 8.4 - 43.2 | 28.0 ± 2.7 | 1 ± 0.4 | 0.08 ± 0.05 | 4 ± 2 | 0.33 ± 0.18 | 3 ± 2 | 0.04 ± 0.02 |
| *Total* | *518 ± 68* | *64.72 ± 4.28* | *7.6 - 177.5* | *34.44 ± 2.84* | *105 ± 2* | *49.40 ± 2.09* | *273 ± 17* | *13.87 ± 0.61* | *140 ± 16* | *1.45 ± 0.16* |
| **Full density** | | | | | | | | | | |
| PISI | 92 ± 12 | 37.70 ± 8.04 | 7.6 - 162.1 | 61.1 ± 8.6 | 67 ± 3 | 36.45 ± 3.77 | 24 ± 6 | 1.17 ± 0.28 | 2 ± 1 | 0.01 ± 0.004 |
| TSHE | 344 ± 78 | 55.60 ± 3.10 | 7.6 - 133.6 | 40.6 ± 3.6 | 111 ± 4 | 42.56 ± 0.74 | 171 ± 25 | 12.47 ± 1.99 | 62 ± 13 | 0.64 ± 0.13 |
| CUNO | 56 ± 56 | 4.82 ± 4.82 | 10.7 - 55.6 | 27.9 ± 0.0 | 0 ± 0 | 0.00 ± 0.00 | 50 ± 0 | 4.71 ± 0.00 | 6 ± 0 | 0.01 ± 0.00 |
| *Total* | *448 ± 88* | *94.33 ± 5.78* | *7.6 - 162.1* | *46.44 ± 5.76* | *178 ± 5* | *79 .08 ± 4.37* | *205 ± 31* | *14.58 ± 2.40* | *65 ± 13* | *0.67 ± 0.13* |
| **All plots** | | | | | | | | | | |
| PISI | 91 ± 20 | 28.0 ± 6.90 | 7.6 -177.5 | 51.5 ± 5.7 | 51 ± 3 | 26.25 ± 2.07 | 37 ± 4 | 1.73 ± 0.18 | 3 ± 0.3 | 0.04 ± 0.01 |
| TSHE | 385 ± 60 | 50.8 ± 5.90 | 7.6 - 133.6 | 35.4 ± 2.7 | 90 ± 4 | 37.90 ± 1.44 | 196 ± 11 | 11.91 ± 0.74 | 99 ± 8 | 1.02 ± 0.08 |
| CHNO | 56 ± 56 | 4.82 ± 4.82 | 10.7 - 55.6 | 27.9 ± 0.0 | 0 ± 0 | 0.00 ± 0.00 | 50 ± 0 | 4.71 ± 0.00 | 6 ± 0 | 0.01 ± 0.00 |
| POTR | 6 ± 6 | 0.80 ± 0.80 | 15.2 - 44.5 | 6.7 ± 6.7 | 2 ± 0 | 0.42 ± 0.00 | 3 ± 0 | 0.37 ± 0.00 | 1 ± 0 | 0.02 ± 0.00 |
| ALRU | 6 ± 5 | 0.44 ± 0.37 | 8.4 - 43.2 | 28.0 ± 2.7 | 1 ± 0.4 | 0.08 ± 0.05 | 4 ± 2 | 0.33 ± 0.18 | 3 ± 2 | 0.04 ± 0.02 |
| *Total* | *482 ± 54* | *79.53 ± 6.0* | *7.6 - 177.5* | *41.11 ± 3.15* | *141 ± 4* | *64.24 ± 2.25* | *239 ± 12* | *14.22 ± 0.83* | *103 ± 8* | *1.06 ± 0.08* |

*PISI = Sitka spruce (*Picea sitchensis*); TSHE = western hemlock (*Tsuga heterophylla*); CHNO = yellow cedar (*Cupressus nootkatensis*); POTR = black cottonwood (*Populus trichocarpa*); ALRU = red alder (*Alnus rubra*)

Note: The data do not include any records of *Tsuga mertensiana* which co-occurs with *Tsuga heterophylla* in many coastal forests in Southeast Alaska. Large individuals of these species can be difficult to differentiate. Thus, we acknowledge the potential for the TSHE category to include minor amounts of *Tsuga mertensiana*.

**Table 2.** Summary values for open areas for 10 Sitka-spruce western hemlock forests in southeast Alaska. Values in parentheses are percent of total plot area in functional canopy gaps per plot. Each plot is a total of 14,164 $m^2$.

| Plot | Total open area ($m^2$) | Area in shadow gap ($m^2$) | Area in geometric gap ($m^2$) |
|---|---|---|---|
| **Medium density** | | | |
| 104 | 4758 | 1399 (9.8) | 2985 (21.1) |
| 130 | 5150 | 441 (3.1) | 3521 (24.9) |
| 132 | 4868 | 944 (6.7) | 3433 (24.2) |
| 141 | 4838 | 531 (3.7) | 2993 (21.1) |
| 220 | 4603 | 957 (6.8) | 3206 (22.6) |
| **Full density** | | | |
| 32 | 2334 | 206 (1.5) | 387 (2.7) |
| 76 | 3384 | 334 (2.4) | 1760 (12.4) |
| 111 | 2804 | 354 (2.5) | 808 (5.7) |
| 143 | 2499 | 0 (0.0) | 406 (2.9) |
| 161 | 3318 | 0 (0.0) | 901 (6.4) |

**Table 3.** Summary statistics for within-stand spatial patterns of widely spaced individual trees (*i.e.* patch size = 1) and patches of trees. A fixed inter-tree distance of 8.88 m was used for overstory trees. BA is basal area in meters squared and SEM is standard error of the mean presented in parentheses.

| **Overstory** | | | | | | |
|---|---|---|---|---|---|---|
| | *Patch size (number of trees)* | | | | | |
| ***Value (SEM)*** | **1** | **2-4** | **5-7** | **8-10** | **11-15** | **16+** |
| Medium density | | | | | | |
| *# Patches ha$^{-1}$* | 10 (2) | 9 (2) | 3 (0) | 2 (0) | 1 (0) | 1 (0) |
| *% Total density* | 9.6 (2.1) | 21.3 (5.7) | 16.4 (1.6) | 14.2 (3.5) | 13.3 (3.3) | 18.2 (3.3) |
| *%Total BA* | 10.5 (2.4) | 24.1 (5.5) | 16.7 (2.0) | 11.5 (3.7) | 15.3 (2.6) | 21.1 (5.7) |
| Full density | | | | | | |
| *# Patches ha$^{-1}$* ± SEM | 4 (1) | 4 (0) | 1(0) | 0 (0) | 0 (0) | 2 (0) |
| *% Total density* | 2.1 (0.5) | 6.1 (1.2) | 4.5 (1.5) | 0.9 (0.9) | 1.9 (1.9) | 84.6 (3.1) |
| *%Total BA* | 2.0 (0.6) | 6.7 (0.9) | 4.8 (1.5) | 0.9 (0.9) | 1.9 (1.9) | 83.2 (3.0) |

## Figures

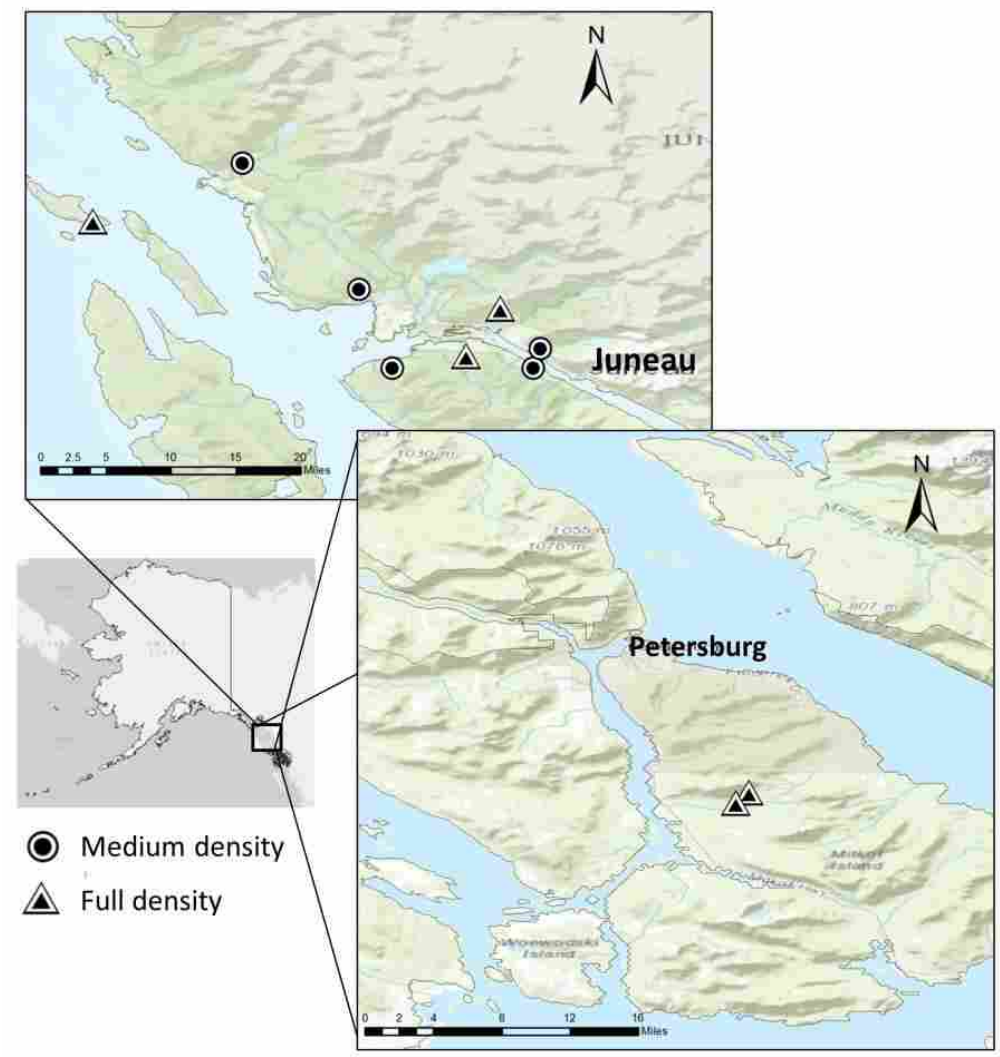


**Figure 1.** Plots were located in the Tongass National Forest in southeast Alaska. Eight plots were located immediately around Juneau and two near Petersburg, Alaska. Plot locations indicated with a circle represent medium density plots and triangles are full density plots.

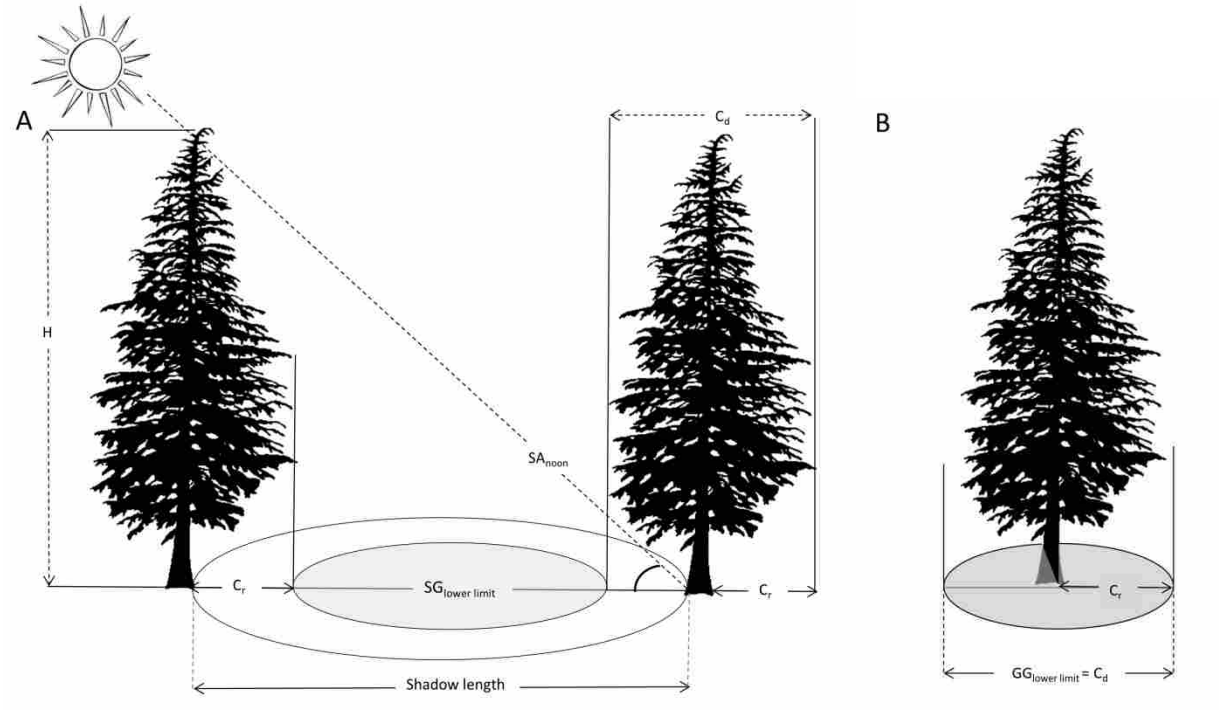


**Figure 2.** Sketch of lower limit of functional gap size. (A) Shadow gap method. $SA_{noon}$ is the solar angel ($^o$) at noon local time; $C_r$ is the length of the crown radius (m); $C_d$ is the length of the crown width (m) which is equal to 2 x $C_r$; H is overstory tree height (25 m); shadow length is the full shadow of a surrounding overstory tree at noon; $SG_{lower\ limit}$ is the lower limit of a shadow gap (m), is equal to shadow length – $C_d$. (adapted from Zhu et al. 2015) (B) Geometric gap method. $GG_{lower\ limit}$ is the lower limit of a geometric gap (m), is equal to $C_d$. Assumptions: (1) slope of the gap location is $0^o$ on flat land; (2) H, of surrounding trees is the same. Hemlock silhouette provided by Natural Resources Canada, https://tidcf.nrcan.gc.ca/en/trees/factsheet/119.

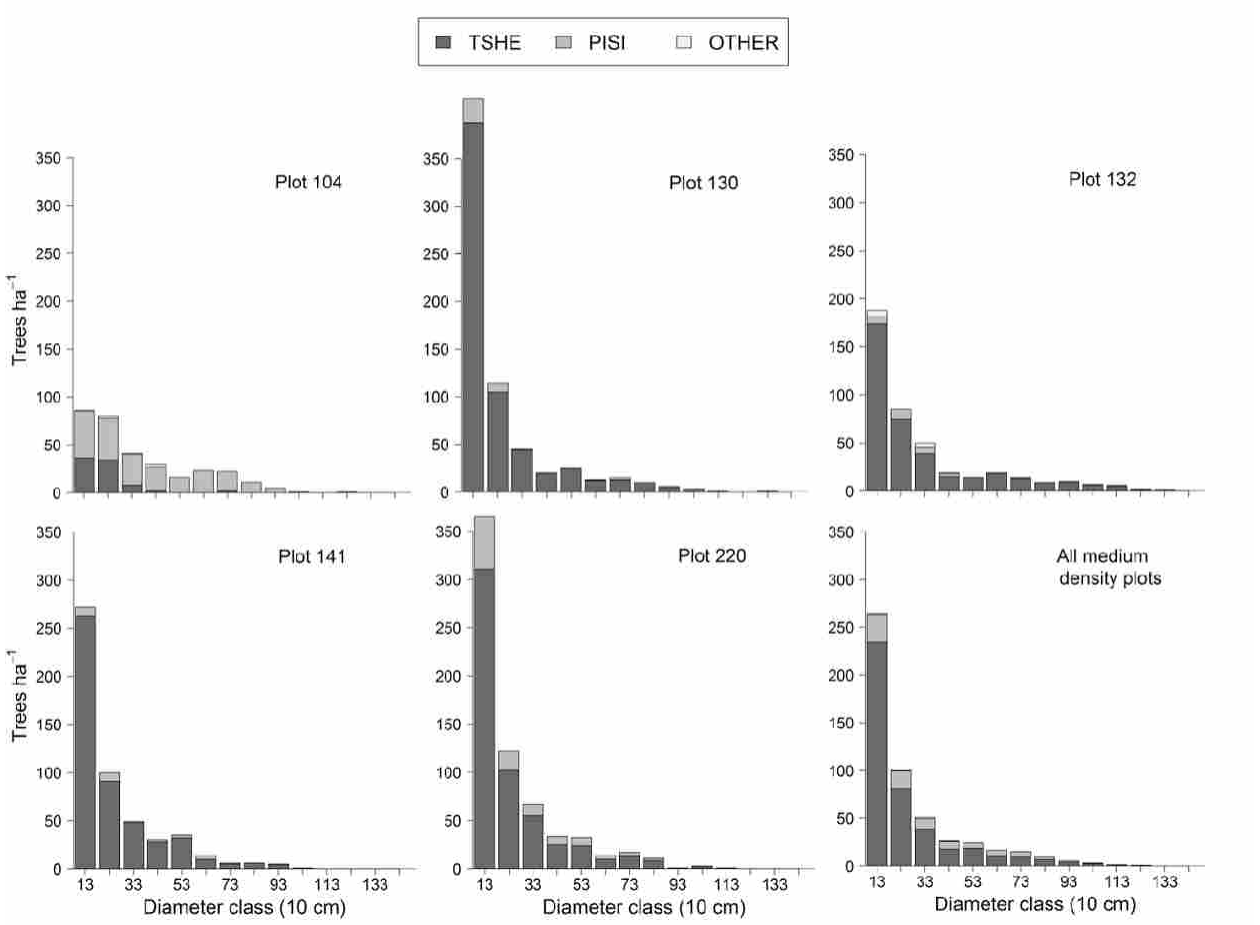


**Figure 3.** Diameter distribution in 10 cm diameter classes for five medium density (40-60% crown closure) plots and pooled values for old-growth Sitka spruce-western hemlock in southeast Alaska. Labels are located at the center point of the 10 cm diameter classes. TSHE: western hemlock, PISI: Sitka spruce, OTHER: includes red alder, black cottonwood, and yellow cedar.

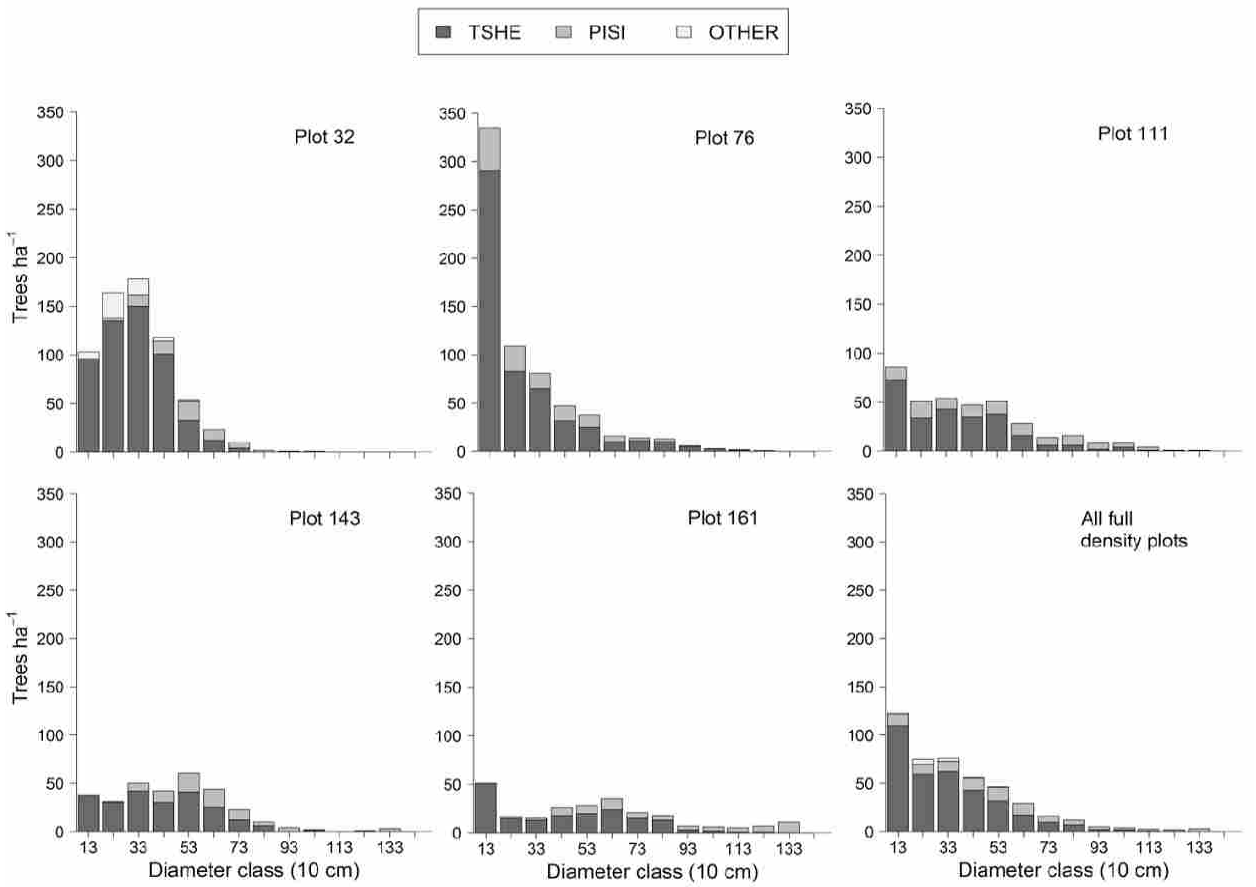


**Figure 4**. Diameter distribution in 10 cm diameter classes for five full density (70-100% crown closure) plots and pooled values for old-growth Sitka spruce-western hemlock in southeast Alaska. Labels are located at the center point of the 10 cm diameter classes. TSHE: western hemlock, PISI: Sitka spruce, OTHER: includes red alder, black cottonwood, and yellow cedar.

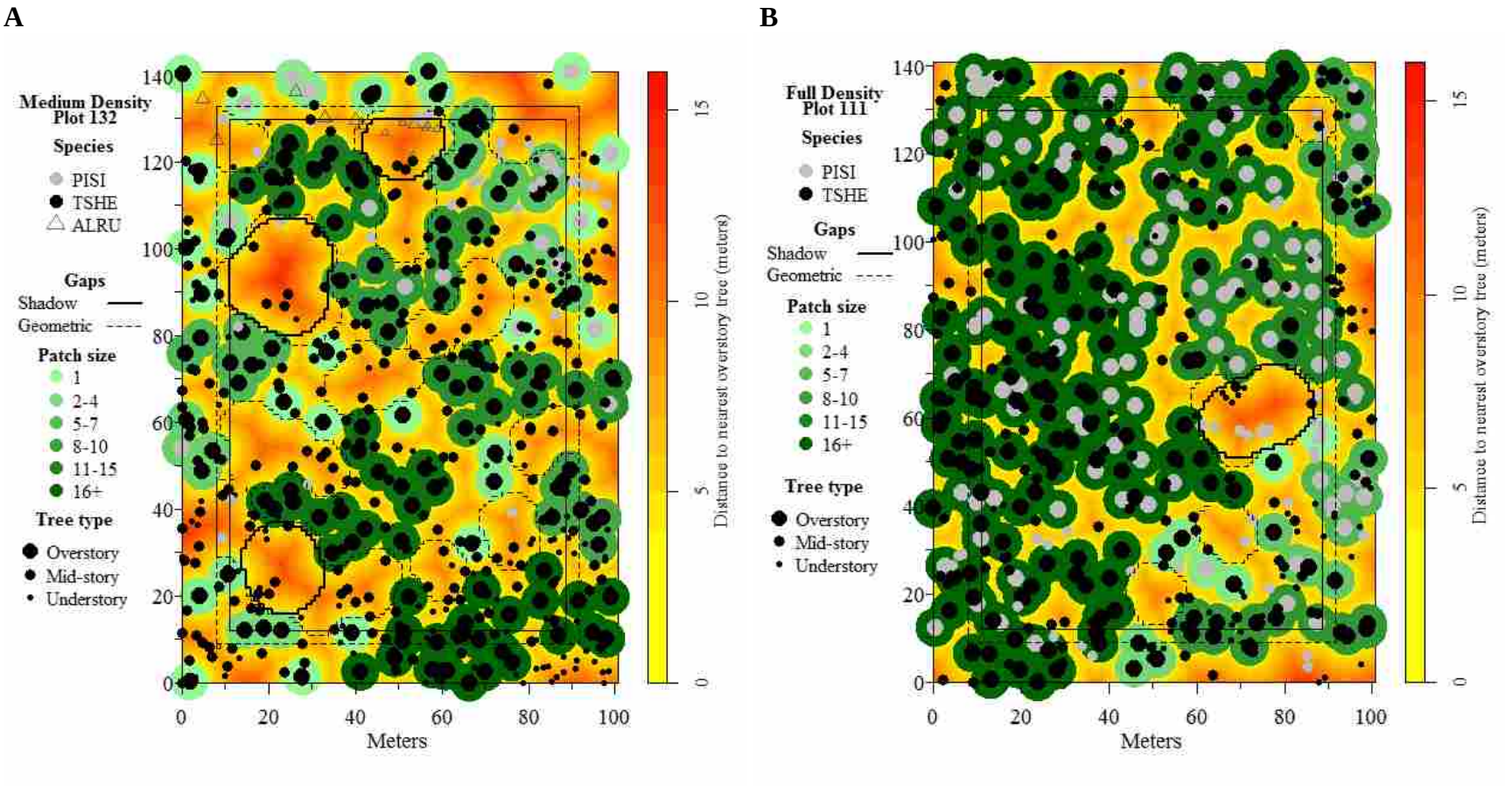


**Figure 5.** Example stem maps for old-growth Sitka spruce – western hemlock forests in southeast Alaska. Tree boles are colored by species and point size represents overstory, mid-story, and understory canopy position. A 4.44 m radius was used to project tree crowns on overstory trees to show patches calculated using a fixed inter-tree distance of 8.88 m. Patch size is on a color gradient following the number of trees in a patch. Gaps and associated buffer distances are shown with a solid or dashed line. Background coloration is a graphical display of open area where colors indicate the distance to the nearest overstory trees in meters. Panel A is a medium density plot. Panel B is a full density plot.

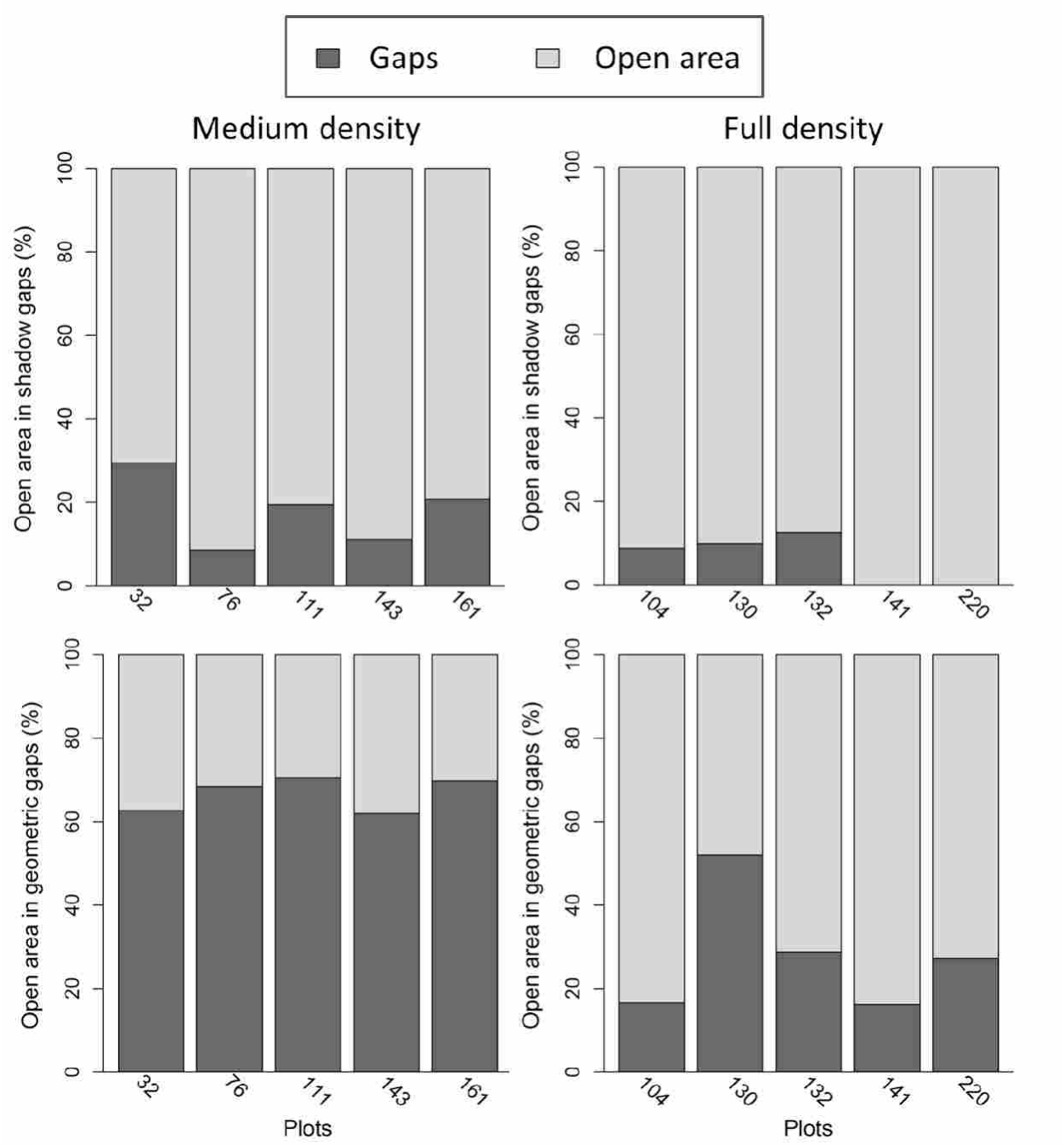


**Figure 6.** Percentage of total open area, defined as area devoid of overstory foliage, considered a functional gap delineated by the shadow or geometric gap definitions, and pooled by density class.

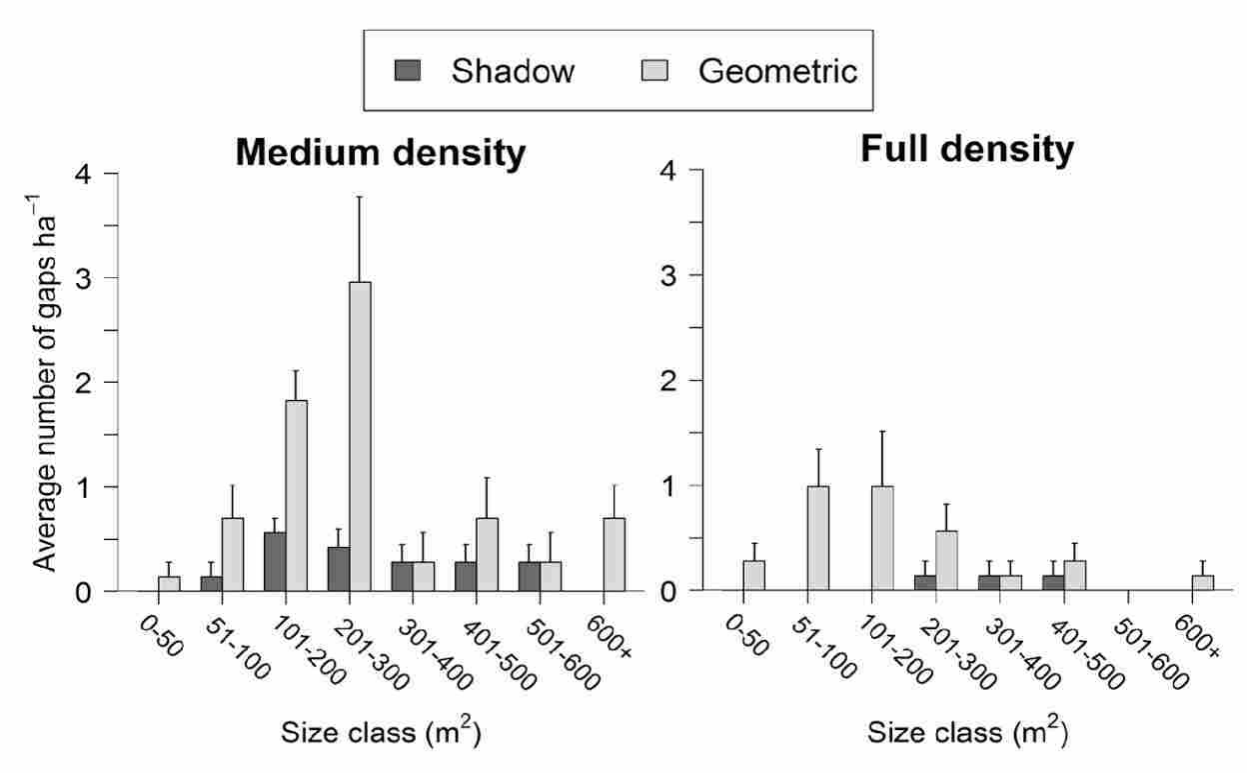


**Figure 7.** Gap size distribution pooled by density class for shadow and geometric gaps. Size class is presented in 50-100 $m^2$ bins. Minimum functional gap size is 42.3 $m^2$ and 15.5 $m^2$ for shadow and geometric gaps respectively.

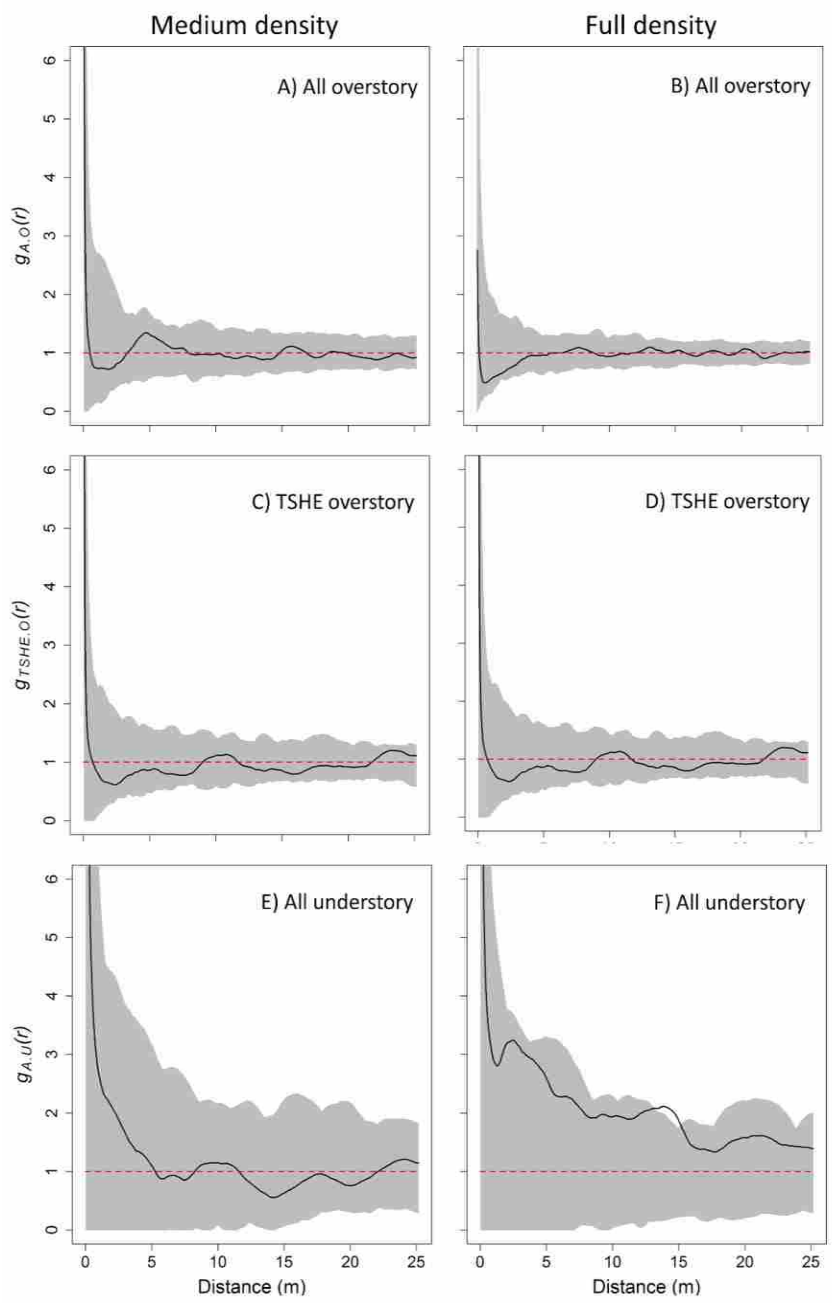


**Figure 8.** Spatial pattern of overstory and understory trees pooled for each density class using a replicated pair correlation function. Analysis was conducted on all overstory trees (≥ 25 m tall; panels A & B), overstory western hemlock (TSHE: panels C & D), and all understory trees (< 10 m tall; panels E & F). The dataset used for panel C was reduced to four plots since one plot had an insufficient sample of overstory hemlock to conduct the analysis. The black line is the empirically observed pattern and the shaded regions represent a simulated 95% confidence envelope. Observed values above (below) the envelope indicates aggregation (uniformity) and within indicate randomness.

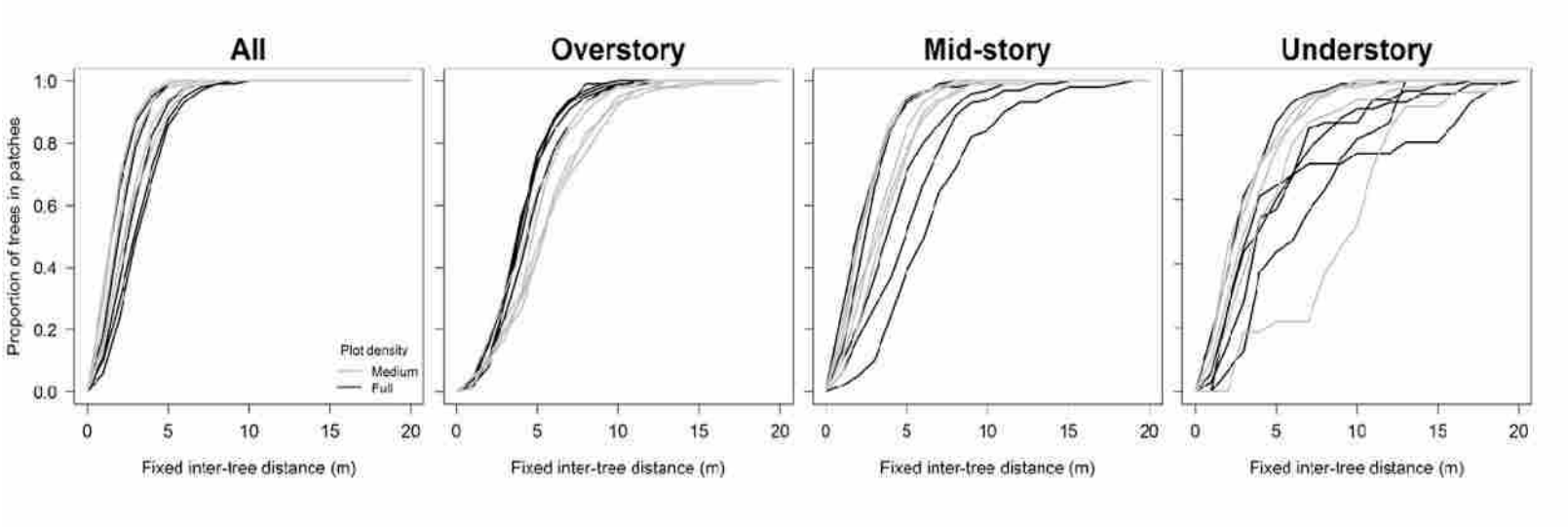


**Figure 9.** Proportional patch size distribution for ten Sitka spruce western hemlock plots. A patch is considered any grouping of two or more trees within a fixed distance of each other. Each line represents one plot. Overstory trees are defined as any tree greater than or equal to 25 m in height, mid-story trees are 10-25 m tall, and understory trees are less than 10 m tall. Plots in full density areas are indicated in black and medium density plots in gray.

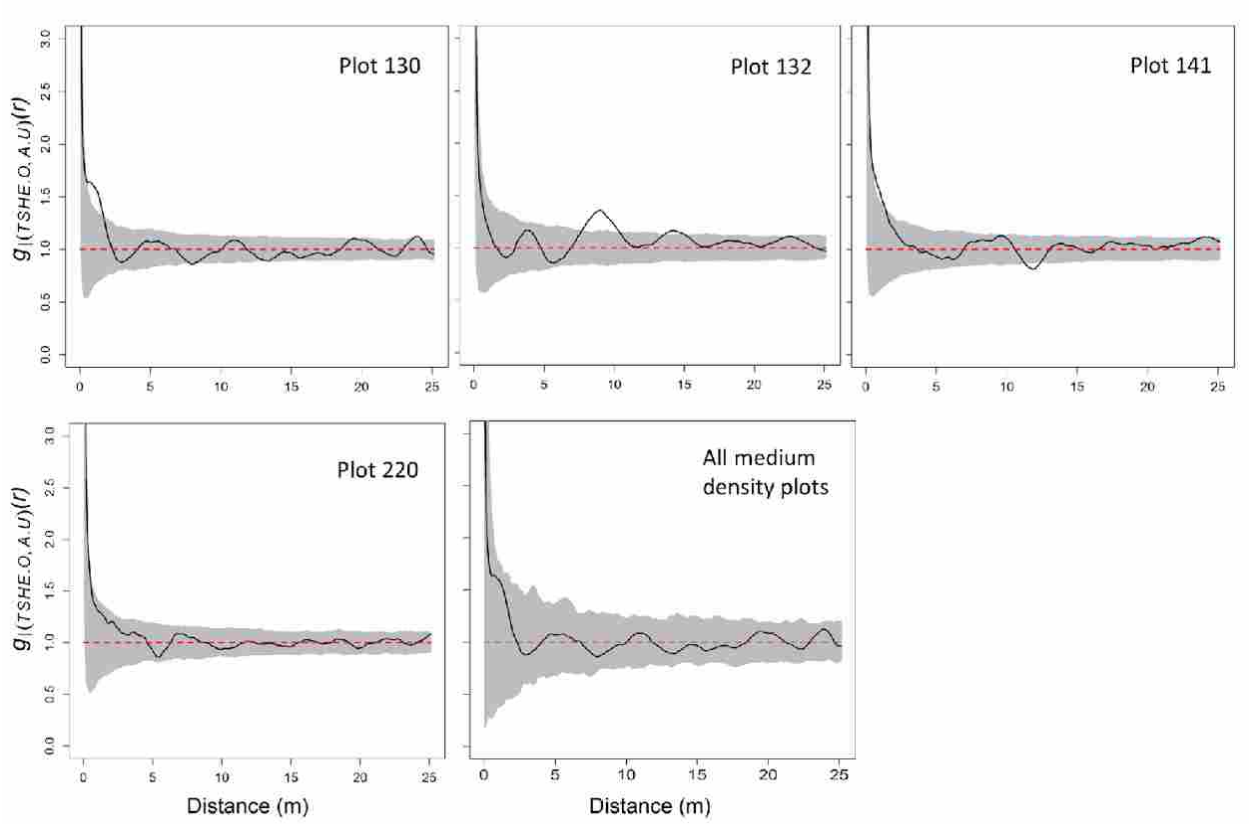


**Figure 10.** Spatial relationships between understory trees (< 25 m tall) and overstory trees (≥ 25 m tall) for the medium density class and pooled value using a replicated bivariate pair correlation function. The analysis was reduced to four plots since plot 104 did not have enough overstory hemlock to conduct the analysis. The black line is the observed pattern and the shaded regions are a simulated 95% confidence envelope. Observed values above (below) the envelope indicates attraction (repulsion) and within indicate independence.

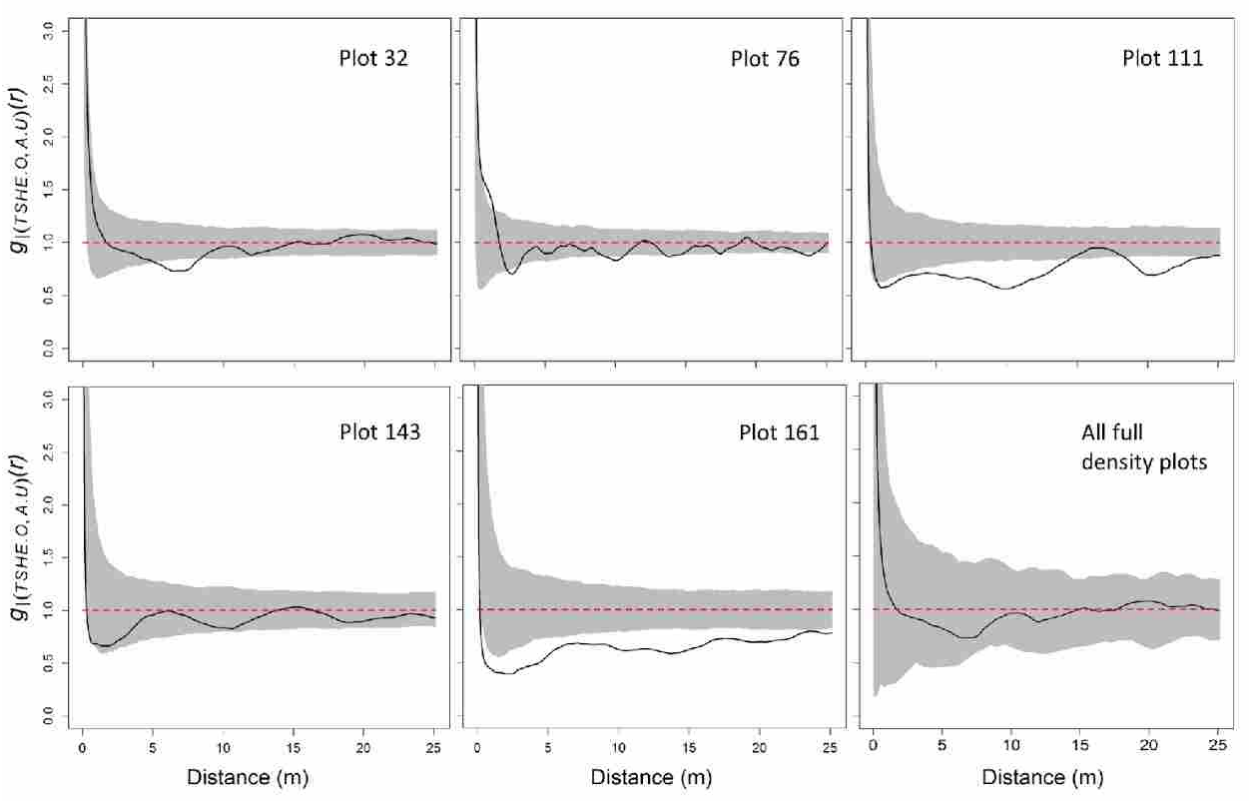


**Figure 11.** Spatial relationships between understory trees (≤ 10 m tall) and overstory trees (≥ 25 m tall) for the full density class and pooled value using a replicated bivariate pair correlation function. The black line is the observed pattern and the shaded regions are a simulated 95% confidence envelope. Observed values above (below) the envelope indicates attraction (repulsion) and within indicate independence.

# CHAPTER 2. Tree spatial patterns modulate peak snow accumulation and snow disappearance


## Abstract

Forests and snow covered regions frequently co-occur across the northern hemisphere. In these environments, forests are structurally and spatially complex mosaics of tree neighborhoods that are intrinsically linked to ecosystem functions. Tree and canopy structures influence snow accumulation and disappearance processes through interception and radiation attenuation. However, it is unclear if spatial heterogeneity within the forest canopy induces heterogeneity in snow accumulation and persistence. We quantitatively identified different tree neighborhoods and tested the differential effects of these within-stand neighborhoods on snow processes. Neighborhood types included individual ponderosa pine (*Pinus ponderosa*), Douglas-fir (*Pseudotsuga menziesii*) and western larch (*Larix occidentalis*) trees, dense overstory tree clumps, openings, and regeneration patches. Intensive measurements of snow accumulation (density and depth) and persistence (disappearance date) were made within replicate neighborhoods for three years. Overall, neighborhood type and year had a significant effect on accumulation and snow disappearance. Openings were significantly different from clumps and individuals, always accumulating more snow. Openings retained snow significantly later than clumps but were not significantly different from individuals. Within the individual tree neighborhood type, a nested species effect indicated no differences in accumulation but significant differences in disappearance between deciduous and evergreen conifers, with snow persisting longer beneath deciduous western larch. Our results suggest that canopy interception is the primary mechanism driving the accumulation phase, while snow disappearance patterns are largely a consequence of spatial variation of longwave radiation. Reducing canopy interception and longwave radiation by increasing the abundance of widely spaced single trees and small openings with silvicultural treatments should increase snow depth and duration, and thus snow water storage. Maintaining a heterogeneous canopy structure that includes tree clumps can be used to meet multiple objectives such as provision of ungulate winter range habitat, and heterogenous understory plant phenology.


## Introduction

Forest vegetation significantly interacts with the processes of snow accumulation and disappearance. Forests and snow-covered regions co-occur over ~25% of the northern hemisphere (Musselman et al. 2012, Dickerson-Lange et al. 2015). Many co-locations occur in mountain watersheds where forest-snow interactions govern local ecology and hydrology (Musselman et al. 2012). In semi-arid regions, such as the western U.S., the annual snowpack in forested watersheds is the primary source of fresh water (Bales et al. 2006). Snow depth and duration influences important ecological functions such as primary productivity (Winkler et al.

2016), wildlife habitat (Mysterud et al. 1999), understory plant phenology (Walker et al. 1993), and microbial activity (Brooks et al. 1996).

Most forests are structurally and spatially complex. Complexity, also referred to as heterogeneity, is characterized by the kind, number, size, and spatial arrangement of structures present at various scales (Franklin et al. 2002). Structural complexity and spatial heterogeneity within forest stands emerge as ordered and random processes occur throughout stand development influence tree establishment, growth, and mortality patterns (Messier et al. 2013). Disturbance type, frequency and intensity also contribute significantly to forest complexity. For example, in western North American dry pine and mixed-conifer forests, complexity is manifest as a mosaic of large openings, widely spaced individual trees, clusters of mature trees, groups of regeneration (Larson and Churchill 2012, Tuten et al. 2015). High understory biodiversity consisting of legacy material and late successional trees such as white pine (*Pinus strobus*) and eastern hemlock (*Tsuga canadensis*) characterize complexity in the Great Lakes region (Webster et al. 2018). Similarly, northern European forests consist of fine-scale patches within continuous multi-aged cover consisting of large early and late successional specialist species and an abundance of dead wood (Brūmelis et al. 2001). Nearly all mature and old-growth temperate forests exhibit structural complexity and spatial heterogeneity, regardless of whether they experience chronic disturbance like gap dynamics in northern Europe and the Great Lakes region, or frequent events like fire and bark beetles in dry pine and mixed conifer forests (Franklin et al. 2002). Forest structural complexity is intrinsically linked to forest ecosystem function, and contributes to resiliency and adaptability (Boyden et al. 2012, Puettmann et al. 2008).

Management for forest structural complexity and within-stand spatial heterogeneity is a common theme in multiple objective forest management systems (Fahey et al. 2018). Technological advances have allowed for greater quantification of complexity, such as tree spatial pattern arrangements or functional trait diversity, and such information is increasingly incorporated into silvicultural prescriptions (Maher et al. 2019). Silvicultural prescriptions that balance multiple objectives using complexity-based approaches are currently being used across a wide range of forest types including variable density thinning, ecological restoration, and complex adaptive systems (North et al. 2009, Tuten et al. 2015, Knapp et al. 2017, Addington et al. 2018, Churchill et al. 2017, Reynolds et al. 2013, Kuuluvainen 2009).

Forest canopy structure influences ecologically and hydrologically significant snowpack attributes, including snow water equivalent (SWE), snow depth, and snow cover duration and extent. SWE is the amount of liquid water held in a given volume of snow and is directly used to forecast the quantity and timing of water availability (Strum et al. 2010). Snow depth is important for winter wildlife habitat (Pauley et al. 1993, Wallmo et al. 1977), efficacy of ground insulation (Zhang 2005), and is a strong driver of species phenology and distributions (Walker et al. 1993). Duration of snow cover is correlated with green-up (Grippa et al. 2005, Ide and Oguma 2013) and is summarized by the snow disappearance date (SDD) or its derivative, fractional snow-covered area (fSCA)—the percent of sample points or area covered by snow.

Tree and canopy structures influence snow accumulation and ablation through interception and radiation attenuation (Jost et al. 2007, Varhola et al. 2010). Interception is thought to be a primary mechanism driving accumulation patterns and can account for up to 60% of incoming precipitation in conifers (Dickerson-Lange et al. 2017, Martin et al. 2013). Intercepted snow can subsequently be returned to the atmosphere via sublimation or removed

from the canopy by mass release or meltwater drip (Storck et al. 2002). Ablation is thought to be controlled by the energy balance where trees can act as longwave radiating bodies increasing subcanopy melt rates, or can shade the snow from incoming shortwave radiation thereby retarding melt (Lawler and Link 2011). Trees also modify local wind patterns and snow redistribution with consequences for below canopy patterns of snow accumulation and persistence (Faria et. al 2000, Jost et al. 2007).

Species composition accounts for differing canopy architectures that include branch size (Brown 1978), strength and pattern, and overall canopy roughness and area (Miller 1964). Differing dominant evergreen conifer species have explained nearly 75% of the variation in peak SWE (Moore and McCaughey 1997, Faria et al. 2000). Among conifers, the greatest functional difference is between deciduousness and evergreen leaf habits, however the effect of this trait on snow processes has received little attention.

This begs the questions, does a heterogeneous forest canopy structure and composition translate to variability in underlying snow characteristics at corresponding spatial scales?

Most research on forest-snow interactions has been done using a stand-average approach. Past studies have compared forested and unforested environments, and also investigated varying shapes and sizes of treeless openings (Kitteridge 1953, Troendle and Leaf 1980, Berndt 1965). Others have examined varying stem densities, total canopy cover or sky view fraction (Gary and Troendle 1982, Hubbart et al. 2015, Dickerson-Lange et al. 2017). As the extent and intensity of forest disturbances have increased, greater attention has been given to the effects forest structural changes due to fire and bark beetle have on snow (Harpold et al. 2014, Boon 2012, Stevens 2017). However, these coarse scale approaches ignore the inherent complexity present in most forests.

Fewer studies have explicitly considered within-stand forest structural complexity or spatial heterogeneity, and the consequences thereof for below-canopy snow dynamics. While still working with stand-average metrics, Woods et al. (2006) and Pickard (2015) compared different tree spatial patterns. Woods et al. (2006) observed significantly more snow in uniform stands than in group retention and control treatments; however variation in snow depth was greater in their group retention treatment. Pickard (2015) found no significant treatment effect of experimentally manipulated tree patterns on snow accumulation (during a very low snow year). Winkler and Moore (2006) did not find a significant effect of within-stand forest structural complexity on snow characteristics; this result was attributed to a mismatch in the spatial scales of structural variation and sampling density. There is a clear need for new studies designed to directly test the effects of forest complexity on below canopy snow attributes.

Our objective was to determine if spatial heterogeneity within the forest canopy induces heterogeneity in snow accumulation and persistence. We quantified tree spatial patterns in an intensively mapped and measured mixed-conifer forest. Within the heterogeneous canopy we identified different tree neighborhoods—individual trees, dense tree clumps, and openings—and hypothesized that snow accumulation and persistence would vary across these neighborhoods due to their differential effects on interception and radiation. Specifically, we used linear contrasts to test the predictions that peak snow accumulation and snow persistence differ between:

5. Openings and clumps;
6. Openings and individuals;
7. Deciduous conifer and evergreen conifer individuals; and
8. Evergreen individuals of different species.

The purpose of this research was to improve our basic understanding of the functional consequences of within-stand structural and spatial heterogeneity for underlying snow processes. Such results can support management approaches that mediate forest structural complexity and tree spatial patterns, and seek to balance multiple management objectives.

## Methods

*Study site*

This study was conducted at Lubrecht Experimental Forest in western Montana, USA (113º27'W, 46º55'N) in the Blackfoot River basin. The study site supports a mature, mixed-conifer forest dominated by Douglas-fir (*Pseudotsuga menziesii;* PSME) and ponderosa pine (*Pinus ponderosa*; PIPO) interspersed with the deciduous conifer, western larch (*Larix occidentalis;* LAOC); and include components of all stages of stand development (Franklin et al. 2002). Located at 1,220 meters a.s.l, with generally flat topography, the site received an annual average of 12.2 cm of snow water equivalent (SWE) from 2014-2017, with snow present from November to March. Average winter temperatures range from -8º C to 2º C (average = -4º C). Winter winds ranged from 0.4 – 1.8 m/s on site in 2016. Existing forest structure and composition reflect recent and historical management regimes defined by early 20$^{th}$ century large tree selection and recent fire exclusion, intermittent grazing, and a thinning in 1984 to a target basal area of 16 m$^2$/ha (Fiedler et al. 2012, Maher et al. 2019). Three adjacent 4.48 ha plots were established within the site to facilitate stem mapping and avoid a centrally bisecting road (Fig. 1, Schneider et al. 2015).

*Forest structure*

To assess structural and spatial heterogeneity all live and dead trees greater than 10.0 cm at breast height were measured and mapped. Each tree was marked with a uniquely numbered tag

and its diameter at breast height (DBH), species, total height, and X-Y coordinates were measured and recorded. A survey grade Leica total station was used to map each structure from a closed traverse loop that allowed us to quantify and correct for mapping error (linear misclosure $\leq 0.49$ m).

*Spatial patterns*

Tree neighborhoods were identified and quantified using a cluster identification algorithm and a canopy opening detection algorithm. Within stand spatial pattern components, henceforth known as neighborhoods, included openings, clumps of overstory trees ("clumps"), individuals, and patches of regeneration ("regen") (Larson and Churchill 2012, Churchill et al. 2018). Openings are defined as areas with no overstory canopy foliage, clumps include trees that are located less than a fixed inter-tree distance from any neighbor or clump member, individuals have no near neighbors, and regeneration patches are clusters of seedlings and saplings (trees less than 10 cm DBH).

A clustering algorithm was used to quantify clumps and individuals. The algorithm evaluates each tree in a point pattern as a member of a clump or as an individual based on a fixed inter-tree distance that extends from tree center to tree center (Plotkin et al. 2002; Larson and Churchill 2008). Clumps consist of at least two trees where membership requires an inter-tree distance less than the fixed distance from at least one existing clump member. The fixed inter-tree distance is related to the average distance between mature trees with interlocking crowns. Consistent with regional values, a fixed inter-tree distance of 6 m was used (Larson and Churchill 2012, Clyatt et al. 2016). Tree crown radii can also be used to establish clump membership, however a fixed distance is more readily translated into management guidelines (Sanchez Meador et al. 2011, Churchill et al. 2017, Maher et al. 2019).

A canopy opening detection algorithm designed for point pattern data was used to identify and calculate the number and size of openings with no overstory canopy foliage within the forest matrix. A minimum opening threshold radius of 9 m was used and corresponds to a minimum area that is functionally distinct from the surrounding forest (Churchill et al. 2017). The algorithm lays a fixed grid over a point pattern (i.e., tree stem map) and calculates the distance from each grid point to the nearest tree bole. A polygon is drawn around all areas exceeding the 9 m minimum threshold. A 3 m tree crown buffer was then applied to each polygon so calculated openings extended from canopy edge to canopy edge. To ensure only the area of complete openings were calculated a 9 m edge buffer was also applied to the plot boundary.

Neighborhoods used for snow sampling (e.g. individuals, clumps, openings) were delineated using the procedures above and selected using a stratified random sampling design (Table S1). Individual trees sampled had a minimum of 7 m to their nearest neighbor to reduce canopy effects from surrounding trees and included the three species present. Six replicates of clumps and openings, and six replicates of each of the three species for individuals were selected for sampling.

Following 2014 field observations of potentially important effects of small trees <10.0 cm DBH on snow characteristics, six regeneration neighborhoods were subjectively located across the site. These regeneration patches contained only tree seedlings and saplings <10.0 cm DBH. To characterize the structure of this neighborhood type, seedlings and saplings were identified to species and censused into size classes using 8.5 m radius plots centered on the snow sampling plot described below. To verify their frequency and structural uniqueness within the site, $n$ = 15, 8.5 m fixed radius plots were randomly located throughout the study area in which

seedlings and saplings were inventoried by species and size class. Because trees <10 cm DBH were not mapped and sampling locations were not randomized, regeneration patches were not included in statistical analyses.

*Snow measurements*

Snowpack characteristics were collected at peak accumulation and through the melt season from 2015-2017 in all neighborhoods, except for peak values in one clump replicate in 2015 and one larch replicate in 2017. Peak snow was sampled February 22, 12, and 23 in 2015, 2016, and 2017 respectively, dates consistent with the local long-term average (Fig. S1). Peak snow depth in clumps, openings and regeneration patches was sampled at 1 m intervals along two 14 m perpendicular transects with a central intersection point using a Standard Federal snow tube (Rickly Hydrological Company, Columbus, OH, USA). Samples were collected at 1 m intervals including the origin for $n$ = 29 measurements per neighborhood. Individuals were sampled every meter along four 7 m transects extending from the tree bole and separated by 90$^{o}$ for $n$ = 32 measurements per individual tree neighborhood. Sampling neighborhoods were marked with 1.5 m tall pieces of wooden lath installed at the end of each transect for easy identification and sampling replication. Wooden lath was chosen as it is a natural, affordable, and minimally conductive material to install as semi-permanent markers. Snow mass values were collected with an electronic scale at every other meter along each transect and used to calculate snow density. SWE was calculated for each point using depth and density values. A total of $n$ = 1,098 points were sampled over 13.44 ha of fully mapped and censused forest. While sampling extreme care was taken to avoid the impacts of altering snow conditions when working on plot.

Following peak accumulation, each sample point across neighborhoods was revisited roughly every three days until no snow remained. A snow disappearance date was assigned to

each sampling point when it was no longer snow covered. Fractional snow-covered area (fSCA) was calculated as the percentage of sample points per neighborhood that remained snow covered during each sampling day and was used to construct melt curves for each neighborhood (Fig. 2; Raleigh et al. 2013, Dickerson-Lange et al. 2015). We reduced individual melt curves to two univariate metrics summarizing snow persistence. We estimated $fSCA_{50}$, the number of days following peak accumulation when 50% of the snow remained in each neighborhood, to provide a common reference point in terms of snow duration which encompasses both accumulation and ablation processes. $fSCA_{50}$ values were estimated by linearly interpolating fSCA between the sample days preceding and following the 50% cover value in each neighborhood. Next we calculated the area under each fSCA melt curve as snow coverage days ($AUC_{fSCA}$). This value describes the form of the melt curve where neighborhoods with quickly melting snow will have a more concave form, while longer lasting snow will have a more convex form.

*Statistical analysis*

Linear mixed effects models with random nested effects and unequal variance were used to test our hypothesis and estimate contrasts. Models were fit using the nlme library and the lme function in R v.3.3.3 (Pinheiro and Bates 2000, R Core Team, 2017). All response variable values were averaged to the replicate level (6 replicates per neighborhood), to obviate the need to account for autocorrelation among snow sampling locations within transects.

A global neighborhood effect was modeled using neighborhood type, year, and an interaction term between neighborhood type and year as fixed effects and neighborhood replicate as a random effect. The random replicate effect was used to acknowledge the repeated measures aspect of the sampling design. In addition, the model allowed for differential variances among replicates across neighborhood types. Neighborhood differences were tested using a set of

contrasts: (1) openings vs. clumps, (2) openings vs. individuals, (3) larch vs. evergreen individuals and (4) ponderosa pine vs. Douglas-fir individuals. The differential effect between neighborhoods was tested using contrasts 1 and 2 where openings were used as the reference point. Nested within the individual tree neighborhood type is a potential species levels effect. We tested for this effect using contrasts 3 and 4. Neighborhood differences and species effects were estimated with the contrast of interest, year, and the interaction between year and contrast. The interaction between contrast and year evaluated the consistency in sign and magnitude of the contrast over years.

The statistical significance of fixed effect terms on snow characteristics was evaluated using F-statistics at the 0.05 level.

## Results

*Forest structure, composition, and spatial patterns*

Structural and spatial heterogeneity define the study site (Fig. 3). Douglas-fir currently dominates the site, accounting for over half the stem density, followed by ponderosa pine at 37% (Table 1, Fig. S2). However, the average ponderosa pine is larger accounting for slightly more basal area across the site (Table 1). Although intermittent and accounting for only 8% of site basal area, the deciduous western larch has an average diameter similar to Douglas-fir.

Neighborhood composition reflected these trends. Regeneration is dominated by Douglas-fir, with most occurring in the 1-5 cm size class (Table 2). Though present throughout the site, the density of seedlings and saplings is 1-2 orders of magnitude larger in sampled regeneration patches than in the forest matrix. Without being analytically identified from stem maps, these results highlight the unique structural attributes of this neighborhood type and verify it as a distinct and potentially important component of forest complexity.

Local spatial analysis identified the presence of individual trees, clumps of various sizes (Table 3), and canopy openings (Table 4). Individuals and small clumps (2-4 trees) occurred most frequently across the site, whereas the largest clumps are long and sinuous accounting for more than half of the total plot density and basal area (Fig. 3). Openings were the rarest spatial pattern component and tended to be small, 100-400 $m^2$ (mean = 300 $m^2$). The largest openings were 772 $m^2$, 523 $m^2$, and 930 $m^2$ in each plot respectively and account for 21% of the total open area at the site.

*Snow accumulation*

Neighborhood type had a significant effect on all snow accumulation and melt characteristics, often significantly interacting with year (Table 5). Openings always accumulated significantly more SWE than clumps or individuals over all sampling years (Fig. 4). Depth followed the same trends as SWE (Fig. 4). On average, openings collected 3.3 cm more SWE and snow was 17.7 cm deeper than clumps, with significantly larger differences observed in the larger snow year of 2017. While smaller, the +1.8 cm SWE and +10.8 cm snow depth differences in openings relative to individuals were significant. Interaction terms with both contrasts and year were significant, but the same pattern held over all sample years. The significant interaction between opening and clumps with year is attributable to the large differences seen in 2017 relative to 2015, while the interaction between year and opening vs. individual is likely sensitive both the heavy snow in 2017 and the unequal variances among neighborhood types.

No statistically significant differences in peak snow accumulation were observed between species. SWE was greatest and snow was deepest under western larch followed by ponderosa pine and Douglas-fir (Fig. 4). Larch on average had 0.8 cm more SWE and was 4.1 cm deeper

than the evergreen species, while ponderosa pine accumulated 0.4 cm more SWE and 2.6 cm more snow than Douglas-fir. A significant interaction between larch and evergreens with year for snow depth was observed, but patterns remained consistent over the years (Table 5, Fig. 4). The fixed effect of year for peak SWE and snow depth was always significant ($p > 0.001$).

On average, regeneration patches accumulated snow with depths and SWE between the canopied and non-canopied neighborhood types (Fig. 4).

*Snow disappearance*

The melt season lasted for 31, 44, and 56 days in 2015, 2016, and2017, respectively. Fractional snow-covered area was plotted for each neighborhood to create melt curves used to determine $fSCA_{50}$ and $AUC_{fSCA}$ (Fig. 2, Fig. S4). Openings differed significantly from clumps in terms of snow persistence, taking on average 9.7 days longer to reach 50% disappearance, which was reflected in significantly more area under the melt curve (Table 5, Fig. 5). No significant difference was seen between openings and individuals, however the interaction between this contrast and year was significant for $fSCA_{50}$ owing to changes in magnitude but not pattern.

The duration of snow and snow disappearance patterns for western larch were significantly different from the two evergreen species (Table 5, Fig. 5, Fig. S4). The interaction between larch and evergreens with year for $AUC_{fSCA}$ was also significant, but again patterns remained consistent through time. Little difference in snow melt characteristics were seen between the evergreen species. The fixed effect of year was always significant ($p > 0.001$) for $fSCA_{50}$ and $AUC_{fSCA}$.

Regeneration patches had $fSCA_{50}$ and $AUC_{fSCA}$ values more often aligned with non-canopied neighborhoods (i.e. openings and western larch) in 2016 and 2017, but were similar to similar to evergreen individuals in 2015.

## Discussion

Heterogeneity in the forest canopy directly affects the variability in peak accumulation and persistence of underlying snow. Our study directly links tree spatial patterns with snow processes by addressing a wide range of within-forest spatial complexity paired with sampling at scales relevant to snow processes. We found that neighborhood type, species, and year significantly influence snow accumulation and disappearance processes in a heterogeneous forest. These findings provide crucial information on the functional consequences of forest structural complexity, which is often a primary silvicultural objective in forests managed for multiple objectives.

Using a meta-analysis, Lundquist et al. (2013) concluded that December-January-February (DJF) climate has a first order effect on how forests impact snow. In warmer and wetter winter climates (DFJ > -1$^{o}$ C) snow is retained longer in openings than in continuous forests. Our site, located in western Montana, is situated in a climatic transition zone between the warmer and wetter maritime and cold, dry continental winter conditions. Three years of consecutive snow data point to snow cover patterns consistent with maritime climate where warmer and wetter conditions lead to more snow and later melt in openings compared to forests. Even with this observation, climate represents a coarse grain factor that may not be able to predict within-stand, micro-scale variability in snow processes created by heterogeneous canopy structure.

The distributional patterns of snow accumulation and ablation are highly variable in space and time. Over the sample years winter temperatures, timing of warming, and total snowfall varied, often giving rise to a significant interaction term in our analysis (Fig. S1). Overall, there was interannual consistency in the patterns of deepest accumulations and the most persistent snow cover, however the magnitude of the differences between neighborhood types

were either compressed or exaggerated (Fig. S4). Other studies have also found interannual variability to be a significant factor for peak snow (Winkler and Moore 2006). It is often noted that under heavy snow conditions an interception threshold is exceeded, and the influence of the trees is muted (Jost et al. 2007, Boon 2009). Our large snow year (2017) exaggerated neighborhood differences (Fig. 4 & 5). We suspect that rather than receiving large storms able to exceed interception capacities, total snowfall occurred in smaller, more frequent events.

*Snow accumulation*

Observed differences in peak accumulation between neighborhoods and species, that span a gradient of canopy densities, suggest that the primary mechanism driving differences in the accumulation process is canopy interception. Previous studies have found that up to 60 % of cumulative snowfall can be intercepted by a forest canopy which can remove up to 40 % of the water storage from the snowpack (Pomeroy et al. 2002, Storck et al. 2002, Martin et al. 2013, Jost et al., 2007, Essery et al. 2003). Under warmer temperatures, consistent with a maritime climate, canopy interception efficiency and storage capacity can approach 80 % (Andreadis et al. 2009).

The amount of snow that can be intercepted also increases with increasing canopy density (Harestad and Bunnell 1981, Teti 2003). Lopez-Moreno and Latron (2008) found a positive linear relationship between canopy density and interception, while in general increasing canopy density by 10% reduces SWE by 4-6% (Moore and McCaughey 1997, Varhola et al. 2010). This trend is apparent in our results: approaching the neighborhoods as a density gradient moving from higher density clumps of mature trees ($n$ = 7-15 stems within the immediate neighborhood), to individuals (evergreens then larch, $n$ = 1 stem in neighborhood), and openings with the lowest canopy density ($n$ = 0 stems) shows a pattern consistent with a canopy density effect.

However, regeneration patches with stem densities from hundreds to thousands are an exception to the density trend. This inconsistency is associated with decreased interception efficiency of small, flexible branches (Lundberg and Halldin 2001). Under juvenile (4 m tall) lodgepole pine in Montana, Hardy and Bristow (1990) found 20% greater snow accumulation compared to a mature spruce forest. Similarly, Winkler et al. (2005) studying juvenile pine stands with stem densities similar to our regeneration patches, observed only 14% less peak snow than in openings. Pfister and Schneebeli (1999) emphasized differences in interception capacity due to branch size, shape and inclination which can be attributed to different species.

Wind and redistribution can also contribute to distributional patterns in peak accumulations. Significant differences in snow accumulation patterns at sites with high average wind speeds were observed following a climate gradient across the Pacific Northwest (Dickerson-Lange et al. 2017). Peak snow depths were equivalent between forests and openings, and snow was retained longer in forests due to preferential snow deposition in the forest. This pattern is consistent across the Northern hemisphere (Lundquist et al. 2013). Our observations of greater accumulations in openings over forests are consistent with sites with low-average wind speeds.

*Snow disappearance*

Differences in peak accumulation between neighborhood types set up by canopy interception, where total snow under trees is less than in non-canopied environments (Fig. 4) contributes to different timing of snow disappearance due to different cold contents (Lundquist et al. 2013, Dickerson-Lange et al. 2017). Net available energy is the primary driver of snowmelt in forested environments (Varhola et al. 2010). In regions where low solar angles and shorter days characterize the melt period, longwave radiation dominates the energy balance as it is dependent

on air temperature rather than solar angle, unlike shortwave radiation (Sicart et al. 2004, Lalwer and Link 2011, Lundquist et al. 2013). Net longwave radiation shifts from positive under closed canopy to negative in openings (Lundquist et al. 2013). Forest canopy can affect the radiation balance in one of two ways: forest canopy can reduce shortwave radiation by shading underlying and adjacent areas resulting in a radiative minima; or the canopy can enhance longwave radiation leading to greater melt under the canopy creating a radiative maxima (Lawler and Link 2011).

We attribute the significant differences in snow disappearance observed between neighborhood types and species to the availability of longwave radiation. The significantly longer time to $fSCA_{50}$ in openings than clumps can be attributed to openings acting as radiative minima, where the surrounding canopy is able to shade the opening and longwave enhancement is minimal. Using sites with characteristics similar to ours (e.g. flat, small radiation differences, discontinuous forest, similar latitude), Lawler and Link (2011) found that small gaps 1-2 tree heights wide, also consistent with the size of our openings (Table S1), experienced minimal radiative input and adjacent forests experienced greater radiative inputs (Golding and Swanson 1978, Berry and Rothwell 1992).

The insignificant difference between openings and pooled individuals is likely driven by the inclusion of larch (see discussion below). However, an average difference of 5.5 days to $fSCA_{50}$ may be an ecologically significant difference, even if it was not statistically significant in our field study with $n = 6$ replicates per neighborhood type.

The significant difference in snow disappearance date and melt pattern observed between larch and the evergreen species suggests a potential biophysical feedback in which the deciduous western larch enhances snow cover duration beneath its crown. The visually striking concentric melt patterns observed around larch stems suggest that bole heating was a factor, and without a

winter canopy there is little overhead mass to trap and enhance longwave radiation below (Lundquist et al. 2013). Crown biomass, which includes branches and foliage can be used to evaluate potential interception and radiation (Brown 1978). For a 30.0 cm DBH tree, Douglas-fir and ponderosa pine maintain 1.5 and 2.5 times more total crown biomass than western larch (Brown 1978). This suggests that the crown architecture (i.e., branch form and biomass) of larch is different from neighboring evergreens, in addition to being deciduous (Gower and Richards 1990). During the winter, a 20 cm DBH Douglas-fir supports 41 $m^2$ of winter foliage area compared to 0 $m^2$ on a western larch of the same size (Gower et al. 1987). A significant interaction for $AUC_{fSCA}$ suggests different melt patterns under western larch relative to co-occurring evergreens.

Previous research on winter interception capacity or ablation mechanisms of *Larix* is nearly absent despite its global distribution and importance as a dominant circumboreal genus (Shuman et al. 2011). Deciduous angiosperms offer a reference point but cannot be directly compared because of very different branch geometry. Conflicting results have been found when comparing deciduous angiosperms and evergreen conifers. Research suggests that deciduous angiosperms tend to accumulate snow like open areas, but with melt rates similar to paired evergreen conifer stands (Lull and Rushmore 1960, Hart 1963). By contrast, Dunford and Niederhof (1944) found that aspen provided enough shelter and shade to reduce wind redistribution and slow melt compared to adjacent evergreen conifers.

We observed greater separation between larch and evergreens in the snowier year of 2017 (Fig. 4). This is likely due to more frequent snow events where snow gradually accumulated under larch, but interception losses were maximized in evergreens with lag times between snow events that did not exceed interception capacity. The significant interaction between leaf habits

and year for peak snow depth also suggests that the difference between these neighborhoods is particularly sensitive to interannual variation of total snowfall (Table 5). *Larix* always accumulated more snow than evergreens and with a larger sample size this difference may have been statistically significant. Because of the unique larch-snow interaction, shifts in species composition from larch to evergreens species will have large scale consequences on hydrology by altering forest composition and structure (Molotch et al. 2009). This trend is already being observed with climate change in Siberia where changes in surface albedo have an amplifying feedback on warming which is predicted to be greater than any carbon gains from biomass accumulation (Shuman et al. 2011, Kharuk et al. 2007).

*Conclusions and Management Implications*

We have demonstrated that structural and spatial heterogeneity within the forest canopy induces heterogeneity on the processes of snow accumulation and disappearance. Understanding the functional consequences of forest complexity is essential to support the development of management principles and silvicultural treatments to meet multiple management objectives (Levin 1992).

If the primary objective is to optimize snow water storage, our results suggest increasing the number of openings and widely spaced individuals. This should increase net accumulation and retain snowpack longer than areas with denser canopy conditions by reducing interception and longwave radiation. However, melt rates are often higher in very large open areas due to increased direct shortwave radiation than in forests and smaller canopy gaps 1-2 tree heights wide (Lawler and Link 2011, Varhola et al. 2010). Increasing the proportions of western larch and ponderosa pine should also modestly increase snow water storage. In dry mixed-conifer forests of the intermountain western US, this is consistent with management guidance to favor

early seral, fire-tolerant species as an ecological restoration and climate change adaptation strategy (Churchill et al. 2013). Yet, maximizing snowpack duration is likely dependent on a heterogeneous forest canopy (Stevens 2017).

Meeting multiple objectives with a single silvicultural prescription is increasingly the norm in forest management (Fahey et al. 2018)—single objective forestry is rare, especially on public lands. Even in municipal watersheds where water provisioning is of primary importance, multiple objectives are being considered to maintain and enhance forest heterogeneity and ecosystem functions. For example, in the Cedar River Municipal Watershed which serves the Seattle, Washington area, management objectives also include restoring forest and riparian ecosystems to provide habitat for species of concern (Richards et al. 2012, Sprugel et al. 2009, Mollot and Bilby 2008). In the Ashland, Oregon, municipal watershed management objectives also include promoting forest health, controlling invasive species, and actively reducing fire risk (Ashland Forest Lands Commission 2016).

Maintaining forest structural complexity and spatial heterogeneity embodied by different neighborhood types allows competing management objectives to be met. If providing winter habitat and energy efficient forge for ungulates is an objective, neighborhoods that accumulate less snow are needed (Armlender et al. 1994). For patches that green up early, neighborhoods with early snow disappearance should be emphasized (Wang et al. 2015). To improve the efficacy of insulation for microbial communities, neighborhoods with deep, persistent snow should be created (Brooks et al. 1996). Thus, multiple-objective forest management may be best served by a portfolio approach in which structurally complex stands include multiple neighborhood types (Franklin et al. 2002). Maintaining or creating structurally and spatially

complex forest stands contributes to forest resiliency and adaptability, which is vital for the perpetuation of forest ecosystem services and function (Franklin et al. 2018).

## References


Addington, R. N., G. H. Aplet, M. A. Battaglia, J. S. Briggs, P. M. Brown, A. S. Cheng, Y. Dickinson, J. A. Feinstein, K. A. Pelz, C. M. Regan, and J. Thinnes. 2018. Principles and practices for the restoration of ponderosa pine and dry mixed-conifer forests of the Colorado Front Range. General Technical Report RMRS-GTR-373. USDA Forest Service, Rocky Mountain Research Station, Fort Collins, Colorado, USA.

Andreadis, K. M., P. Storck, and D. P. Lettenmaier. 2009. Modeling snow accumulation and ablation processes in forested environments. Water Resources Research 45(5):WO549.

Armleder, H. M., M. J. Waterhouse, D. G. Keisker, and R. J. Dawson. 1994. Winter habitat use by mule deer in the central interior of British Columbia. Canadian Journal of Zoology 72(10):1721-1725.

Ashland Forest Lands Commission. 2016. 2016 Ashland Forest Plan. http://www.ashland.or.us/Files/2016%20Ashland%20Forest%20Plan%20Final2.pdf.

Bales, R. C., N. P. Molotch, T. H. Painter, M. D. Dettinger, R. Rice, and J. Dozier. 2006. Mountain hydrology of the western United States. Water Resources Research, 42(8):W08432.

Berndt, H.W. 1965. Snow accumulation and disappearance in lodgepole pine clearcut blocks in Wyoming. Journal of Forestry, 63(2):88-91.

Berry, G. J., and R. L. Rothwell. 1992. Snow ablation in small forest openings in southwest Alberta. Canadian Journal of Forest Research 22(9):1326-1331.

Boon, S. 2009. Snow ablation energy balance in a dead forest stand. Hydrological Processes: An International Journal 23(18):2600-2610.

Boon, S. 2012. Snow accumulation following forest disturbance. Ecohydrology, 5(3):279-285.

Boyden, S., R. Montgomery, P. B. Reich, and B. Palik. 2012. Seeing the forest for the heterogeneous trees: stand-scale resources distributions emerge from tree scale structure. Ecological Applications 22(5):1578-1588.

Brooks, P. D., M. W. Williams, and S. K. Schmidt. 1996. Microbial activity under alpine snowpacks, Niwot Ridge, Colorado. Biogeochemistry 32(2):93-113.

Brown, J. K. 1978. Weight and density of crowns of Rocky Mountain conifers. Research Paper INT-197. USDA Forest Service, Intermountain Forest and Range Experiment Station, Ogden, Utah, USA.

Brūmelis, G., B. G. Jonsson, J. Kouki, T. Kuuluvainen, and E. Shorohova. 2011. Forest naturalness in northern Europe: perspectives on processes, structures and species diversity. Silva Fennica 45(5): 807–821.

Churchill, D. J., G. C. Carnwath, A. J. Larson, and S. A. Jeronimo. 2017. Historical forest structure, composition, and spatial pattern in dry conifer forests of the western Blue Mountains, Oregon. General Technical Report PNW-GTR-956. USDA Forest Service, Pacific Northwest Research Station, Portland, Oregon, USA.

Churchill, D. J., A. J. Larson, M. C. Dahlgreen, J. F. Franklin, P. F. Hessburg, and J. A. Lutz. 2013. Restoring forest resilience: from reference spatial patterns to silvicultural prescriptions and monitoring. Forest Ecology and Management 291:442-457.

Churchill, D. J., S. T. Seager, A.J. Larson, E. E. Schneider, K. B. Kemp, and C. Bienz. 2018. Ecological Functions of Spatial Patterns in Dry Forests: Implications for Forest Restoration. The Nature Conservancy, Portland, OR. 7 p.

Clyatt, K. A., J. S. Crotteau, M. S. Schaedel, H. L. Wiggins, H. Kelley, D. J. Churchill and A. J. Larson. 2016. Historical spatial patterns and contemporary tree mortality in dry mixed-conifer forests. Forest Ecology and Management 361:23-37.

Dickerson-Lange, S. E., R. F. Gersonde, J. A. Hubbart, T. E. Link, A. W. Nolin, G. H. Perry, T. R. Roth, N. E. Wayand, and J. D. Lundquist. 2017. Snow disappearance timing is dominated by forest effects on snow accumulation in warm winter climates of the Pacific Northwest, United States. Hydrological processes 31(10):1846-1862.

Dickerson-Lange, S. E., J. A. Lutz, R. Gersonde, K. A. Martin, J. E. Forsyth, and J. D. Lundquist, J.D. 2015. Observations of distributed snow depth and snow duration within diverse forest structures in a maritime mountain watershed. Water Resources Research 51(11):9353-9366.

Dunford, E. G., and C. H Niederhof. 1944. Influence of aspen, young lodgepole pine, and open grassland types upon factors affecting water yield. Journal of Forestry 42(9):673-677.

Essery, R., J. Pomeroy, J. Parviainen, and P. Storck. 2003. Sublimation of snow from coniferous forests in a climate model. Journal of Climate 16(11):1855-1864.

Fahey, R. T., B. C. Alveshere, J. I. Burton, A. W. D'amato, Y. L. Dickinson, W. S. Keeton, C. C. Kern, A. J. Larson, B. J. Palik, K. J. Puettmann, and M. R. Saunders. 2018. Shifting conceptions of complexity in forest management and silviculture. Forest Ecology and Management 421:59-71.

Faria, D. A., J. W. Pomeroy, and R. L. H. Essery. 2000. Effect of covariance between ablation and snow water equivalent on depletion of snow covered area in a forest. Hydrological Processes 14(15):2683-2695.

Fiedler, C. E., K. L. Metlen, and E. K. Dodson. 2010. Restoration Treatment Effects on Stand Structure, Tree Growth, and Fire Hazard in a Ponderosa Pine/Douglas-Fir Forest in Montana. Forest Science 56:18–31.

Franklin, J. F., T. A. Spies, R. Van Pelt, A. B. Carey, D. A. Thornburgh, D. R. Berg, D. B. Lindenmayer, M. E. Harmon, W. S. Keeton, D. C. Shaw, and K. Bible. 2002. Disturbances and structural development of natural forest ecosystems with silvicultural implications, using Douglas-fir forests as an example. Forest Ecology and Management 155(1-3):399-423.

Franklin, J. F., K.N. Johnson, and D. L. Johnson. 2018. Ecological forest management. Waveland Press, Long Grove, IL.

Gary, H. L., and C. A. Troendle. 1982. Snow accumulation and melt under various stand densities in lodgepole pine in Wyoming and Colorado. USDA Forest Service, Rocky Mountain Forest and Range Experiment Station. Volume 417.

Golding, D. L., and R. H. Swanson. 1978. Snow accumulation and melt in small forest openings in Alberta. Canadian Journal of Forest Research 8(4):380-388.

Gower, S. T., and J. H. Richards. 1990. Larches: deciduous conifers in an evergreen world. BioScience 40(11):818-826.

Gower, S. T., C. C. Grier, D. J. Vogt, and K. A. Vogt. 1987. Allometric relations of deciduous (Larix occidentalis) and evergreen conifers (Pinus contorta and Pseudotsuga menziesii) of the Cascade Mountains in central Washington. Canadian Journal of Forest Research 17(7):630-634.

Grippa, M., L. Kergoat, T. Le Toan, N. M. Mognard, N. Delbart, J. L'hermitte, and S. M. Vicente-Serrano. 2005. The impact of snow depth and snowmelt on the vegetation variability over central Siberia. Geophysical Research Letters 32(21):L21412.

Hardy, J. P., and K. J. Hansen-Bristow. 1990. Temporal accumulation and ablation patterns in forests representing varying stages of growth. Paper presented at 58th Western Snow Conference, Sacramento, California.

Harestad, A. S., and F. L. Bunnell. 1981. Prediction of snow-water equivalents in coniferous forests. Canadian Journal of Forest Research 11(4):854-857.

Harpold, A. A., J. A. Biederman, K. Condon, M. Merino, Y. Korgaonkar, T. Nan, L. L. Sloat, M. Ross, and P. D. Brooks. 2014. Changes in snow accumulation and ablation following the Las Conchas Forest Fire, New Mexico, USA. Ecohydrology 7: 440–452.

Hart, G. 1963. Snow and frost conditions in New Hampshire, under hardwoods and pines and in the open. Journal of Forestry 61(4): 287-289.

Hubbart, J. A., T. E. Link, and J. A. Gravelle. 2015. Forest canopy reduction and snowpack dynamics in a northern Idaho watershed of the continental-maritime region, United States. Forest Science 61(5):882-894.

Ide, R. and H. Oguma. 2013. A cost-effective monitoring method using digital time-lapse cameras for detecting temporal and spatial variations of snowmelt and vegetation phenology in alpine ecosystems. Ecological Informatics, 16:25-34.

Jost, G., M. Weiler, D. R. Gluns, and Y. Alila. 2007. The influence of forest and topography on snow accumulation and melt at the watershed-scale. Journal of Hydrology 347: 101-115.

Kharuk, V., K. Ranson, and M. Dvinskaya. 2007. Evidence of evergreen conifer invasion into larch dominated forests during recent decades in central Siberia. Eurasian Journal of Forest Research 10(2):163-171.

Kittredge, J. 1953. Influences of forests on snow in the ponderosa, sugar pine, fir zone of the central Sierra Nevada. Hilgardia 22:1-96.

Knapp, E. E., J. M. Lydersen, M. P. North, and B. M. Collins. 2017. Efficacy of variable density thinning and prescribed fire for restoring forest heterogeneity to mixed-conifer forest in the central Sierra Nevada, CA. Forest Ecology and Management 406:228-241.

Kuuluvainen, T., 2009. Forest management and biodiversity conservation based on natural ecosystem dynamics in northern Europe: the complexity challenge. AMBIO: A Journal of the Human Environment 38:309-315.

Larson, A. J., and D. Churchill. 2008. Spatial patterns of overstory trees in late-successional conifer forests. Canadian Journal of Forest Resesarch 38:2814–2825.

Larson, A. J., and D. Churchill. 2012. Tree spatial patterns in fire-frequent forests of western North America, including mechanisms of pattern formation and implications for designing fuel reduction and restoration treatments. Forest Ecology and Management 267:74-92.

Lawler, R. R., and T. E. Link. 2011. Quantification of incoming all-wave radiation in discontinuous forest canopies with application to snowmelt prediction. Hydrological Processes 25(21):3322-3331.

Levin, S.A. 1992. The problem of pattern and scale in ecology: the Robert H. MacArthur award lecture. Ecology, 73(6):1943-1967.

López-Moreno, J. I., and J. Latron. 2008. Spatial heterogeneity in snow water equivalent induced by forest canopy in a mixed beech–fir stand in the Pyrenees. Annals of Glaciology 49:83-90.

Lull, H. W., and F. M. Rushmore. 1960. Snow accumulations and melt under certain forest conditions in the Adirondacks. USDA Forest Service Station Paper NE-138. Upper Darby, PA: Northeastern Forest Experiment Station. 16 p., 138.

Lundberg, A., and S. Halldin. 2001. Snow interception evaporation. Review of measurement techniques, processes, and models. Theoretical and Applied Climatology 70:117-133.

Lundquist, J. D., S. E. Dickerson-Lange, J. A. Lutz, and N. C. Cristea. 2013. Lower forest density enhances snow retention in regions with warmer winters: a global framework developed from plot-scale observations and modeling. Water Resources Research 49: 1-15.

Maher, C. T., E. Oja, A. Marshall, M. Cunningham, L. Townsend, G. Worley-Hood, L. Robinson, T. Margot, D. Lyons, S. Fety, E. E. Schneider, S. M. A. Jeronimo, D. J. Churchill, A. J. Larson. 2019. Real-time monitoring with a tablet app improves implementation of treatments to enhance forest structural diversity. Journal of Forestry. *In press*.

Martin, K. A., J. T. Van Stan II, S. E. Dickerson-Lange, J. A. Lutz, J. W. Berman, R. Gersonde, and J. D. Lundquist. 2013. Development and testing of a snow interceptometer to quantify canopy water storage and interception processes in the rain/snow transition zone of the North Cascades, Washington, USA. Water Resources Research 49:3243-3256.

Messier, C., K. J. Puettmann, and K. D. Coates, eds. 2013. Managing forests as complex adaptive systems: building resilience to the challenge of global change. Routledge.

Miller, D. H. 1964. Interception processes during snowstorms. USDA Forest Service Res. Paper PSW-RP-18. Berkeley, CA: Pacific Southwest Forest & Range Experiment Station, 24 p, 18.

Mollot, L.A. and R. E. Bilby. 2008. The use of geographic information systems, remote sensing, and suitability modeling to identify conifer restoration sites with high biological potential for anadromous fish at the Cedar River Municipal Watershed in western Washington, USA. Restoration ecology 16(2):336-347.

Molotch, N. P., P. D. Brooks, S. P. Burns, M. Litvak, R. K. Monson, J. R. McConnell, and K. Musselman. 2009. Ecohydrological controls on snowmelt partitioning in mixed-conifer sub-alpine forests. Ecohydrology: Ecosystems, Land and Water Process Interactions, Ecohydrogeomorphology 2(2):129-142.

Moore, C. A., and W. W. McCaughey. 1997. Snow accumulation under various forest stand densities at Tenderfoot Creek Experimental Forest, Montana, USA. In: 65th annual meeting, western snow conference: joint meeting with the 54th annual eastern snow conference and Canadian Geophysical Union.; 1997 May 4-8; Banff, Alberta, Canada. Brush Prairie, WA: Western Snow Conference. p. 42-51. (pp. 42-51).

Musselman, K. N., N. P. Molotch, S. A. Margulis, P. B. Kirchner, and R. C. Bales. 2012. Influence of canopy structure and direct beam solar irradiance on snowmelt rates in a mixed conifer forest. Agricultural and Forest Meteorology 161:46-56.

North, M., P. Stine, K. O'Hara, W. Zielinski, and S. Stephens. 2009. An ecosystem management strategy for Sierran mixed-conifer forests. General Technical Report PSW-GTR-220. USDA Forest Service Pacific Southwest Research Station, Albany, CA Department of Agriculture, Forest Service, USA.

Mysterud, A., and E. Østbye, E. 1999. Cover as a habitat element for temperate ungulates: effects on habitat selection and demography. Wildlife Society Bulletin 27(2):385-394.

Pauley, G. R., J. M. Peek, and P. Zager. 1993. Predicting white-tailed deer habitat use in northern Idaho. The Journal of wildlife management 57(4):904-913.
Pfister, R., and M. Schneebeli. 1999. Snow accumulation on boards of different sizes and shapes. Hydrological processes 13(14-15):2345-2355.
Pickard, M.R. 2015. Influence of within-stand tree spatial arrangement on snowpack distribution and ablation in the Sierra Nevada, CA. Dissertation. University of California Merced, California, USA.
Pinheiro, J.C., and D. M. Bates. 2000. Mixed-Effects Models in S and S-PLUS. Springer.
Plotkin, J. B., J. Chave, and P. S. Ashton. 2002. Cluster analysis of spatial patterns in Malaysian tree species. The American Naturalist 160(5):629-644.
Pomeroy, J. W., D. M. Gray, N. R. Hedstrom, and J. R. Janowicz. 2002. Prediction of seasonal snow accumulation in cold climate forests. Hydrological Processes 16(18):3543-3558.
Puettmann, K. J., C. C. Messier, and K. D. Coates. 2008. A critique of silviculture: managing for complexity. Island Press, Washington, D.C., USA.
R Core Team. 2017. R: A language and environment for statistical computing. R Foundation for Statistical Computing, Vienna, Austria. https://www.R-project.org/.
Raleigh, M. S., K. Rittger, C. E. Moore, B. Henn, J. A. Lutz, and J. D. Lundquist. 2013. Ground-based testing of MODIS fractional snow cover in subalpine meadows and forests of the Sierra Nevada. Remote Sensing of Environment 128:44-57.
Richards, W. H., R. Koeck, R. Gersonde, G. Kuschnig, W. Fleck, and E. Hochbichler. 2012. Landscape-scale forest management in the municipal watersheds of Vienna, Austria, and Seattle, USA: commonalities despite disparate ecology and history. Natural Areas Journal 32:199-207.
Sánchez Meador, A. J., P. F. Parysow, and M. M. Moore. 2011. A New Method for Delineating Tree Patches and Assessing Spatial Reference Conditions of Ponderosa Pine Forests in Northern Arizona. Restoration Ecology 19:490–499.
Schneider, E. E., and A. J. Larson. 2017. Spatial aspects of structural complexity in Sitka spruce–western hemlock forests, including evaluation of a new canopy gap delineation method. Canadian Journal of Forest Research 47(8):1033-1044.
Schneider, E. E., A. J. Larson, and K. G Jencso. 2015. The influence of a heterogeneous mixed-conifer canopy on snow accumulation and melt. *In* 83rd Annual Western Snow Conference. Grass Valley, CA.
Shuman, J. K., H. H. Shugart, and T. L. O'halloran. 2011. Sensitivity of Siberian larch forests to climate change. Global Change Biology 17(7):2370-2384.
Sicart, J. E., R. L. Essery, J. W. Pomeroy, J. Hardy, T. Link, and D. Marks. 2004. A sensitivity study of daytime net radiation during snowmelt to forest canopy and atmospheric conditions. Journal of Hydrometeorology 5(5):774-784.
Sprugel, D. G., K. G. Rascher, R. Gersonde, M. Dovčiak, J. A. Lutz, and C. B. Halpern. 2009. Spatially explicit modeling of overstory manipulations in young forests: effects on stand structure and light. Ecological Modelling 220(24):3565-3575.
Stevens, J. T. 2017. Scale-dependent effects of post-fire canopy cover on snowpack depth in montane coniferous forests. Ecological Applications 27(6):1888-1900.
Storck, P., D. P. Lettenmaier, and S. M. Bolton. 2002. Measurement of snow interception and canopy effects on snow accumulation and melt in a mountainous maritime climate, Oregon, United States. Water Resources Research 38(11):1223.

Sturm, M., B. Taras, G. E. Liston, C. Derksen, T. Jonas, and J. Lea. 2010. Estimating snow water equivalent using snow depth data and climate classes. Journal of Hydrometeorology 11(6):1380-1394.

Troendle, C. A. and C. F., Leaf. 1980. Effects of timber harvesting in the snow zone on volume and timing of water yield. *In* Interior West Watershed Symposium, Spokane, W A.

Teti, P. 2003. Relations between peak snow accumulation and canopy density. The Forestry Chronicle 79(2):307-312.

Tuten, M. C., A. S. Meador, and P. Z. Fulé. 2015. Ecological restoration and fine-scale forest structure regulation in southwestern ponderosa pine forests. Forest Ecology and Management 348:57-67.

Varhola, A., N. C. Coops, M. Weiler, and R. D. Moore. 2010. Forest canopy effects on snow accumulation and ablation: an integrative review of empirical results. Journal of Hydrology 392:219-233.

Walker, D. A., J. C. Halfpenny, M. D. Walker, and C. A. Wessman. 1993. Long-term studies of snow-vegetation interactions. BioScience 43(5):287-301.

Wallmo, O. C., L. H. Carpenter, W. L. Regelin, R. B. Gill, and D. L. Baker. 1977. Evaluation of deer habitat on a nutritional basis. Journal of Range Management 30:122-127.

Wang, K., L. Zhang, Y. Qiu, L. Ji, F. Tian, C. Wang, and Z. Wang. 2015. Snow effects on alpine vegetation in the Qinghai-Tibetan Plateau. International Journal of Digital Earth 8(1):58-75.

Webster, C. R., Y. L. Dickinson, J. I. Burton, L. E. Frelich, M. A. Jenkins, C. C. Kern, P. Raymond, M. R. Saunders, M. B. Walters, and J. L. Willis. 2018. Promoting and maintaining diversity in contemporary hardwood forests: Confronting contemporary drivers of change and the loss of ecological memory. Forest Ecology and Management. *In press*.

Winkler, D. E., K. J. Chapin, and L. M. Kueppers. 2016. Soil moisture mediates alpine life form and community productivity responses to warming. Ecology 97(6):1553-1563.

Winkler, R. D., and R. D. Moore. 2006. Variability in snow accumulation patterns within forest stands on the interior plateau of British Columbia, Canada. Hydrological Processes 20:3683-3695.

Winkler, R. D., D. L. Spittlehouse, and D. L. Golding. 2005. Measured differences in snow accumulation and melt among clearcut, juvenile, and mature forests in southern British Columbia. Hydrological Processes: An International Journal 19(1):51-62.

Woods, S. W., R. Ahl, J. Sappington, and W. McCaughey. 2006. Snow accumulation in thinned lodgepole stands, Montana, USA. Forest Ecology and Management 235:202-211.

Zhang, T. 2005. Influence of the seasonal snow cover on the ground thermal regime: An overview. Reviews of Geophysics 43(4):RG4002.

## Tables

**Table 1.** Summary of structural characteristics for all trees > 10.0 cm dbh by plot and site for a mixed conifer forest in western Montana. Site values are given as mean ± standard deviation. TPH is trees per hectare, QMD is quadratic mean diameter, species: PIPO = ponderosa pine (*Pinus ponderosa*), PSME = Douglas-fir (*Pseudotsuga menziesii*), LAOC = western larch (*Larix occidentalis*), PICO = lodgepole pine (*Pinus contorta*). Dead includes all upright snags with a height greater than 1.37 m that are greater than 10.0 cm dbh.

| Species | Density (TPH) | Basal area ($m^2$/ha) | DBH range (cm) | QMD (cm) |
|---|---|---|---|---|
| **Plot 1** | | | | |
| PIPO | 112 | 13.60 | 10.2 - 79.5 | 39.3 |
| PSME | 148 | 10.43 | 10.0 - 71.2 | 29.9 |
| LAOC | 1 | 0.08 | 10.7 - 41.9 | 27.5 |
| Dead | 11 | 0.74 | 10.1 - 77.9 | 28.7 |
| **Plot 2** | | | | |
| PIPO | 119 | 13.02 | 10.0 - 77.7 | 37.3 |
| PSME | 174 | 10.65 | 10.0 - 67.4 | 27.9 |
| LAOC | 13 | 0.99 | 12.1 - 58.8 | 31.5 |
| Dead | 19 | 0.97 | 10.0 - 57.8 | 25.4 |
| **Plot 3** | | | | |
| PIPO | 81 | 7.91 | 10 .0 - 73.0 | 35.2 |
| PSME | 115 | 9.33 | 10.0 - 64.8 | 32.1 |
| LAOC | 85 | 4.80 | 10.0 - 62.3 | 26.9 |
| PICO | < 1 | 0.06 | 28.6 | 28.6 |
| Dead | 21 | 1.34 | 10.0 - 77.5 | 28.4 |
| **Site average** | | | | |
| PIPO | 104 ± 20 | 11.51 ± 3.13 | 10.0 -79.5 | 37.2 ± 2.0 |
| PSME | 146 ± 29 | 10.14 ± 0.70 | 10.0 -71.2 | 30.0 ± 2.1 |
| LAOC | 33 ± 45 | 1.96 ± 2.51 | 10.0 - 62.3 | 28.6 ± 2.5 |
| PICO | < 1 ± 0 | <0.01 ± 0.00 | 28.6 | 28.6 ± 0.0 |
| Dead | 17 ± 5 | 1.02 ± 0.30 | 10.0 - 77.9 | 27.5 ± 1.8 |

**Table 2.** Mean densities of seedlings and saplings (≤ 10.0 cm DBH) within the research site estimated from randomly located plots, and in subjectively selected regeneration neighborhoods. Size classes are diameter at breast height.

| Size class (cm) | TPH | SD | Range |
|---|---|---|---|
| Randomly located plots (*n* = 15) | | | |
| 0-1 | 179 | 200 | 0 – 617 |
| 1-5 | 579 | 904 | 0 - 3,260 |
| 5-10 | 59 | 84 | 0 – 264 |
| Subjectively selected regeneration patches (*n* = 6) | | | |
| 0-1 | 1,219 | 787 | 352 - 2,247 |
| 1-5 | 5,955 | 3,548 | 2,643 - 12,732 |
| 5-10 | 1,116 | 535 | 573 - 1,366 |

**Table 3.** Distribution of individual trees and clumps across a mixed-conifer forest using a fixed inter-tree distance of 6 m. Total density is total number of mapped stems by plot and BA is basal area.

| | | Clump size (number of trees) | | | | |
|---|---|---|---|---|---|---|
| | | **1** | **2 - 4** | **5 - 9** | **10 - 15** | **16+** |
| **Plot 1** | *# Clumps ha$^{-1}$* | 16 | 15 | 5 | 2 | 4 |
| | *% Total density* | 6 | 16 | 13 | 12 | 53 |
| | *% Total BA* | 10 | 19 | 14 | 11 | 46 |
| **Plot 2** | *# Clumps ha$^{-1}$* | 11 | 11 | 6 | 2 | 4 |
| | *% Total density* | 4 | 11 | 13 | 10 | 63 |
| | *% Total BA* | 6 | 12 | 15 | 9 | 58 |
| **Plot 3** | *# Clumps ha$^{-1}$* | 15 | 11 | 6 | 1 | 4 |
| | *% Total density* | 5 | 11 | 14 | 4 | 65 |
| | *% Total BA* | 9 | 14 | 16 | 5 | 56 |
| **Site** | *# Clumps ha$^{-1}$* | 14 ± 3 | 12 ± 2 | 6 ± 1 | 2 ± 1 | 4 ± 0 |
| **average** | *% Total density* | 5 ± 1 | 13 ± 3 | 13 ± 1 | 9 ± 4 | 60 ± 6 |
| | *% Total BA* | 8 ± 2 | 15 ± 4 | 15 ± 1 | 8 ± 3 | 54 ± 6 |

**Table 4.** Description and distribution of openings within a mixed-conifer forest. Values are presented for each 4.48 ha (44,800 $m^2$) plot and averaged across the site. Each open area is any canopy opening extending at least 9 m from any live tree bole. Open area is the total plot area devoid of overstory foliage. Means ± standard deviation.

| | **Openings $ha^{-1}$** | **Mean area ($m^2$)** | **Open area ($m^2$)** | **Open area (%)** |
|---|---|---|---|---|
| Plot 1 | 2 | 327.1 ± 186.8 | 3,598.00 | 8.0 |
| Plot 2 | 3 | 280.8 ± 119.2 | 3,651.00 | 8.1 |
| Plot 3 | 2 | 326.0 ± 230.5 | 3,260.00 | 7.3 |
| Site avg. | 2 | 311.3 ± 178.9 | 3,503.00 | 7.8 |

| | Number of openings in size class ($m^2$) | | | | | | | |
|---|---|---|---|---|---|---|---|---|
| | **0-50** | **51-100** | **101-200** | **201-300** | **301-400** | **401-500** | **501-600** | **601+** |
| Plot 1 | 0 | 1 | 2 | 2 | 4 | 1 | 0 | 1 |
| Plot 2 | 0 | 0 | 5 | 3 | 3 | 1 | 1 | 0 |
| Plot 3 | 0 | 0 | 2 | 4 | 2 | 1 | 0 | 1 |
| Site avg. | 0 ± 0 | 1 ± 1 | 3 ± 2 | 3 ± 1 | 3 ± 1 | 1 ± 0 | 0 ± 1 | 1 ± 1 |

**Table 5.** ANOVA summary results for snow accumulation and melt characteristics for neighborhood type and a neighborhood type year interaction. O is opening, C is clump, I is individuals pooled across species, L is larch, E is evergreen species pooled, Pi is ponderosa pine, and Ps is Douglas-fir, Num is numerator, Den is denominator, Diff. stands for average difference across years. When days is used as a unit it is days since peak snow. Statistically significant values are bolded.

| | **Snow water equivalent (cm)** | | | | **Snow depth (cm)** | | | | **$fSCA_{50}$ (days)** | | **$AUC_{fSCA}$ (fSCA*days)** | |
|---|---|---|---|---|---|---|---|---|---|---|---|---|
| | Num df | Den df | p-value | Diff. ± SD | p-value | Diff. ± SD | Num df | Den df | p-value | Diff. ± SD | p-value | Diff. ± SD |
| **Neighborhood Type** | 4 | 25 | **<0.0001** | | **<0.0001** | | 4 | 25 | **<0.0001** | | **<0.0001** | |
| O vs. C | 1 | 25 | **<0.0001** | 3.3 ± 0.5 | **<0.0001** | 17.7 ± 2.8 | 1 | 25 | **<0.0001** | 9.7 ± 1.9 | **<0.0001** | 984.1 ± 192.3 |
| O vs. I | 1 | 25 | **0.0001** | 1.8 ± 0.4 | **<0.0001** | 10.8 ± 2.2 | 1 | 25 | 0.1320 | 5.5 ± 1.8 | 0.1826 | 578.4 ± 177.0 |
| L vs. E | 1 | 25 | 0.1468 | 0.8 ± 0.4 | 0.2359 | 4.1 ± 2.3 | 1 | 25 | **0.0082** | 3.2 ± 1.0 | **0.0027** | 290.0 ± 86.5 |
| Pi vs. Ps | 1 | 25 | 0.2914 | 0.4 ± 0.4 | 0.3297 | 2.6 ± 2.6 | 1 | 25 | 0.4069 | 1.1 ± 1.0 | 0.6759 | 75.2 ± 105.7 |
| **Neighborhood:year** | 8 | 48 | **0.0043** | | **0.0003** | | 8 | 50 | **0.0246** | | **0.0084** | |
| O vs. C | 2 | 48 | **0.0001** | | **<0.0001** | | 2 | 50 | 0.0775 | | 0.0678 | |
| O vs. I | 2 | 48 | 0.0647 | | **0.0122** | | 2 | 50 | **0.0413** | | 0.1335 | |
| L vs. E | 2 | 48 | 0.3560 | | **0.0523** | | 2 | 50 | 0.2689 | | **0.0091** | |
| Pi vs. Ps | 2 | 48 | 0.6306 | | 0.0602 | | 2 | 50 | 0.2591 | | 0.4381 | |

## Figures

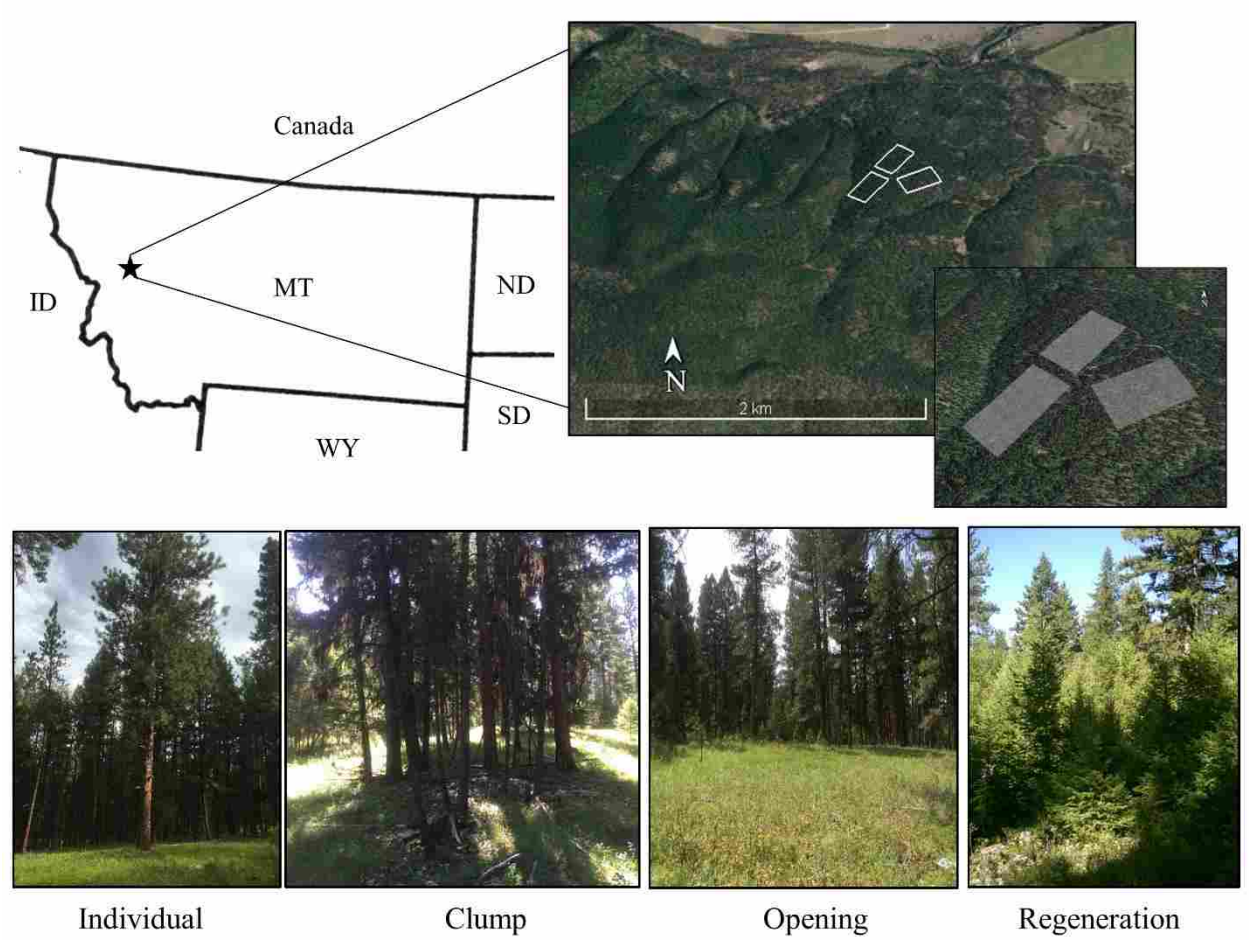


**Figure 1.** Study site located in western Montana, USA. Top image shows local topography and forest conditions. The inset, taken from an oblique angle indicates the position of each 4.48 ha (160 x 280 m) plot within the forest bisected by a central gravel road. The lower images provide an example of each local neighborhood environment sampled.

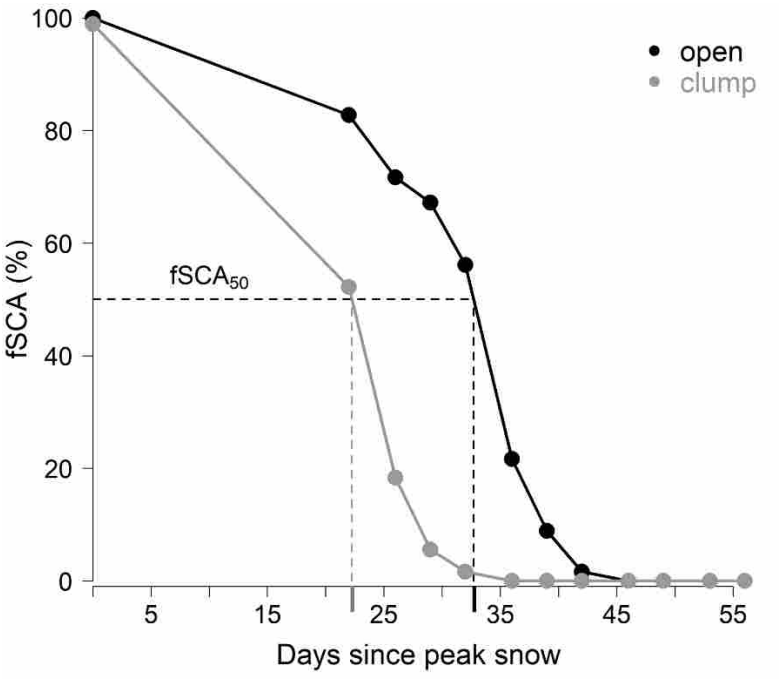


**Figure 2**. Example of two fractional snow cover melt curves from the 2017 season. Fifty percent of sample points remain snow covered along the horizontal dashed line and the vertical dashed lines represent the day since peak snow when 50% cover is reached.

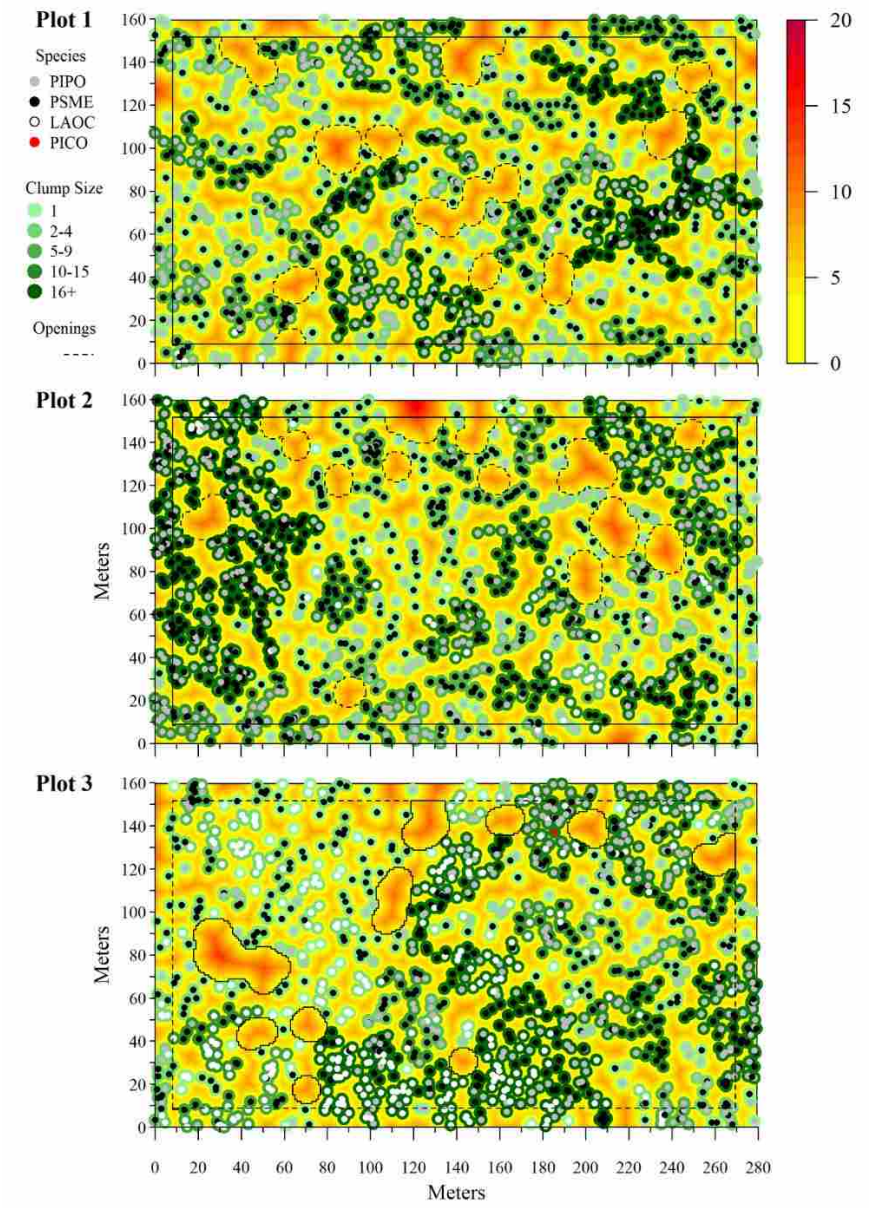


**Figure 3**. Stem maps of a mixed-conifer forest in western Montana. Tree locations are colored by species with a projected 6 m canopy diameter. Clump size follows a color gradient from light to dark. Openings are delineated by the solid black line and the buffer distance a dashed line. Background coloration illustrates nearest neighbor distances in meters.

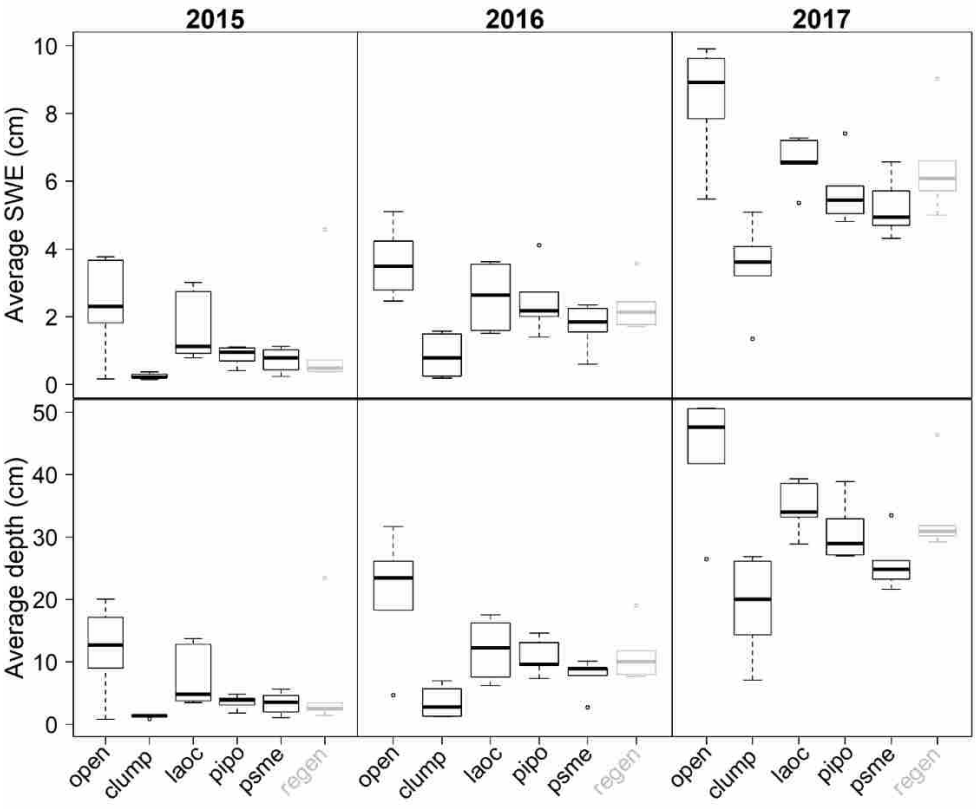


**Figure 4.** The relationship between average snow accumulation characteristics and neighborhood type across years. Boxes extend from the 25$^{th}$ to 75$^{th}$ percentiles, the central bold line the median, whiskers extend 1.5 times the interquartile range, and outliers are represented as individual points.

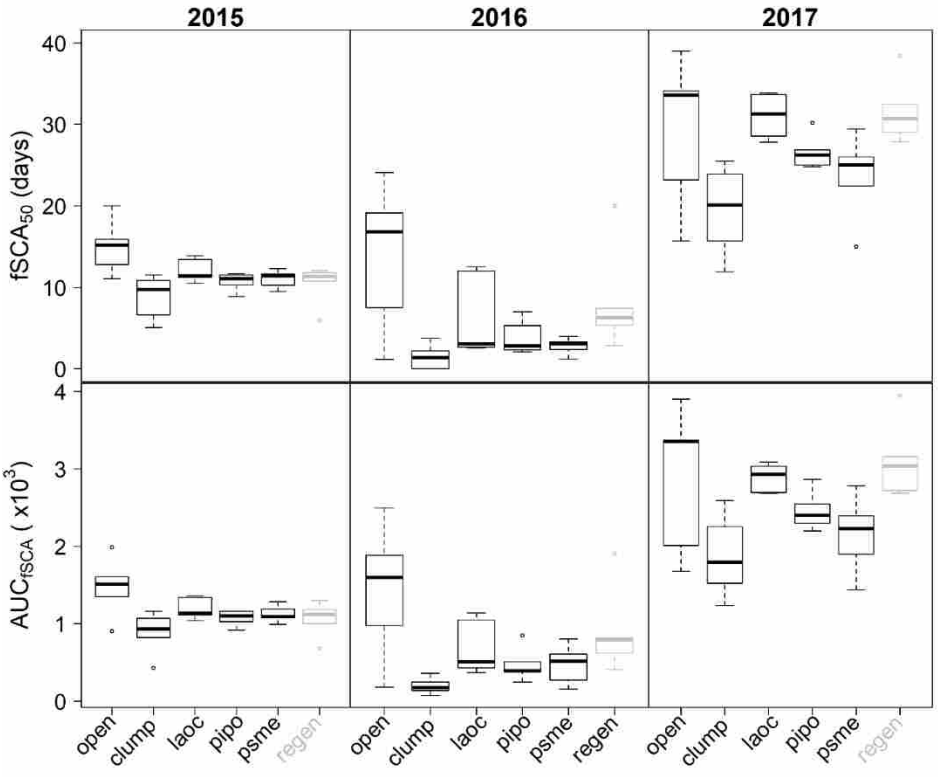


**Figure 5.** Relationship between average snow melt characteristics based on fSCA melt curves, by neighborhood type across sampling years. Box and whiskers are the same as in Figure 4. $fSCA_{50}$ are best fit model estimates of the day at which 50% of the snow remained in each neighborhood. $fSCA_{50}$ days is days since peak snow.

# CHAPTER 3. Ground and LiDAR derived forest canopy metrics perform equally in estimating snow accumulation and persistence in a mixed-conifer forest

**Abstract**
The spatiotemporal patterns of snow accumulation and disappearance in montane forests control the annual timing and availability of freshwater. Patterns of snow characteristics have been modeled using 1-2 year of data and regression trees, with vegetation classes. We used four years of high resolution snow measurements paired with random forest models and detailed forest structural predictors from ground and LiDAR data that influence the physical processes of forest-snow interactions. Ground based and LiDAR derived models performed equally well in estimating snow accumulation (SWE) and disappearance (SDD). Peak SWE and SDD were best predicted with the Hegyi index and tree density from ground metrics and crown density and coefficient of variation for height with LiDAR metrics. Local stem density of *Larix* was also important for SWE. In general, SWE increased with decreases in overstory density and cover. Peak snow density was not predictable with canopy or terrain metrics. Importance of the same variables for peak SWE as SDD suggest that the hydrologic processes are driven by the same principles, and that canopy metrics explain one-third to nearly half the variation in accumulation and melt. The use of LiDAR metrics over ground metrics offers resource managers a rapid, spatially continuous, and increasingly cost-effective tool for predicting ecohydrologic processes following changes to forest canopy structure due to silvicultural practices or natural disturbances. Capturing a range of annual snow conditions also provides insight into future snow patterns under climate change.

## Introduction

The spatiotemporal patterns of snow accumulation and disappearance in mountain forests control the annual timing and availability of much of the freshwater runoff globally (Cheng 2003). This runoff is critical for downstream ecosystems, communities, and economies (Bales et al. 2006). Climate and elevation exert first order controls on snow accumulation and ablation, while vegetation and topography control heterogeneous patterns of snowpack at local scales (Varhola et al 2010a). Variability in snow properties over short distances make it particularly difficult to model. However, current runoff predictions are made using data sources that avoid the influence of vegetation, and typically perform well only under long-term average conditions, which are becoming less frequent with climate change (Balk and Elder 2000, Molotch et al.

2005). A better understanding of vegetation's role in snow accumulation and melt responses are needed to improve models of ecohydrologic processes (Varhola et al. 2010a).

There is a complex interplay between forest vegetation and the mass and energy balance of the snowpack (Moeser et al. 2015). Conifer canopies can intercept up to 60% of the total incoming snowfall (Martin et al. 2013), which can sublimate back to the atmosphere, or can later be removed from the canopy by mass release or meltwater drip, generally decreasing snow accumulation (Storck et al 2002). Forest canopies absorb and reflect incoming shortwave radiation, shading the snow beneath and retarding melt (Lawler and Link 2011); and they emit and trap longwave radiation which can enhance melt beneath (Musselmann et al. 2013). The vertical profile of the forest also alters turbulent heat transfer and wind redistribution (Link and Marks 1999). This leads to difficulties in quantifying and attribution of canopy structural effects on snow in space and over time. Addressing this limitation requires longitudinal, high-resolution forest structure and snow measurements paired at process relevant scales.

Modeling can help to elucidate, and test conceptualizations of the mechanistic controls observed at micro-scales to management relevant units (Musselmann et al. 2008). Statistical models trained on field data, particularly regression tree models have proved promising for exploring the non-linear relationships between snow accumulation and melt patterns, and local terrain features (slope, aspect, net radiation) and cover type (forest vs. no forest) (Molotch et al. 2005, Erxleben et al. 2002, Musselmann et al. 2008, Elder et al. 1995). Spatially distributed regression tree models that account for the location of these predictor variables often outperform (Balk and Elder 2000, Molotch et al. 2005) regression trees (Elder et al. 1995, 1998) or geospatial techniques alone (Carroll and Cressie 1996). This reinforces the results of Moeser et al. (2015) which highlight the importance of feature location, not just average canopy

characteristics for predicting snow processes. However, most snow models are too coarse to explicitly account for the fine-scaled processes controlled by structural and spatial complexity of the forest canopy (Uhlmann et al. 2018).

Light detection and ranging (LiDAR) offers an alternative approach for quantifying fine-scale surface and vegetation features (Kostadinov et al. 2019). Traditional ground-based snow sampling and forest measurements are time consuming, expensive and limited in extent compared to LiDAR (Deems et al. 2013, Jeronimo et al. 2018), which has become a readily accessible data source for researchers and land managers. Næsset et al. (2002), Kane et al. (2010b), and Wiggins et al. (2018) have found high levels of correlation between field measurements and LiDAR based canopy metrics. LiDAR has been used to describe forest structural and spatial complexity from individual trees to spatial patterns including tree clumps and openings over increasingly large extents (Kane et al. 2011, Kane et al. 2010b, Kane et al. 2010a, Jeronimo et al. 2018). LiDAR derived metrics of: $95^{th}$ percentile height, mean height, the L moments of height, canopy cover or density, and rumple (a measure of canopy surface roughness) have accurately captured forest structural complexity (Jeronimo et al. 2018, Moran et al. 2018, Kane et al. 2011). Despite the prevalence and extensive use of airborne LiDAR derived forest canopy metrics in other disciplines, and the known significant influence of canopy complexity on snow distribution (Schneider et al. 2019), these metrics have not been used as predictors in a spatially explicit regression tree models to estimate snow properties. Rather, hydrologic studies have used LiDAR surface models to estimate and map snow depth, snow water equivalent (SWE), melt rates or snow covered area (Harplod et al. 2014, Zheng et al. 2016, Hopkinson et al. 2004, Nolan et al. 2015, Broxton et al. 2019).

The objectives of this study were to assess the roles of forest structure in explaining the variation in snow characteristics to better understand the controls of complex forest structure on snow driven ecohydrologic processes at multiple scales by developing a spatially explicit, regression tree model. Precisely geolocated forest structure and snow sampling locations enabled snow and vegetation characteristics to be explicitly linked. We first report snow properties within and between years to confirm and describe the presence of spatial heterogeneity across the site. We were then able to ask if forest canopy metrics can explain the observed variation in snow properties within the forest. We further asked how two different methods for deriving forest canopy metrics (ground vs. LiDAR) performed in predicting snow characteristics, as LiDAR is a widely available, cost efficient alternative to ground based measurements.

## Methods

*Study area*

We conducted this research in Lubrecht Experimental Forest, 50 km northeast of Missoula, Montana, USA (46°55´N, 113°27´W). Three, 4.48 ha plots were installed to quantify forest vegetation and within stand snow characteristics (Figure 1). The site is characterized by a structurally complex and spatially heterogeneous forest dominated by Douglas-fir (*Pseudotsuga menziesii;* 55%*)*, ponderosa pine (*Pinus ponderosa;* 37%), and a lesser component of western larch (*Larix occidentalis*; LAOC 8%). Average site density is 283 trees per hectare (≥10 cm dbh), average basal area is 23.62 $m^2ha^{-1}$ and overstory tree diameters at breast height range from 10.0-79.5 cm. Forest structure and composition at the study site are the product of early $19^{th}$ century large-tree harvest, fire exclusion, periodic grazing and a more recent (*ca*. 1984) thinning to a target basal area of 16 $m^2\,ha^{-1}$ (Maher et al. 2019). Schneider et al. (2019) provides a detailed

description of forest structure, composition, and spatial characteristics for the site. The study site is located at 1,220 m a.s.l.

Peak SWE, peak snow density and snow disappearance were measured within the study area annually from 2014-2017. During the study period mean winter temperature was -4$^{o}$ C (range: -8$^{o}$ – 2$^{o}$ F), with snow present from November to March (Figure S1). Peak accumulation occurred between February 13 and March 5, which is consistent with the local long-term average (Lubrecht Flume SNOTEL 604, NRCS, https://wcc.sc.egov.usda.gov/nwcc/site?sitenum=604). Wind ranged from 0 – 1.8 m/second on site during the winter of 2016.

*Snow characteristics*

*Accumulation*

Snow accumulation was characterized by peak snow water equivalent and snow density. Peak accumulation is defined as the point at which cumulative increases in snowfall have ceased and the snowpack is isothermal allowing liquid water to be released. The timing of peak sampling was determined using a local SNOTEL site (Lubrecht Flume) and extended forecasts for the area. Peak accumulation was measured on March 5, February 20, February 13, and February 21 for 2014-2017.

Peak snow depth and bulk density were collected along a fixed 20 m x 20 m grid (9 rows x 15 columns; $n$ = 135/plot) in each plot (Figure 2-layer A). Sub-grid variation (Schneider et al. 2015) was assessed using “intensive” samples collected along two, 9 m transects separated by 90$^{o}$ (Figure 2-layer B). Intensive samples were located on one randomly selected grid point per column and sampled at 1 m intervals ($n$ = 270/plot). Snow depth was collected at each point and density at approximately every other point (Figure 2-bottom highlight). Following the 2014 snow season, it was determined that sampling points did not span the full range of within forest canopy

conditions. Additional sampling points referred to as “neighborhoods” were added across the site (*see* Schneider et al. 2019). Neighborhoods consisted of two, centrally bisecting 14 m transects sampled at 1 m intervals (Figure 2-layer C). Depth was collected at each point and density at every other point (Figure 2-upper highlight). Snow depth and density were collected with a standard Federal snow sampling tube and scale (Rickly Hydrological Company, Columbus, OH, USA). SWE values were calculated using observed snow depth and density values.

*Disappearance*

Our high-resolution snow disappearance monitoring protocols were designed to capture as much spatial variation under various canopy conditions as possible. Snow disappearance was monitored at all peak snow sampling points and at an additional 2,700 points per plot. Additional points were distributed at 1 m intervals along fifteen, 160 m transects extending the length of each grid column (Figure 2-layer D). Sampling occurred approximately every third day from peak accumulation until no snow remained at any of the sampling points. A snow disappearance date (SDD) was assigned to each point corresponding to the sampling day snow no longer covered each point. This resulted in an interval censored variable with a precision based on the days between sampling campaigns. Snow disappearance was only monitored in plot 1 in 2016 due to time constraints.

Fractional snow covered area (fSCA), the number of snow covered points over the total number of sampling points, was used to provide plot scale metrics for snow disappearance (Dickerson-Lange et al. 2015).

*Predictor variables*

*Ground measurements*

All overstory trees, defined as trees with a diameter at breast height (DBH) greater than 10.0 cm were mapped and measured. For each plot, mapping was done with a Leica survey grade total station, and a control loop used to quantify mapping error (linear misclosure ≤0.49 m). Each tree was tagged with a unique number; and species, DBH, total height, and canopy depth were measured.

Mapped locations were georeferenced using an Emlid Reach RS unit (point error less than 3.0 cm). Local coordinates were converted to global coordinates by rotating local coordinates by the angle of difference between local and global positioning of plot origin to the first point on the control loop. Rotation RMSE was 0.44 m on plot 2 using thirteen control points. The angle of rotation was determined using the same methods for the remaining plots. Alignment was visually assessed using a LiDAR model of maximum heights.

*Ground based predictors*

Predictor variable selection was based on our understanding of the mechanistic processes that influence snow accumulation and disappearance processes. Field measured predictors included stem density (Lundquist et al. 2013; Hubbart et al. 2015), number of neighboring *Larix* (Schneider et al. 2019), canopy strata (intermediate, co-dominant, dominant), Hegyi index, sum of nearest neighbor distance (Moeser et al. 2015), slope, aspect, and January-June shortwave radiation (Musselmann et al. 2008, Elder et al. 1995). SWE was used as a predictor variable for density and SDD (Dickerson-Lange et al. 2017; Table 1).

Vertical canopy strata were used to characterize layering within of the canopy profile (Kane et al. 2011). Designations were based on the local distribution of heights and height-DBH relationships (Schneider et al 2019). Intermediate trees had a DBH < 17.1 cm, co-dominant trees were 17.1-35.5 cm DBH, and dominant trees were >35.5 cm DBH. These values closely

correspond with the 25th, 50th and 75th percentiles of heights. The Hegyi index is a measure of competition that accounts for the size and distance of neighboring trees (Contreras et al. 2011). To calculate a standardized Hegyi index for each snow sampling point the "focal tree" dbh was fixed at 10 cm. Nearest neighbor distance was calculated using the spatstat package and distmap function in R.v.3.5.3. at a 1 m resolution (Baddeley et al. 2015, R Core Team 2017). The pixel image is a function of the shortest distance from each sampling point to every tree on site. This image was rasterized and imported into ArcGIS 10.1 to extract point values. Net daily shortwave radiation was modeled using a 1m DTM and the Potential Incoming Radiation module using System for Automated Geoscientific Analysis (SAGA GIS) software and summed from January to June for each sampling point (Conrad et al. 2015).

*LiDAR acquisition*

LiDAR data collection was conducted in June of 2015 by Quantum Spatial using a Leica ALS70 laser sensor with a pulse rate of 180-193 kHz (https://quantumspatial.com). Low flight altitude (1450 m), multiple returns per pulse, 60% side-lap (100% overlap) and opposing directional flight paths were utilized to optimize vegetation detection. Vertical accuracy was 0.097 m ($n$ = 211) and first return point density was 20.07 points/$m^2$. Calibration corrections, filtering of erroneous points, and point classifications were carried out by Quantum Spatial. A digital terrain model (DTM) was created using 1 m mean elevations in a triangulated irregular network. To normalize point height, the elevation of LiDAR points was subtracted from underlying DTM values. Forest canopy metrics were calculated using FUSION software and a 1 m DTM (McGaughey 2015).

*LiDAR based predictors*

We used the four L-moment height features, coefficient of variation for height, 95$^{th}$ percentile height, 99$^{th}$ percentile height, and canopy density as predictors (Table 1). All metrics describe the vertical distribution of forest canopy structure except canopy density which characterizes the horizontal distribution (Kane et al. 2010b, Jeronimo et al 2018, Moran et al. 2018, Varhola et al 2010a). The four L-moments are ordered statistics that are analogous to distributional descriptors of mean (L-1), standard deviation (L-2), skewness (L-2) and kurtosis (L-4). These metrics have been used to describe canopy structure (Moran et al. 2018, Frazer et al. 2011, Valbuena et al. 2017). 99$^{th}$ percentile height represents maximum height values that are free from outlying maximum height points.

All vegetation predictor variables were calculated over a range of distances from each sample point. A circular area with a radius ranging from 1-15 m (1-8 m for LiDAR metrics due to computational limits) was centered on each sample point. Ground and LiDAR metrics were calculated within this area. For ground metrics, sample size was reduced with increasing radial distance due to buffering for edge effects since forest structure outside of the plots is unknown. A linear mixed effects model was used to regress each predictor variable on each snow response across all radial distances. Fixed effects where the metric of interest, year, and an interaction between the metric and year. Sample point was modeled as a random effect allowing the model to acknowledge the repeated measures aspect of the study. Fit was assessed using AIC (Table S1, S2). LiDAR metrics of skewness and kurtosis could not be fit with the random factors due to a lack of convergence, so a simplified fixed effects model was used. Analysis was done using the lmer4 package in R.v.3.5.3 (R Core Team 2017, Bates et al. 2015).

*Modeling*

Regression trees are hierarchical, non-parametric, machine learning algorithms where predictor variables are recursively partitioned based on a set of decision rules (Prasad et al. 2006). Because regression tree models account for interactions and non-linear relationships between variables, they are often used to model the distribution of snow (Elder et al. 1995, Winstral et al 2002). Regression trees predict the response variable, in this case snow characteristics, based on recursive partitioning of a dataset utilizing a set of decision rules (Breiman et al. 1984). Random forests (RF) offer an improvement in prediction accuracy over traditional regression trees by reducing the variance of single trees by aggregating multiple bootstrap trees (Breiman and Cutler 2003). Within each bootstrap sample, a tree is grown where each split is based on a random selection of a subset of possible predictor variables which reduces correlation among trees. Trees over all samples are averaged, yielding the most influential variables. However, the gain in prediction accuracy is at the expense of interpretability. Variable importance measures the influence of a predictor on model accuracy and gives an idea of the strength of a variable's relationship with the response. Permutation importance is measured as the difference in MSE between the out-of-bag (OOB) sample tree and a tree using the same OOB sample, where the values of each variable are randomly permuted separately and then averaged over all trees in the forest. Mean variable importance values were calculated from 100 permutations of each predictor (Table 1). For each RF, an 80:20 random partitioning into a training and validation dataset was constructed allowing for a 20 fold cross-validation.

To account for the first order effects of annual climate variability all response variables were normalized within year. Normalization was carried out by subtracting the annual mean and dividing by the standard deviation.

Increased performance of regression trees with the use of residual interpolation has also been observed for snow characteristics (Balk and Elder 2000, Erxleben et al. 2002). Ordinary kriging (OK) was used to model any remaining spatial dependencies in the regression model residuals. Interpolated residual estimates were added to the regression tree models and examined for increased performance. All RF model performance was evaluated using cross-validated RMSE values.

## Results

### *Snow characteristics*

#### *Accumulation*

Spatial variation defines the patterns of peak SWE, snow density, and snow disappearance beneath a heterogeneous forest canopy. Year-to-year climate variability exerted a strong first order control on the amount of peak SWE and patterns of snow disappearance captured by our four year collection period (Table 2 and 3). 2014 was an above average snow year (Figure S1). Peak accumulation occurred earlier with more mid-winter melt events in 2015 than other years. 2016 was a dry year with below average snowfall. The 2017 snow season was above average with a large, late snow event.

Within the forest, SWE covered a range of values which always included locations with no snow and averaged between 1.1 and 8.4 cm from 2014-2017 within the study area (Table 2). The greatest variation (CV = 1.36 and 0.71) in peak SWE occurred in years with lower SWE (2015 & 2016), exhibiting a reverse J distribution (Figure 3). In above average years the distribution of SWE was less variable and followed a normal distribution (Figure 3, Table 2). Despite different winter conditions, average snow density was near 20% normally distributed with a slight right skew across all years (Figure 4). Sampled at a 2:1 ratio with snow depth, peak

snow densities ranged from 0.02 – 0.49 g/cm$^3$ in 2014, 0.04 – 0.47 g/cm$^3$ in 2015, 0.06 – 0.85 g/cm$^3$ in 2016, and 0.02 – 0.82 g/cm$^3$ in 2017 (Table 2). Average peak SWE (used as a proxy for snow depth) was around 1.5 times more variable than snow density, except in 2015 where SWE was four time more variable (Table 2).

*Disappearance*

The snow melt season lasted between 31 and 59 days and the snowpack had mostly or completely melted by April 1 (Table S3). A transition point in the rate of snow disappearance, from a steady decline to rapid drop in fSCA was a defining feature across all years, but the time of this point depended on annual snow conditions (Figure 5). In 2015 and 2016 the transition to rapid melt occurred around a quarter of the way through the melt season, while in 2014 and 2017 this point was much later in the season, occurring more than halfway through the melt season (Table S3).

*Random Forest Modeling*

Random forest (RF) models parameterized with ground and LiDAR derived canopy metrics performed nearly identically when estimating snow characteristics (Table 3). RFs parameterized with forest canopy metrics provided better predictions for peak SWE and the timing of snow disappearance than snow density (Figure 6). Our models were able to explain 30 and 35% of the variation in peak SWE using ground and LiDAR metrics respectively with an associated RMSE of 0.93 cm and 0.91 cm (Table 3). 47% of the variation in SDD was explained with ground and LiDAR canopy metrics. However, the predictive accuracy for peak snow density was very poor with $R^2$ of 0.05 and 0.00 for ground and LiDAR methods respectively. Because residual interpolation did not improve the fit of SWE or density models and contributed

to marginal improvements in SDD estimation (data not shown), it was not included in the final models.

The optimal radius for predictor variable calculation was constant within each ground based predictor variable, often the largest distances having the smallest AIC (Figure S2, Table S1). Radial distance selection varied within and between snow responses for LiDAR predictors, with the lowest AIC values falling in mid-range distances (Table S2). Overall, there were weak to moderate correlations (0 – 0.54) between ground and LiDAR predictor metrics (Figure S3). Based on cross-validation the optimal number of variables selected at each node ranged from 4-5 for ground metrics and 3-4 for LiDAR values, which is consistent with the RF default values.

All predictor variables contributed to model learning, however the Hegyi index and tree density were most important for SWE and SDD (Figure 7). Although used by the models, many of the explanatory variables had little predictive power. The Hegyi competition index was 4 and 2.7 time more important than the next most influential variable, tree density, for predicting SWE and SDD respectively. The effect of the Hegyi index on peak SWE was linear, with decreasing snow water with increasing Hegyi values (Figure 8). SDD decreased (i.e., earlier melt) with increasing Hegyi, with the earliest snow melt occurring in areas with a Hegyi index greater than 20 (Figure 9). In general, as local tree density increased peak SWE was reduced, while increasing *Larix* stem density increased peak SWE.

Canopy density (CD) was the most influential LiDAR predictor of SWE and SDD, reducing the amount of SWE and leading to earlier melt (Figure 8 & 9). The amount of variation (CV) and the distribution of biomass in the canopy (skewness) were also important LiDAR predictors of SWE (Figure 7). As the amount of alternating areas of open and dense canopy increases across the horizontal canopy surface (i.e. CV) and the vertical biomass is focused at the

top or bottom of the canopy (i.e. skewness) there is a general increase in SWE (Figure 8). Figure 9 shows that when canopy foliage is focused in the lowest portions of the canopy (negative skewness) and local tree height exceeded 5 m, the LiDAR RF model predicted the earliest disappearance dates.

Although all predictor variables were used by the RF models of snow density, they explained little to no variation with and $R^2$ of 0.05 and 0.00 for ground and LiDAR models respectively (Figure 7, Table 3). Ground method performance was primarily driven by peak SWE, followed by net shortwave radiation, slope, and the Hegyi index. Partial dependency plots indicated a linear relationship between snow density and SWE and Hegyi which plateaued around 10 (Figure 10). The relationships between density with shortwave radiation and slope are non-linear with density minimized around 440,000 $kJ/m^2$ and maximized around 10% slope. All variables led to similar improvements in accuracy within the LiDAR model (Figure 6). Canopy density and the variation in canopy heights (CV) were slightly more important with density increases associated with an increase in both variables but plateauing around 0.65 for CV (Figure 10).

## Discussion

Understanding the mechanisms driving the patterns in snow accumulation and disappearance in mountain forests is critical for accurately forecasting water availability. We found that detailed forest canopy metrics and the most basic terrain features account for one-third to nearly half of the variation in peak snow accumulation and snow disappearance processes in a mountain forest. Model performance did not depend on the source of canopy metrics. Ground and LiDAR parameterized models performed equally well. Thus, models based on LiDAR derived measures of forest canopy structure may offer an efficient, cost effective tool for

managers to predict snow characteristics, including outcomes of silvicultural practices and disturbance processes over management relevant extents (Winkler and Moore 2006, Varhola et al. 2010a).

*Snow characteristics*

Patterns of snow accumulation and disappearance beneath a complex forest canopy are highly variable. A gradient of interception capacities present within the forest is thought to drive greater variation in peak snow beneath the forest than in adjacent non-forested areas (Musselmann et al. 2008, Woods et al. 2006, Winkler et al. 2005, Jost et al. 2007). We observed the coefficient of variation for peak SWE to range on average from 0.36-1.36 within the forest (Table 2). All but the largest CV values are consistent with reported CV values (0.1 – 0.70) for peak SWE in watersheds with varying amounts of forest vegetation (Varhola et al. 2010a, Balk and Elder 2000, Molotch et al. 2005, Jost et al. 2007, Woods et al. 2006).

The greatest variation in peak SWE (CV = 1.36) occurred during 2015, a snow season characterized by early onset of melt and multiple mid-winter melt events (Table 2, Figure S1). Earlier melt and increases in the frequency of mid-winter melt are expected with climate change in the western U.S. (Lute et al. 2015). The results of this study suggest that greater variation in peak SWE could be expected in forested watersheds as climate change leads to warmer winters. Greater variation of SWE (and SDD) will have strong impacts on microclimate dynamics and key ecosystem processes such as patterns of species diversity and nutrient cycling (Vanwalleghen and Meentemeyer 2009).

Melt curves highlight the interannual variability of snow characteristics with different dates for peak SWE, fSCA at peak, and different curve shapes (Figure 5, Table S3). This is not surprising as climate exerts a first order control on annual snowpack characteristics (Lundquist et

al. 2013, Varhola et al. 2010b). A consistent pattern in SDD emerged over time, where fSCA transitioned from a steady decrease to a rapid drop. This pattern is captured in other work where the fSCA was changing by 6% in the first part of the melt season but increased to 62% midway through the melt season (Molotch et al. 2005, Elder et al. 1995, Varhola et la. 2010a). Field observations suggest that this threshold may be related to nightly low temperatures or advective warming from an increasing fraction of adjacent bare ground with a lower albedo.

Adequately capturing snow density is necessary to accurately calculate water availability as density provides the link between snow depth and water content. However, snow density is typically assumed to be much less variable than snow depth, and consequently sampled at much lower frequencies (30:1; Sturm et al. 2010). Estimates of snow water using a single average density value may misrepresent the total amount of snow water stored in a watershed (Wetlaufer et al. 2016). Our high sampling ratio of snow density to depth (2:1) at micro-scales (1-20 m), unmatched by previous studies, may contribute to the larger CV for snow density observed (0.27 – 0.45; Table 2). Using fewer samples, but at 1 m resolution, Molotch et al. (2005) observed a CV of 0.17 for snow density in the Sierra Nevada alpine. Whereas high frequency measurements taken at a larger resolution (>100 m) in the Spanish Pyrenees had a snow density CV range of 0.05-0.32 (López-Morano et al. 2013). A global analysis of peak snow densities revealed a CV range of 0.08-0.23 (Jonas et al. 2009). Greater variation in snow density at our site may be driven by stronger temperature and radiation gradients within the forest compared to more sparsely vegetated sites or due to mid-winter melt events at our lower elevation (López-Morano et al. 2013). These results emphasize the need for increased sampling to capture the variability of peak density, where even small differences in density lead to large differences in calculated SWE and predicted water output (Wetlaufer et al. 2016).

*Modelling*

Different statistical models with varying terrain and or vegetation explanatory variables have been widely used to describe the patterns in snow accumulation and ablation. Recently, the use of machine learning techniques such as random forests are being used as an alternative for increased predictive power over regression tree and linear models (Breiman 2001). Our RF models using detailed ground and LiDAR forest canopy predictors and basic terrain features explained 30% and 35% of the variation in peak SWE respectively (Table 3).

The outcome of snow distribution models depends on various environmental and data conditions. The geographic location of a study site determines the dominant winter conditions (i.e. average winter temperature) which drive forest-snow patterns and determine the prevalence of contributing factors such as wind (Lundquist et al. 2013, Dickerson-Lange et al. 2017). Catchment size is also important because the factors that control local snow dynamics function over a small range of conditions leading to better model performance in smaller watersheds (Elder 1995). Most snow modelling studies also characterize accumulation with snow depth, however the variation observed in SWE has been found to be primarily driven by the variation in depth (Balk and Elder 2000). Sample size, the type of predictors used, and the length of regression trees grown also contribute to model performance. Larger regression trees are typically able to explain more variation, but this may lead to overfitting and poor predictive power (Molotch et al. 2005).

Regression tree models using terrain features alone (e.g., slope, aspect, radiation) were able to explain 34 – 37% of the variation in peak snow depths in the alpine of the Sierra Nevada (Molotch et al. 2005). The addition of vegetation type or distance to canopy predictors to terrain features explained 17 – 68% of the variation in peak snow depth from the steep relief in Rocky

Mountain National Park to the alpine of New Mexico and the flatter forests of the Colorado Front Range (Balk and Elder 2000, Erxleben et al. 2002, Musselmann et al. 2008, Elder et al. 1995). Using both ground and LiDAR based canopy metrics consistent with ours, with multiple linear regression, Varhola et al. (2010a) found models with LiDAR metrics explained 51% of variation while ground based canopy metrics explained only 25% of the variation in peak SWE in the boreal forests of British Columbia.

Although these studies provide context for our results, they differ in important ways. This study involved random forest modelling of high resolution snow measurements within a small, fully forested site on gentle topography. The relatively flat nature of our site may have eliminated some of the more complex terrain interactions, as terrain features were not prominent drivers in our models (Figure 7). The smaller extent of our study area may also potentially alter the relationships observed between snow distribution and predictors due to the resolution of controlling factors (Molotch et al. 2005, Elder 1995).

Variables related to the amount, size, and location of neighboring trees were most important for predicting SWE and SDD (Figure 7). Overlapping variables for peak SWE and disappearance suggest that these hydrologic processes are driven by the same principles. This is consistent with studies that found a similar effect on snow accumulation and melt processes following changes to forest structure (Anderson and Gleason 1960, Hardy et al. 1998, McGuaghey and Farnes 2001, Jost et al. 2007). Our study predictors explained more variation in SDD than peak accumulation suggesting that there is more variation in the factors influencing accumulation processes that may not be captured by our current understanding. Further research is needed into identify these additional mechanisms.

The predictive power of forest canopy metrics affirms the long-standing observation that forest vegetation is a strong secondary driver of variation in snow accumulation and melt patterns (Varhola et al. 2010a, b). Decreasing SWE with increases in tree density and Hegyi index is consistent with the interception hypothesis where variation in peak SWE is primarily driven by overhead interception capacity (Martin et al. 2015, Dickerson-Lange et al. 2017, Schneider et al. 2019). Using ground and LiDAR predictors, Varhola et al. 2010a also found LiDAR derived canopy cover, equivalent to our canopy density, was the best predictor of the distribution of SWE.

The positive relationship between disappearance date and tree density from 10 to 32 neighborhood trees (Figure 9) is not supported by the literature or field observations. (Dickerson-Lange et al. 2016; Varhola et al. 2010a, Lundquist et al. 2013). However, the highest density areas (> 32 trees) were associated with the latest snow disappearance dates. This later portion of this relationship is likely due to thickets of the smallest trees which have low interception efficiency and provide deep shade retarding melt. The relationship between mean tree height and SDD within the LiDAR model add further support. When the local neighborhood is composed of trees less than 5 m tall final snow disappearance occurs later. These observations are consistent with disappearance dynamics in dense regeneration neighborhoods (Schneider et al. 2019).

Melt dynamics are primarily driven by the amount of available energy (Lawler and Link 2011). In early spring sun angles are still low and the radiation balance is dominated by air temperature (i.e., longwave radiation; Lundquist et al. 2013). Under these conditions bole heating, and the radiation attenuation of forest structures in general, strongly influence below canopy ablation processes by controlling energy availability (Musselman et al. 2012, Bohren et al. 1973, Link and Marks 1999, Davis et al. 1997). An early melt season (February – April) and

the primary importance of canopy metrics in our snow disappearance models is explained and supported by these previous findings. The absence of our radiation predictor variable which quantifies incoming shortwave radiation adds further evidence to the dominance of longwave radiation as the mechanistic driver of observed melt dynamics.

*Larix,* a deciduous conifer, was also important for estimating peak SWE. The importance of *Larix* in modeling the distribution of snow accumulation is expected with reduced interception capacity in the winter during times of foliage loss, however little research on *Larix*-snow dynamics is available (Schneider et al. 2019). The global extent of *Larix*, the potential importance of their unique biophysical feedbacks with snow accumulation and melt for global climate, and their susceptibility to climate change highlight the importance of this circumboreal genus for future empirical research and the incorporation of functional traits (deciduousness) in linked vegetation-earth system models.

Little to no variation in peak snow density was explained by canopy structure or terrain metrics (Figure 4 & 6, Table 3). The importance of SWE, radiation, and slope as predictor variables for explaining some variation in ground density models ($R^2 = 0.05$, Figure 6) is consistent with current research and hydrologic theory, where increases in radiation and the weight of overlying snow causes compaction and greater density (Figure 10; Sturm et al. 2010, Jonas et al. 2013, López-Morano et al. 2013, Bormann et al. 2013, Kojima et al. 1967, Molotch et al. 2005, Balk and Elder 2000, Wetlaufer et al. 2016, Svoma 2011). However, these same predictors were unable to explain any variation when paired with LiDAR canopy metrics.

Unlike our models, Broxton et al. (2019) was able to explain 30% of density patterns using topographic and canopy features with a neural network, an alternative machine learning approach. Multiple linear regression (MLR) and regression tree (RT) techniques were also more

successful at predicting snow density than our RF approach. Radiation and elevation were used to describe 39% (MLR) and 41% (RT) of variation in snow density in southwestern Montana (Wetlaufer et al. 2016), while radiation and slope only captured 10% (RT) of the spatial distribution of snow density in the Sierra Nevada (Molotch et al. 2005). Poor model performance may be attributed to our much larger sample size capturing a fuller range of variation. Our choice of variables also did not fully account for all unique combinations or interactions between potentially important physiographic parameters like the temporal variability in temperature and precipitation and their interactions with forest structural components.

Ground and LiDAR derived metrics produced RF models that performed equally well in predicting SWE and SDD. This suggests that the elements of structural complexity captured by LiDAR metrics characterizing the arrangement and density of canopy cover are related to snow interception and ablation processes. We expected LiDAR data to perform better than ground metrics, as observed by Varhohla et al. (2010a), since the biomass of the canopy directly over snow sampling points intercepting incoming snowfall and reflecting radiation, is also reflecting laser pulses. Whereas the position of tree boles does not always correspond to direct overhead canopy biomass due to tree lean, no accounted for by our ground based measurements (Wiggins et al. 2019). In addition, ground surveys captured only overstory trees (≥ 10 cm), while LiDAR captured all forest biomass above 2 m, including dense areas of regenerating saplings.

The comparison between ground and LiDAR metrics also inadvertently examined the role of tree density based metrics to canopy cover attributes as the source of better predictive outcomes for snow dynamics. Ground based predictors used metrics calculated from stem size, functional traits (evergreen conifers vs. deciduous *Larix*) and location; while LiDAR metrics described the vertical and horizonal distribution of canopy cover. The equal model performance

and generally low correlation of ground and LiDAR predictor variables (Figure S3) suggest that these contrasting vegetation measurements are capturing different mechanisms through which vegetation influences snow characteristics.

## Conclusions

Our results emphasize the importance of forest canopy structure on the processes of snow accumulation and ablation. The presence of overlapping predictors between accumulation and snow disappearance implies that the same factors are driving these linked processes (Anderson and Gleason 1960, Hardy et al. 1998, McCaughey and Farnes 2001). Previous research indicates a clearer delineation between controlling factors with snow accumulation driven by canopy interception, and snow disappearance driven by the energy balance than we found in this study, especially in relation to snow disappearance (Dickerson-Lange et al 2017, Schneider et al. 2019). Our inability to explain observed variation of snow density means we still have an incomplete understanding of controlling physical processes and interactions. Our study highlights the need for further investigation into the most accurate and efficient variables that capture the most important processes influencing the spatial distribution of snow accumulation and ablation. Climate change is already having an impact in these environments so being able to accurately predict the amounts and location of snowpack, and the melt dynamics under a range of winter conditions, is needed to forecast water resource availability.

### *Management Implications*

Climate change is contributing to winter conditions and snow characteristics beyond the range of long-term averages. In this context it is important to develop predictive models that accurately estimate snowpack characteristics and account for vegetation heterogeneity at management relevant scales (Musselmann et al. 2008). Existing research already supports the use

of LiDAR a primary data source for canopy metrics (Kane et al. 2011, 2013, Asner et al. 2013). The superior performance of LiDAR canopy metrics for predicting snow properties found by Varhola et al. (2010a) and the near equivalent model performance between ground and LiDAR derived canopy metrics of this study for estimating snow accumulation and ablation further emphasize the importance of LiDAR as a management tool. The use of LiDAR derived forest canopy metrics with predictive models such as ours offers managers a quick, affordable, and repeatable method for estimating snow characteristics that are critical for forecasting the timing and quantity of water availability (Kane et al. 2013). Models such as ours may also be used to help estimate alterations in snow controlled hydrologic processes following changes in the forest canopy structure.

**References**


Altmann A, Toloşi L, Sander O, Lengauer T. 2010. Permutation importance: a corrected feature importance measure. Bioinformatics 26:1340–1347.

Asner, G., Kellner, J., Kennedy-Bowdoin, T., Knapp, D., Anderson, C., & Martin, R. 2013. Forest canopy gap distributions in the Southern Peruvian Amazon. Plos One, 8(4), e60875.

Baddeley, A., Rubak, E. and Turner, R. 2015. Spatial Point Patterns: Methodology and Applications with R. Chapman and Hall/CRC Press.

Bales, R. C., N. P. Molotch, T. H. Painter, M. D. Dettinger, R. Rice, and J. Dozier. 2006. Mountain hydrology of the western United States. Water Resources Research, 42(8): W08432.

Balk, B. and Elder, K., 2000. Combining binary decision tree and geostatistical methods to estimate snow distribution in a mountain watershed. Water Resources Research, 36(1): 13-26.

Bates, D., Mächler, M., Bolker, B. and Walker, S. 2015. Fitting linear mixed-effects models using lme4. Journal of Statistical Soft-ware, 67(1): 48. DOI: 10.18637/jss.v067.i01.

Bohren, C.F. and Thorud, D.B. 1973. Two theoretical models of radiation heat transfer between forest trees and snowpacks. Agricultural Meteorology, 11: 3-16.

Breiman L, Cutler A. 2003. Setting up, using, and understanding Random Forests v4.0. [online] URL: http://www.stat.berkeley.edu/users/breiman/rf.html.

Breiman L, Freidman J, Olshen R, Stone C. 1984. Classification and regression trees. Belmont (CA): Wadsworth, 358 p.

Conrad, O., Bechtel, B., Bock, M., Dietrich, H., Fischer, E., Gerlitz, L., Wehberg, J., Wichmann, V., and Böhner, J. 2015. System for Automated Geoscientific Analyses (SAGA) v. 2.1.4, Geosci. Model Dev., 8, 1991-2007, doi:10.5194/gmd-8-1991-2015.

Contreras, M.A., Affleck, D. and Chung, W. 2011. Evaluating tree competition indices as predictors of basal area increment in western Montana forests. Forest Ecology and Management, 262(11):1939-1949.

Carroll, S.S. and Cressie, N. 1996. A Comparison of Geostatistical Methodologies Used to Estimate Snow Water Equivalent 1. JAWRA Journal of the American Water Resources Association, 32(2): 267-278.

Deems, J.S., Painter, T.H. and Finnegan, D.C. 2013. Lidar measurement of snow depth: a review. J. Glaciology, 59(215): 467-479.

Dickerson-Lange, S.E., Gersonde, R.F., Hubbart, J.A., Link, T.E., Nolin, A.W., Perry, G.H., Roth, T.R., Wayand, N.E. and Lundquist, J.D. 2017. Snow disappearance timing is dominated by forest effects on snow accumulation in warm winter climates of the Pacific Northwest, United States. Hydrological Processes, 31(10):1846-1862.

Dickerson-Lange, S.E., Lutz, J.A., Gersonde, R., Martin, K.A., Forsyth, J.E., Lundquist, J.D. 2015. Observations of distributed snow depth and snow duration within diverse forest structures in a maritime mountain watershed. Water Resources Research, 51 (11): 9353–9366.

Elder, K., Rosenthal, W. and Davis, R.E., 1998. Estimating the spatial distribution of snow water equivalence in a montane watershed. Hydrological Processes, 12(10-11): 1793-1808.

Elder, K., Michaelsen, J., Dozier, J. 1995. Small basin modeling of snow water equivalence using binary regression tree methods. In Biogeochemistry of Seasonally Snow-Covered Catchments. [Ed.] Tonnessent, K.A., IAHS Publishing, 228: 129-139.

Erxleben, J., Elder, K. and Davis, R. 2002. Comparison of spatial interpolation methods for estimating snow distribution in the Colorado Rocky Mountains. Hydrological Processes, 16(18): 3627-3649.

Frazer, G.W., Magnussen, S., Wulder, M.A., Niemann, K.O. 2011. Simulated impact of sample plot size and co-registration error on the accuracy and uncertainty of LiDAR derived estimates of forest stand biomass. Remote Sens. Environ. 115, 636–649.

Harpold, A.A., Guo, Q., Molotch, N., Brooks, P.D., Bales, R., Fernandez-Diaz, J.C., Musselman, K.N., Swetnam, T.L., Kirchner, P., Meadows, M.W. and Flanagan, J. 2014. LiDAR-derived snowpack data sets from mixed conifer forests across the Western United States. Water Resources Research, 50(3): 2749-2755.

Hopkinson, C., Chasmer, L., Young-Pow, C. and Treitz, P., 2004. Assessing forest metrics with a ground-based scanning lidar. Canadian Journal of Forest Research, 34(3): 573-583.

Hubbart, J.A., Link, T.E., Gravelle, J.A. 2015. Forest canopy reduction and snowpack dynamics in a northern Idaho watershed of the continental-maritime region, United States. Forest Science, 61 (5): 882–894.

Jeronimo, S.M., Kane, V.R., Churchill, D.J., McGaughey, R.J. and Franklin, J.F. 2018. Applying LiDAR individual tree detection to management of structurally diverse forest landscapes. Journal of Forestry, 116(4): 336-346.

Kane, V.R., Bakker, J.D., McGaughey, R.J., Lutz, J.A., Gersonde, R.F. and Franklin, J.F., 2010a. Examining conifer canopy structural complexity across forest ages and elevations with LiDAR data. Canadian Journal of Forest Research, 40(4): 774-787.

Kane, V.R., Gersonde, R.F., Lutz, J.A., McGaughey, R.J., Bakker, J.D. and Franklin, J.F., 2011. Patch dynamics and the development of structural and spatial heterogeneity in Pacific Northwest forests. Canadian Journal of Forest Research, 41(12): 2276-2291.

Kane, V.R., Lutz, J.A., Roberts, S.L., Smith, D.F., McGaughey, R.J., Povak, N.A. and Brooks, M.L., 2013. Landscape-scale effects of fire severity on mixed-conifer and red fir forest structure in Yosemite National Park. Forest Ecology and Management, 287: 7-31.

Kane, V.R., McGaughey, R.J., Bakker, J.D., Gersonde, R.F., Lutz, J.A. and Franklin, J.F. 2010b. Comparisons between field-and LiDAR-based measures of stand structural complexity. Canadian Journal of Forest Research, 40(4): 761-773.

Kostadinov, T.S., Schumer, R., Hausner, M., Bormann, K.J., Gaffney, R., McGwire, K., Painter, T.H., Tyler, S. and Harpold, A.A. 2019. Watershed-scale mapping of fractional snow cover under conifer forest canopy using lidar. Remote Sensing of Environment, 222: 34-49.

Lawler, R. R., and T. E. Link. 2011. Quantification of incoming all-wave radiation in discontinuous forest canopies with application to snowmelt prediction. Hydrological Processes 25(21):3322-3331.

López-Moreno, J.I., Fassnacht, S.R., Heath, J.T., Musselman, K.N., Revuelto, J., Latron, J., Morán-Tejeda, E. and Jonas, T. 2013. Small scale spatial variability of snow density and depth over complex alpine terrain: Implications for estimating snow water equivalent. Advances in Water Resources, 55: 40-52.

Link, T.E. and Marks, D. 1999. Point simulation of seasonal snow cover dynamics beneath boreal forest canopies. Journal of Geophysical Research: Atmospheres, 104(D22): 27841-27857.

Lundquist, J.D., Dickerson-Lange, S.E., Lutz, J.A. and Cristea, N.C. 2013. Lower forest density enhances snow retention in regions with warmer winters: A global framework developed

from plot-scale observations and modeling. Water Resources Research, 49(10): 6356-6370.
Lute, A. C., J. T. Abatzoglou, K. C. Hegewisch. 2015. Projected changes in snowfall extremes and interannual variability of snowfall in the Western United States. Water Resources Research 51:960–972.
Maher, C. T., E. Oja, A. Marshall, M. Cunningham, L. Townsend, G. Worley-Hood, L. Robinson, T. Margot, D. Lyons, S. Fety, E. E. Schneider, S. M. A. Jeronimo, D. J. Churchill, A. J. Larson. 2019. Real-time monitoring with a tablet app improves implementation of treatments to enhance forest structural diversity. Journal of Forestry, DOI: 10.1093/jofore/fvz003.
Martin, K. A., J. T. Van Stan II, S. E. Dickerson-Lange, J. A. Lutz, J. W. Berman, R. Gersonde, and J. D. Lundquist. 2013. Development and testing of a snow interceptometer to quantify canopy water storage and interception processes in the rain/snow transition zone of the North Cascades, Washington, USA. Water Resources Research 49:3243-3256.
McGaughey, R.J., 2015. FUSION v3.5. USDA Forest Service, Pacific Northwest Research Station, Olympia, WA. http://forsys.cfr.washington.edu/.
Molotch, N.P. and Bales, R.C., 2005. Scaling snow observations from the point to the grid element: Implications for observation network design. Water Resources Research, 41(11).
Moran, C.J., Rowell, E.M. and Seielstad, C.A. 2018. A data-driven framework to identify and compare forest structure classes using LiDAR. Remote Sensing of Environment, 211: 154-166.
Moeser, D., Morsdorf, F. and Jonas, T. 2015. Novel forest structure metrics from airborne LiDAR data for improved snow interception estimation. Agricultural and forest meteorology, 208: 40-49.
Musselman, K.N., Molotch, N.P., Margulis, S.A., Kirchner, P.B., Bales, R.C., 2012. Influence of canopy structure and direct beam solar irradiance on snowmelt rates in a mixed conifer forest. Agriculture and Forest Meteorology. 161, 46–56.
Musselman, K.N., Molotch, N.P. and Brooks, P.D. 2008. Effects of vegetation on snow accumulation and ablation in a mid-latitude sub-alpine forest. Hydrological Processes: An International Journal, 22(15): 2767-2776.
Næsset, E., 2002. Predicting forest stand characteristics with airborne scanning laser using a practical two-stage procedure and field data. Remote Sensing of Environment, 80: 88–99.
Nolan, M., Larsen, C.F. and Sturm, M. 2015. Mapping snow-depth from manned-aircraft on land scape scales at centimeter resolution using Structure-from-Motion photogrammetry. Cr yosphere Discussions, 9(1).
Prasad, A.M., Iverson, L.R. and Liaw, A. 2006. Newer classification and regression tree techniqu es: bagging and random forests for ecological prediction. Ecosystems, 9(2): 181-199.
R Core Team (2017). R: A language and environment for statistical computing. R Foundation for Statistical Computing, Vienna, Austria. URL https://www.R-project.org/.
Schneider, E.E., Affleck, L.R., and Larson, A.J. 2019. Tree spatial patterns modulate peak snow accumulation and snow disappearance. Forest Ecology and Management 441: 9-19.
Schneider, E. E., A. J. Larson, and K. G Jencso. 2015. The influence of a heterogeneous mixed-conifer canopy on snow accumulation and melt. *In* 83rd Annual Western Snow Conference. Grass Valley, CA.

Storck, P., D. P. Lettenmaier, and S. M. Bolton. 2002. Measurement of snow interception and canopy effects on snow accumulation and melt in a mountainous maritime climate, Oregon, United States. Water Resources Research 38(11):1223.

Sturm, M., Taras, B., Liston, G.E., Derksen, C., Jonas, T. and Lea, J. 2010. Estimating snow water equivalent using snow depth data and climate classes. Journal of Hydrometeorology, 11(6): 1380-1394.

Svoma, B. M. 2011. Winter Climatic Controls on Spring Snowpack Density in the Western United States. Arctic, Antarctic, and Alpine Research, 43(1): 118-126.

Tinkham, W.T., Smith, A.M., Marshall, H.P., Link, T.E., Falkowski, M.J. and Winstral, A.H. 2014. Quantifying spatial distribution of snow depth errors from LiDAR using Random Forest. Remote sensing of environment, 141: 105-115.

Trujillo, E., Molotch, N.P., Goulden, M.L., Kelly, A.E. and Bales, R.C. 2012. Elevation-dependent influence of snow accumulation on forest greening. Nature Geoscience, 5(10): 705.

Uhlmann, Z., Glenn, N.F., Spaete, L.P., Hiemstra, C., Tennant, C. and McNamara, J., 2018, July. Resolving the Influence of Forest-Canopy Structure on Snow Depth Distributions with Terrestrial Laser Scanning. In IEEE International Geoscience and Remote Sensing Symposium, IEEE: 6284-6286.

Vanwalleghem, T. and Meentemeyer, R. K. 2009. Predicting forest microclimate in heterogeneous landscapes. Ecosystems, 12(7): 1158-1172.

Varhola, A., Coops, N.C., Bater, C.W., Teti, P., Boon, S. and Weiler, M. 2010a. The influence of ground-and lidar-derived forest structure metrics on snow accumulation and ablation in disturbed forests. Canadian Journal of Forest Research, 40(4): 812-821.

Varhola, A., N. C. Coops, M. Weiler, and R. D. Moore. 2010b. Forest canopy effects on snow accumulation and ablation: an integrative review of empirical results. Journal of Hydrology 392:219-233.

Valbuena, R., Maltamo, M., Mehtatalo, L., Packalen, P. 2017. Key structural features of boreal forests may be detected directly using L-moments from airborne lidar data. Remote Sensing of Environment, 194: 437–446.

Walker, D.A., Halfpenny, J.C., Walker, M.D. and Wessman, C.A. 1993. Long-term studies of snow-vegetation interactions. BioScience, 43(5): 287-301.

Wetlaufer, K., Hendrikx, J. and Marshall, L. 2016. Spatial heterogeneity of snow density and its influence on snow water equivalence estimates in a large mountainous basin. *Hydrology*, *3*(1): 3.

Wiggins, H.L., Nelson, C.R., Larson, A.J. and Safford, H.D., 2019. Using LiDAR to develop high-resolution reference models of forest structure and spatial pattern. Forest ecology and management, 434: 318-330.

Winkler, R.D. and Moore, R.D. 2006. Variability in snow accumulation patterns within forest stands on the interior plateau of British Columbia, Canada. *Hydrological Processes*, 20: 3683-3695.

Winstral, A., Elder, K. and Davis, R.E., 2002. Spatial snow modeling of wind-redistributed snow using terrain-based parameters. Journal of hydrometeorology, 3(5): 524-538.

Woods, S.W., Ahl, R., Sappington, J., McCaughey, W. 2006. Snow accumulation in thinned lodgepole stands, Montana, USA. Forest Ecology and Management, 235: 202-211.

Zheng, Z., Kirchner, P.B., Bales, R.C. 2016. Topographic and vegetation effects on snow accumulation in the southern Sierra Nevada: a statistical summary from lidar data. Cryosphere 10 (1): 257–269.

## Tables

**Table 1.** Canopy structure predictor variables used in regression analysis with snow accumulation and disappearance. Radius indicates the radial distance of a circular around each sampling point the given variable was calculated within listed for SWE, density, SDD. Range (obsv.) is the range of values observed within the given radius.

| Source | Variable (Abbreviation) | Units | Radius (m) | Range (obsv.) | Description |
|---|---|---|---|---|---|
| **Ground** | Density (t.den) | count | 15, 4, 15 | 2 - 55 \| 0 - 11 | Total number of trees within the given radius. |
| | Larch (Abs.LAOC) | count | 15, 4, 15 | 0 - 29 \| 0 - 7 | Total number of western larch within the given radius. Describes the species compositions |
| | Intermediate (Abs.intermed) | count | 15, 4, 15 | 0 - 25 \| 0 - 7 | Total number of trees in the intermediate strata. Describes the density of the lowest canopy layer. |
| | Codominant (Abs.codom) | count | 15, 4, 15 | 0 - 38 \| 0 - 6 | Total number of trees in the codominant strata. Describes the density of the middle canopy layer. |
| | Dominant (Abs.dom) | count | 15, 4, 15 | 0 - 15 \| 0 - 4 | Total number of trees in the dominant strata. Describes the density of the tallest canopy layer. |
| | Hegyi index (Hegyi) | None (index) | 15, 4, 15 | 1.11 - 163.14 \| 0 - 156.167 | $\sum_{i=1}^{n} {d_i}/{(d \times dist_{i})}$ Competition index based on size and distance of neighboring trees (Contreras et al. 2011). Focal point given a 10 cm diameter. |
| | Sum Nearest Neighbor (NN.Sum) | meters | 15, 4, 15 | 0 - 2604.02 \| 0 - 445.09 | Total of the distance transformed nearest neighbor pattern of trees with in the given radius. |
| | Slope | % | point | 0 - 21.6 | Steepness of the ground surface. |
| | Aspect | degrees | point | 0 - 360 | Direction of sun exposure, influencing temperature. |

| | | | | | |
|---|---|---|---|---|---|
| **LiDAR** | Mean Height (mean.ht) | meters | 3, 3, 4 | 0.02 - 22.88 \| 0.02 - 20.3 | Average value of height returns. |
| | Standard deviation (SD) | meters | 2, 3, 2 | 0 - 6.37 \| 0 - 6.46 | 2nd L-moment: standard deviation of height returns. Describes vertical canopy complexity. |
| | Coefficient of Variation of Height (CV) | None (ratio) | 4, 6, 6 | 0.17 - 0.94 \| 0.25 - 0.94 | Coefficient of variation of height returns. A normalizes metric of vertical canopy complexity. |
| | Skewness (skew) | None (ratio) | 4, 4, 5 | -0.39 - 0.95 | Ratio of 3rd/2nd L-moments. Describes the symmetry of the height distribution; bottom or top-loading. |
| | Kurtosis (Kurt.) | None (ratio) | 2, 4, 5 | -0.25 - 0.99 \| -0.21 - 0.91 \| -0.20 - 0.89 | Ratio of 4th/2nd L-moments. Describes the tailed nature of the vertical foliage distribution. |
| | 95th Percentile Height (ht.95) | meters | 2, 2, 2 | 0.04 - 32.18 | 95th percentile of height returns. |
| | 99th Percentile Height (ht.99) | meters | 2, 2, 2 | 0.04 - 32.54 | 99th percentile of height returns. Describes maximum tree height. |
| | Canopy density (CD) | % | 3, 5, 4 | 0 - 100 \| 0 - 94.7 \| 0 - 98.2 | Similar to canopy cover. The percent of first laser returns above 2 m to the total number of returns. |

**Table 2**. Snow accumulation metrics for four consecutive snow years within 3 mixed-conifer stands forming a single research site. n is sample size, CV is coefficient of variation, ± standard deviation.

| | | SITE | | PLOT 3 | | PLOT 2 | | PLOT 1 | |
|---|---|---|---|---|---|---|---|---|---|
| Year | | SWE (cm) | Density (%) | SWE (cm) | Density (%) | SWE (cm) | Density (%) | SWE (cm) | Density (%) |
| **2014** | *n* | 809 | 569 | 405 | 284 | 404 | 285 | NA | NA |
| | *CV* | 0.36 ± 0.06 | 0.28 ± 0.01 | 0.40 | 0.28 | 0.32 | 0.27 | NA | NA |
| | *average* | 8.4 ± 0.4 | 20.1 ± 1.8 | 8.7 | 21.3 | 8.1 | 18.8 | NA | NA |
| | *range* | 0 - 18.0 | 2.4 - 49.7 | 0 - 18 | 3.7 - 49.7 | 0 - 16.4 | 2.4 - 44.1 | NA | NA |
| **2015** | *n* | 2196 | 329 | 812 | 198 | 687 | 62 | 697 | 69 |
| | *CV* | 1.37 ± 0.22 | 0.33 ± 0.06 | 1.12 | 0.30 | 1.45 | 0.40 | 1.53 | 0.30 |
| | *average* | 1.1 ± 0.2 | 20.6 ± 2.5 | 1.4 | 22.9 | 1 | 17.9 | 1 | 21.1 |
| | *range* | 0 - 11.9 | 4.1 - 46.6 | 0 - 11.2 | 5.0 - 46.6 | 0 - 11.9 | 4.1 - 39.8 | 0 - 6.7 | 11.1 - 37.3 |
| **2016** | *n* | 2104 | 1349 | 744 | 396 | 699 | 498 | 661 | 455 |
| | *CV* | 0.71 ± 0.04 | 0.44 ± 0.02 | 0.74 | 0.45 | 0.74 | 0.42 | 0.67 | 0.45 |
| | *average* | 2.4 ± 0.3 | 22.7 ± 0.3 | 2.5 | 22.6 | 2.1 | 23 | 2.7 | 22.5 |
| | *range* | 0 - 14.9 | 5.5 - 85.3 | 0 - 8.7 | 5.7 - 74.6 | 0 - 9.3 | 6.0 - 74.6 | 0 - 14.9 | 5.5 - 85.3 |
| **2017** | *n* | 2214 | 1326 | 819 | 493 | 697 | 416 | 698 | 417 |
| | *CV* | 0.47 ± 0.02 | 0.31 ± 0.03 | 0.49 | 0.34 | 0.46 | 0.31 | 0.46 | 0.28 |
| | *average* | 6.2 ± 0.2 | 19.3 ± 0.6 | 6.2 | 18.6 | 6 | 19.8 | 6.4 | 19.6 |
| | *range* | 0 - 14.9 | 2.3 - 82.1 | 0 - 14.9 | 2.3 - 59.7 | 0 - 14.2 | 3.0 - 67.9 | 0 - 14.2 | 4.3 - 82.1 |

**Table 3.** Summary of RF model optimization and performance. mtry is the number of random variables selected at each split, # trees is the total number of bootstrapped trees computed for each split. The squared correlation coefficient and root means squared error is given for RF model predictions and standardized response variables using a 20 fold cross-validation. Influential variables are variables that the RF model significantly relies on for estimates.

| | | mtry | # trees | $R^2$ | RMSE |
|---|---|---|---|---|---|
| **Ground** | **SWE** | 5 | 500 | 0.30 | 0.93 |
| | **Density** | 5 | 500 | 0.05 | 0.95 |
| | **SDD** | 4 | 500 | 0.47 | 0.94 |
| **LiDAR** | **SWE** | 4 | 500 | 0.35 | 0.91 |
| | **Density** | 3 | 500 | 0.00 | 1.43 |
| | **SDD** | 3 | 500 | 0.47 | 0.91 |

## Figures

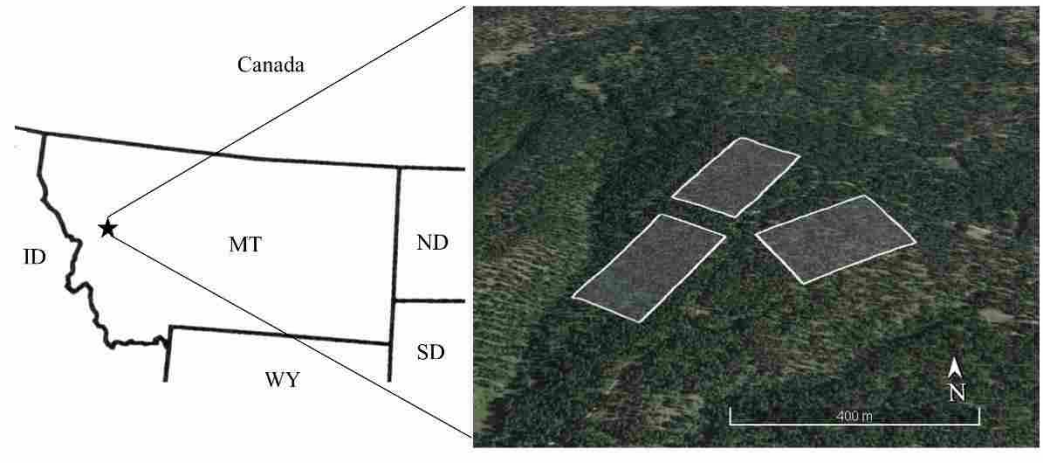


**Figure 1**. Study site located in western Montana, USA. The site is populated by a mixed-conifer forest. Three plots were installed to aid in stem mapping and avoid a centrally bisecting road.

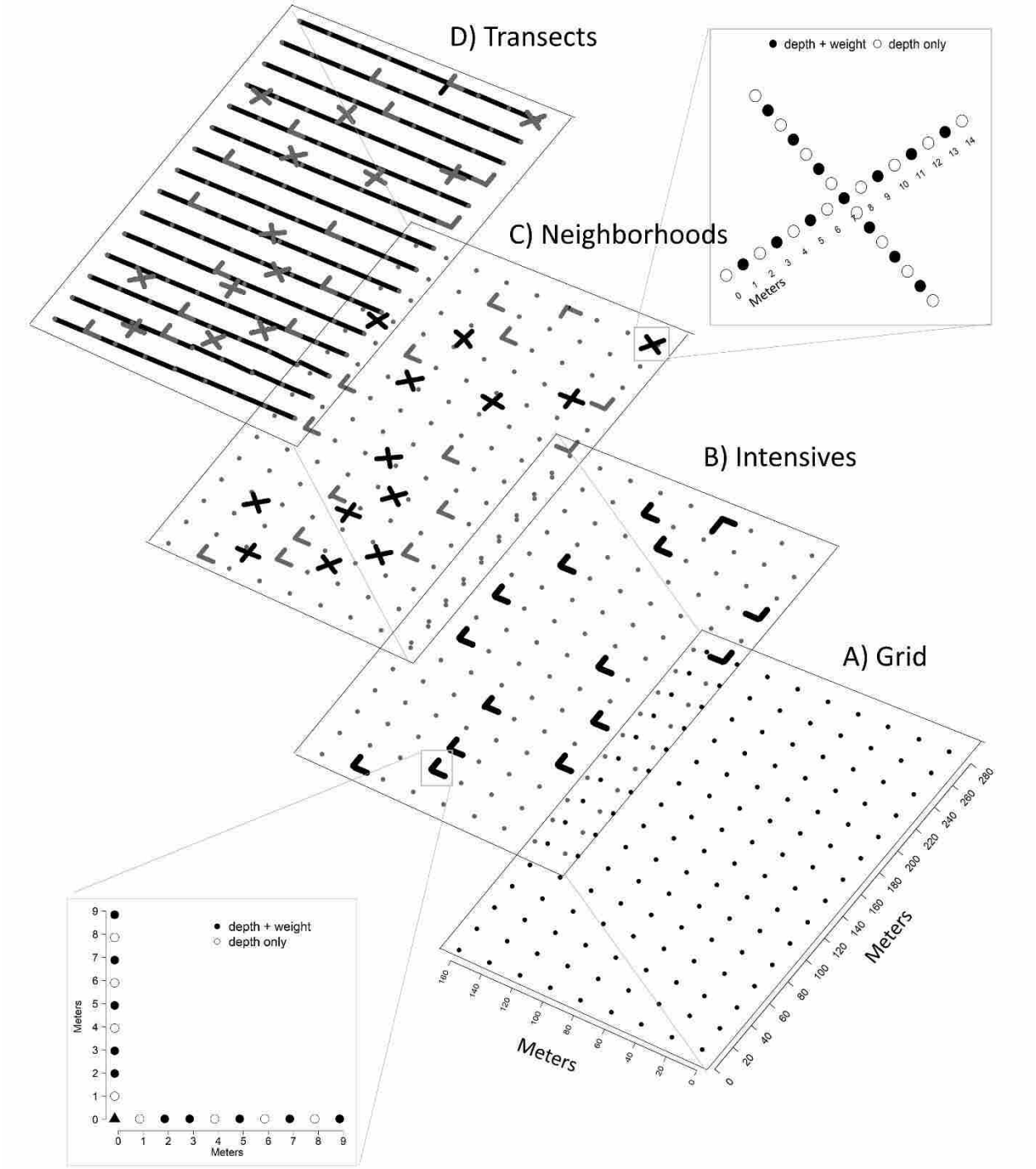


**Figure 2.** Snow sampling diagram. Point sampling layers were added progressing from A-D in each plot. Snow depth and density was measured at all points in layer A. In layers B and C snow depth was collected at all points and depth + weight was collected at every other point along each intensive (layer B bottom highlight) and neighborhood (layer C top highlight) to yield snow density. Snow disappearance was measured at all points in layers A-D.

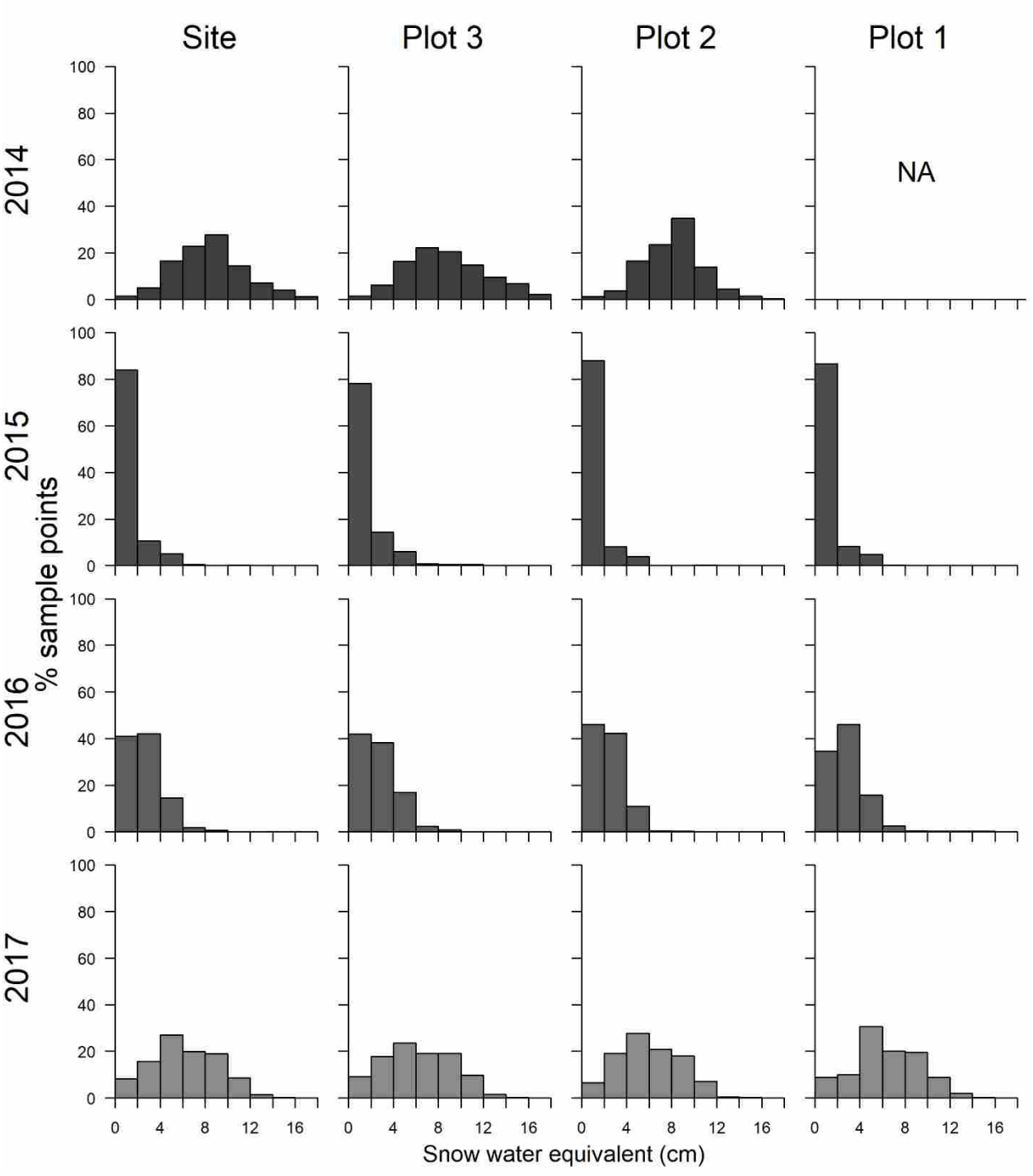


**Figure 3.** Distribution of peak snow water equivalent as % of points from 2014 – 2017 across a mixed-conifer forest. SWE is in 2 cm size classes.

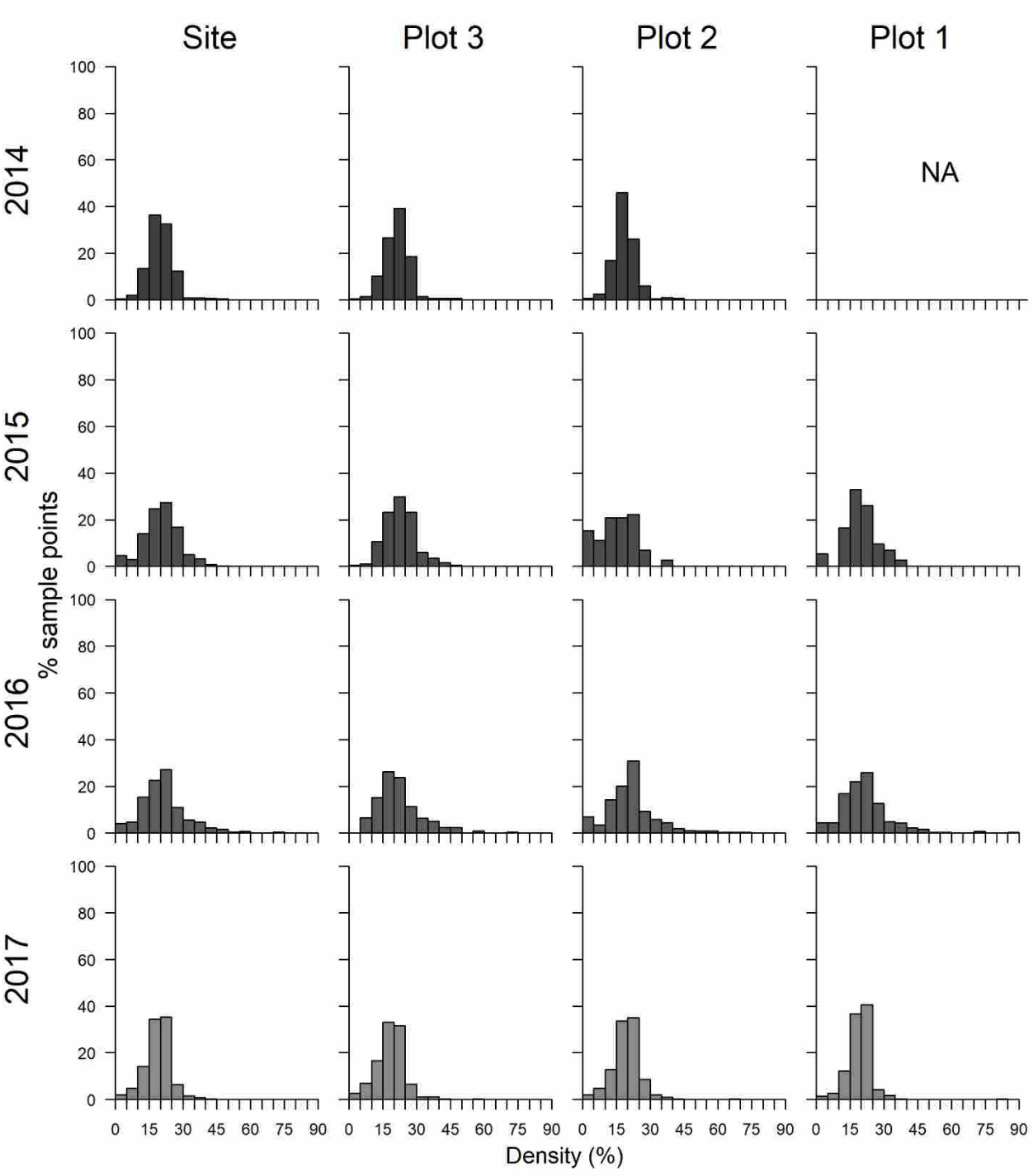


**Figure 4.** Distribution of peak snow density as % of points from 2014 – 2017 across a mixed-conifer forest. Density is in 5% size classes.

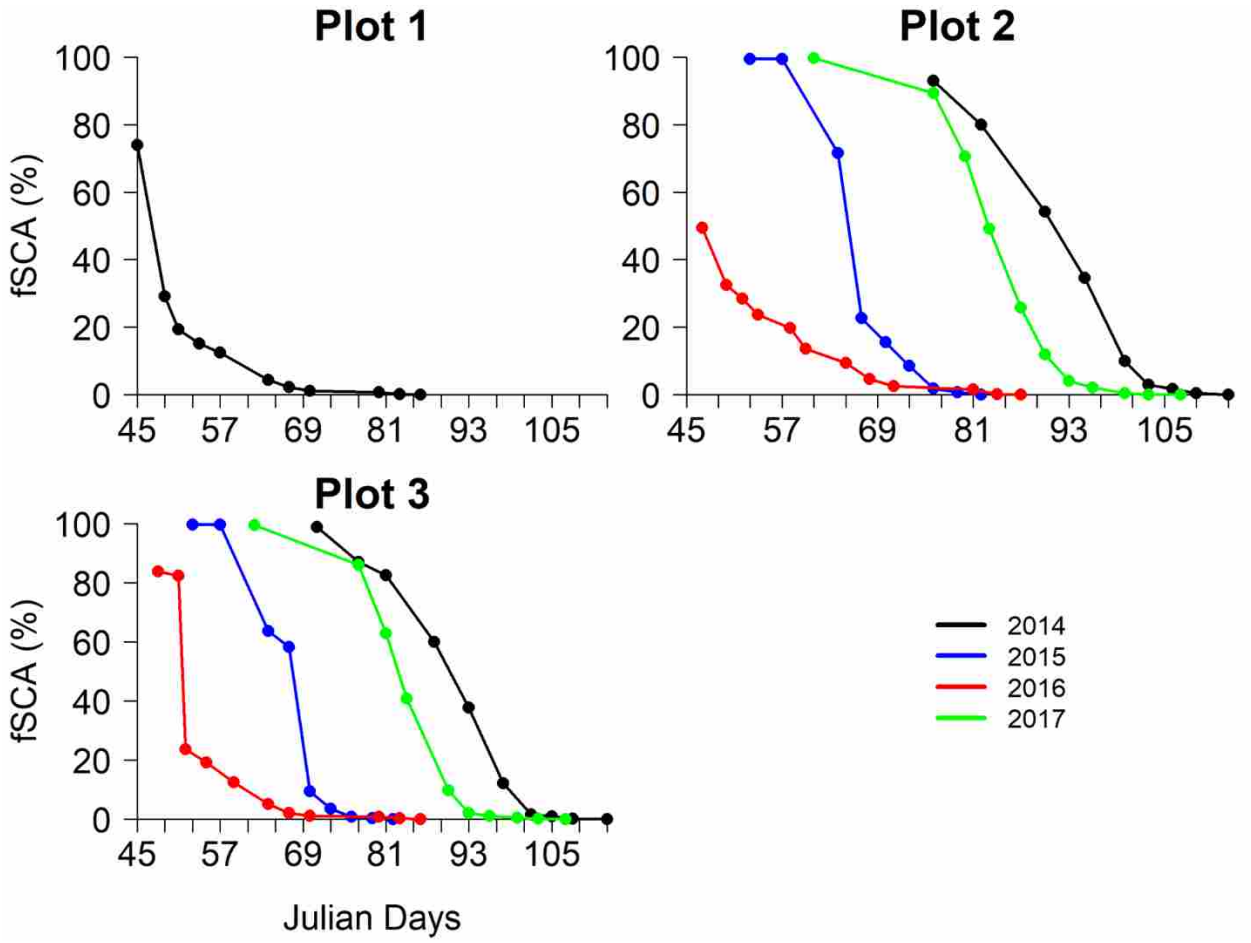


**Figure 5.** Melt curves across four different snow seasons. fSCA is the percentage of sample points with snow cover remaining for each given day.

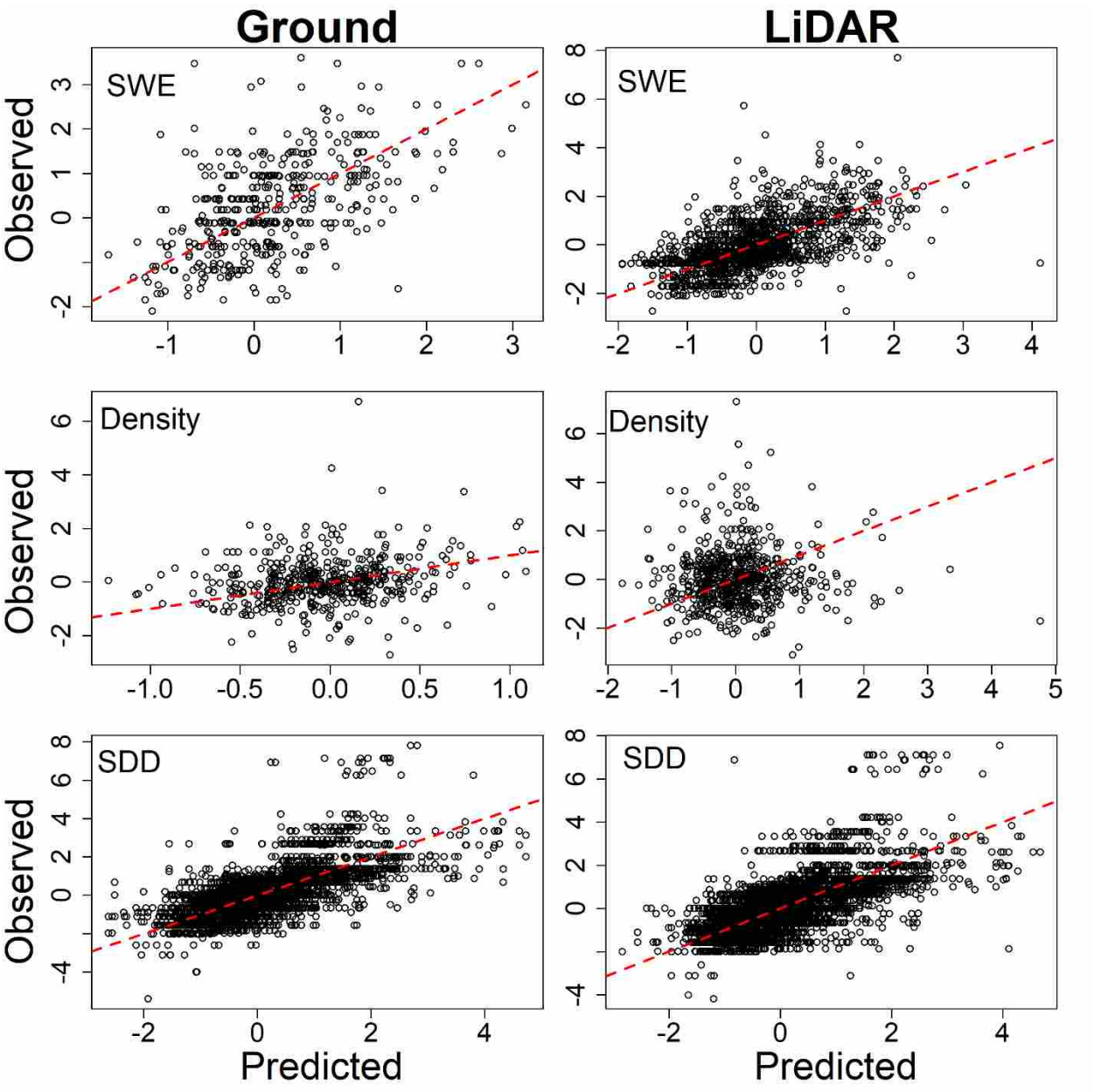


**Figure 6.** Fit for random forest models of snow characteristics using ground and lidar based canopy predictors. Response variables have been normalized by year. The dashed line is a 1:1 line indicating perfect model fit.

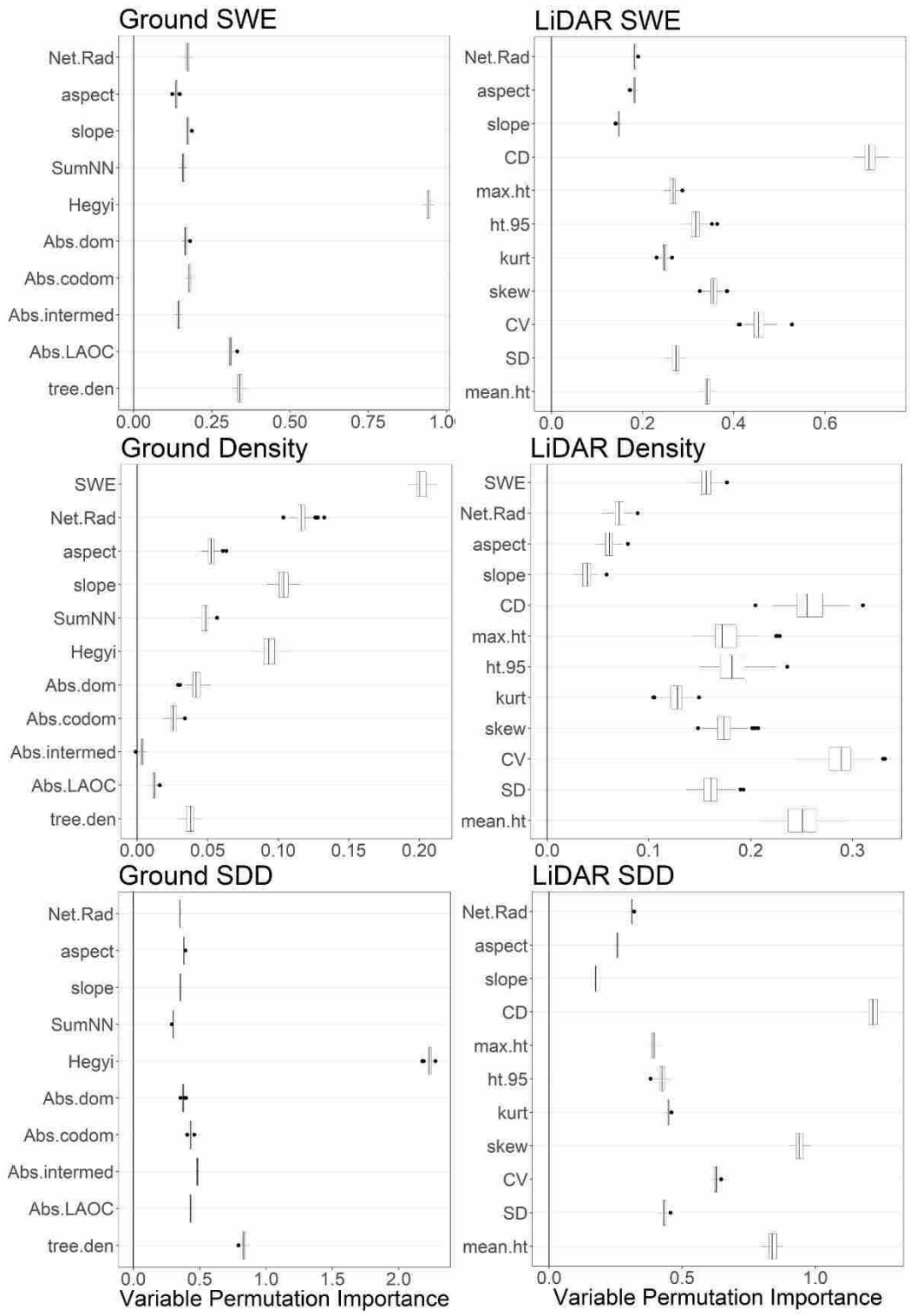


**Figure 7.** The marginal permutation importance for ground and LiDAR predictor variables for SWE, snow density, and SDD. learning. Central vertical lines display the mean increase in model accuracy from 100 random permutation of the variable. Variables below the solid zero line do not contribute to model performance.

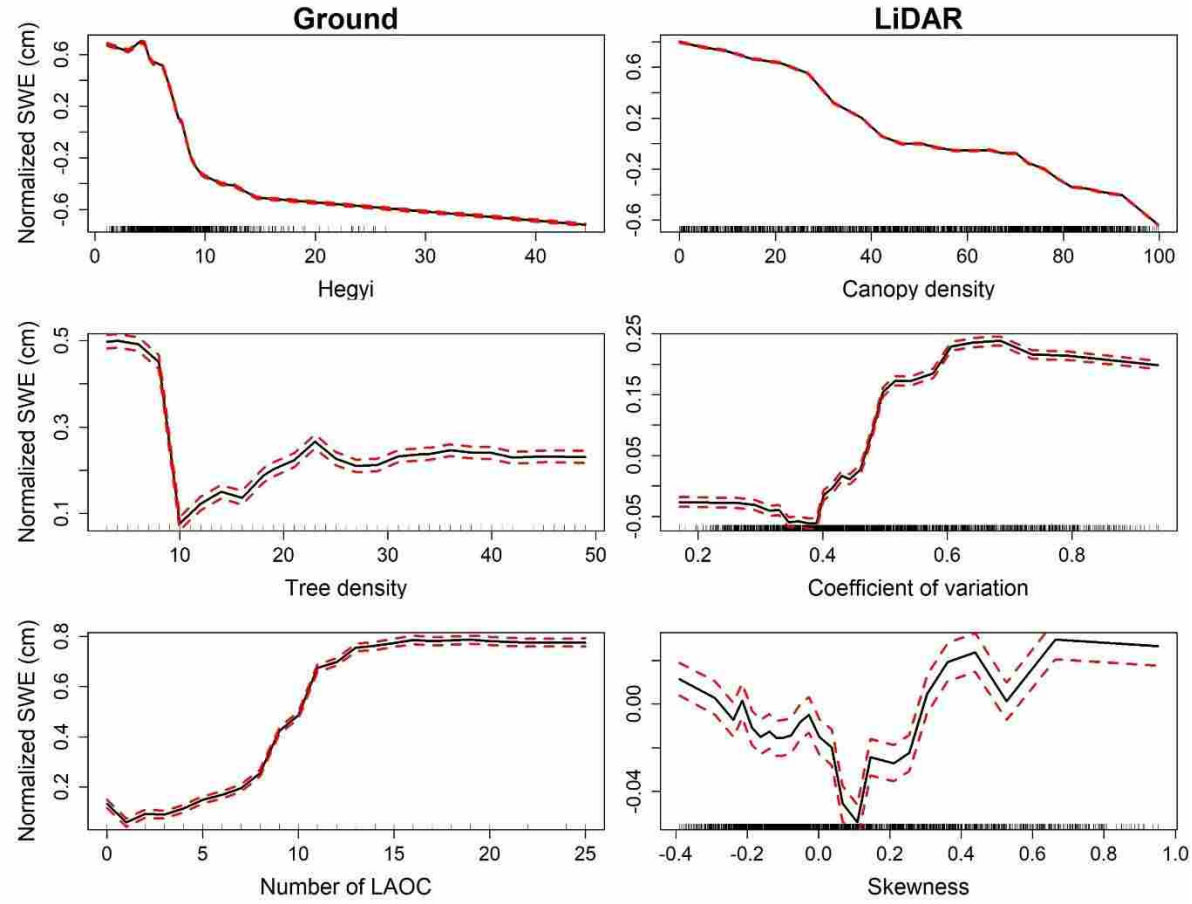


**Figure 8.** Partial dependency plot of the marginal effects of significantly important of forest canopy predictors on the estimates of SWE from a RF model. Rug plots indicate the distribution of predictions. Dashed lines enclose a 95% confidence interval. Response variables are normalized by year.

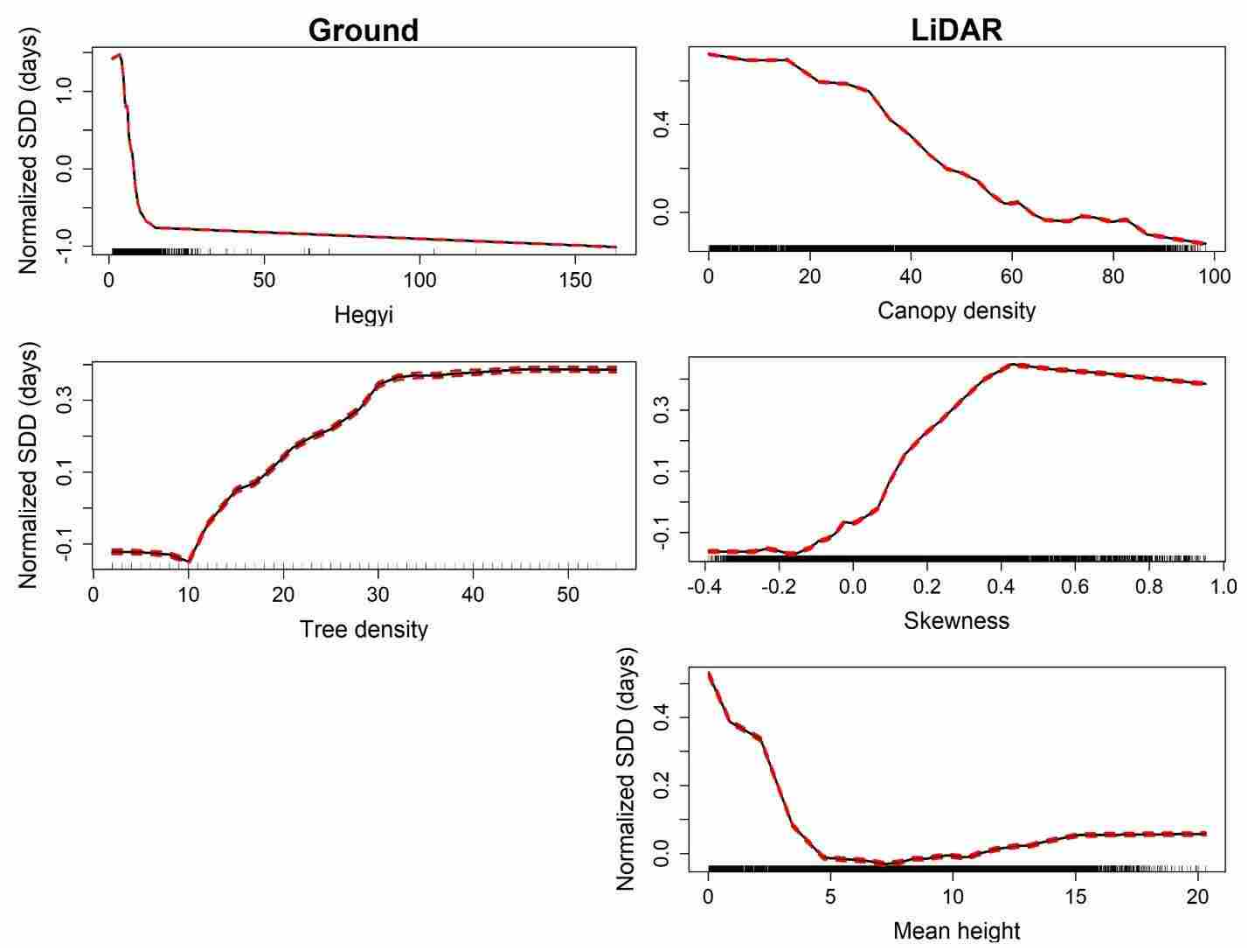


**Figure 9.** Partial dependency plot of the marginal effects of significantly important of forest canopy predictors on the estimates of SDD from a RF model. Rug plots indicate the distribution of predictions. Dashed lines enclose a 95% confidence interval. Response variables are normalized by year.

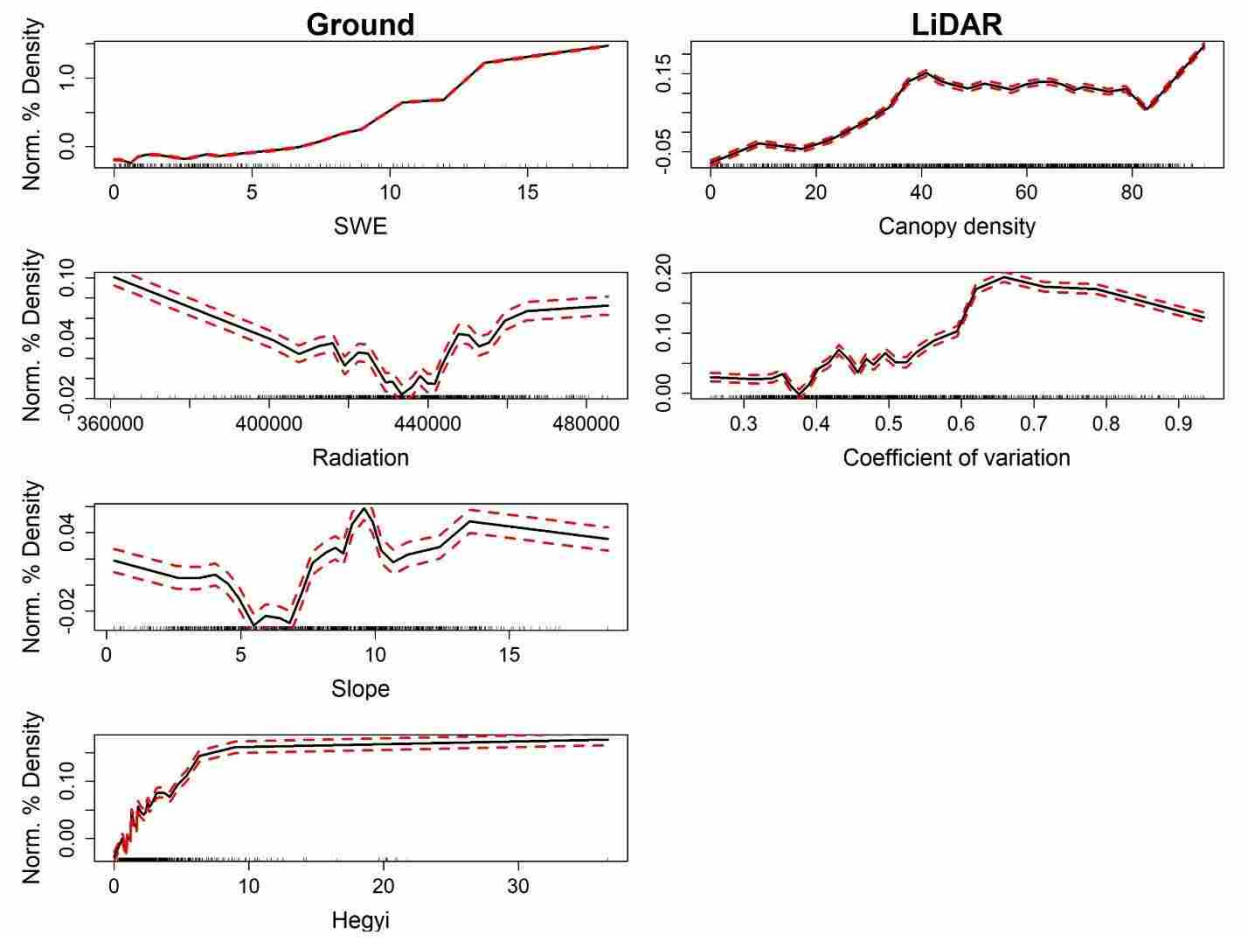


**Figure 10.** Partial dependency plot of the marginal effects of significantly important forest canopy structural predictors on the estimates of snow density from a RF model. Rug plots indicate the distribution of predictions. Response variables have been normalized by year. Dashed lines enclose a 95% confidence interval.

## CHAPTER 1 Supplementary Material

**Table S1:** Stand structure and compositional attributes of 10 old-growth Sitka spruce-western hemlock forest stands. Medium density represents forests with 40-60% canopy closure and full density is 70-100% canopy closure. Overstory, midstory, and understory trees are ≥ 25 m, 10-25 m, and <10 m in height respectively. TPH is trees per hectare. PISI = Sitka spruce; TSHE = western hemlock; CHNO = yellow cedar; POTR = black cottonwood; ALRU = red alder.

| | | All | | | | Overstory | | Midstory | | Understory | |
|---|---|---|---|---|---|---|---|---|---|---|---|
| | **Species** | **Density (TPH)** | **Basal area ($m^2$/ha)** | **DBH range (cm)** | **QMD (cm)** | **Density (TPH)** | **Basal area ($m^2$/ha)** | **Density (TPH)** | **Basal area ($m^2$/ha)** | **Density (TPH)** | **Basal area ($m^2$/ha)** |
| **Medium density** | | | | | | | | | | | |
| **Plot 104** | PISI | 226 | 55.25 | 7.6 - 122.2 | 46.8 | 109 | 49.18 | 110 | 6.02 | 6 | 0.05 |
| | TSHE | 82 | 5.08 | 7.6 - 77.5 | 23.6 | 4 | 1.66 | 63 | 3.27 | 15 | 0.14 |
| | POTR | 6 | 0.80 | 15.2 - 44.5 | 33.7 | 2 | 0.42 | 3 | 0.37 | 1 | 0.02 |
| | ALRU | > 1 | 0.07 | 30.7 | 30.7 | 0 | 0.00 | 1 | 0.07 | 0 | 0.00 |
| | *Total* | *315* | *61.20* | *7.6 - 122.2* | *41.8* | *115* | *51.26* | *177* | *9.73* | *22* | *0.21* |
| **Plot 130** | PISI | 42 | 4.28 | 7.6 - 97.0 | 30.1 | 6 | 3.26 | 33 | 1.00 | 4 | 0.20 |
| | TSHE | 623 | 59.40 | 7.6 - 132.6 | 29.2 | 86 | 42.33 | 323 | 14.84 | 213 | 2.22 |
| | *Total* | *665* | 63.67 | 7.6 - 132.6 | 29.3 | *92* | *45.59* | *356* | *15.84* | *217* | *2.24* |
| **Plot 132** | PISI | 33 | 10.98 | 7.9 - 177.5 | 54.5 | 11 | 9.77 | 21 | 1.20 | 1 | 0.01 |
| | TSHE | 379 | 67.56 | 7.6 - 123.2 | 40.0 | 90 | 55.95 | 191 | 10.54 | 98 | 1.06 |
| | ALRU | 11 | 0.81 | 8.4 - 43.2 | 25.3 | 1 | 0.15 | 6 | 0.59 | 5 | 0.07 |
| | *Total* | *423* | *79.34* | *7.6 - 177.5* | *41.0* | *102* | *65.87* | *218* | *12.33* | *104* | *1.14* |

| | | | | | | | | | | | |
|---|---|---|---|---|---|---|---|---|---|---|---|
| **Plot 141** | PISI | 32 | 7.04 | 7.9 - 101.3 | 44.1 | 13 | 6.27 | 17 | 0.76 | 2 | 0.02 |
| | TSHE | 487 | 46.00 | 7.6 - 95.3 | 29.1 | 84 | 31.19 | 234 | 13.03 | 169 | 1.76 |
| | *Total* | *519* | *53.03* | *7.6 - 101.3* | *30.3* | *97* | *37.46* | *251* | *13.80* | *171* | *1.78* |
| **Plot 220** | PISI | 113 | 14.37 | 7.6 - 100.6 | 33.8 | 33 | 11.79 | 72 | 2.53 | 8 | 0.06 |
| | TSHE | 553 | 52.00 | 7.6 - 109.0 | 29.0 | 85 | 35.02 | 289 | 15.12 | 179 | 1.84 |
| | *Total* | *666* | *66.37* | *7.6 - 109.0* | *29.9* | *118* | *46.81* | *361* | *17.65* | *187* | *1.90* |
| **Full density** | | | | | | | | | | | |
| **Plot 32** | PISI | 67 | 21.76 | 20.1 - 101.6 | 53.7 | 62 | 21.00 | 6 | 0.42 | 0 | 0.00 |
| | TSHE | 531 | 66.00 | 7.6 - 75.7 | 33.4 | 146 | 37.09 | 343 | 28.47 | 41 | 0.43 |
| | CHNO | 56 | 4.82 | 10.7 - 55.6 | 27.9 | 0 | 0.00 | 50 | 4.71 | 6 | 0.10 |
| | *Total* | *654* | *92.58* | *7.6 - 101.6* | *35.6* | *208* | *58.43* | *399* | *33.61* | *47* | *0.53* |
| **Plot 76** | PISI | 129 | 20.56 | 7.6 - 111.8 | 37.8 | 47 | 17.13 | 76 | 3.38 | 7 | 0.05 |
| | TSHE | 535 | 59.13 | 7.6 - 120.7 | 31.5 | 94 | 41.96 | 266 | 15.38 | 174 | 1.80 |
| | *Total* | *664* | *79.70* | *7.6 - 120.7* | *32.8* | *141* | *59.09* | *342* | *18.76* | *181* | *1.85* |
| **Plot 111** | PISI | 109 | 40.97 | 8.1 - 113.3 | 58.0 | 74 | 39.29 | 34 | 1.66 | 2 | 0.01 |
| | TSHE | 259 | 52.96 | 7.6 - 133.6 | 42.8 | 108 | 44.73 | 103 | 7.76 | 47 | 0.48 |
| | *Total* | *368* | *93.93* | *7.6 - 133.6* | *47.8* | *182* | *84.02* | *137* | *9.42* | *49* | *0.49* |
| **Plot 143** | PISI | 84 | 40.57 | 23.9 - 135.6 | 65.9 | 82 | 40.41 | 2 | 0.16 | 0 | 0.00 |
| | TSHE | 224 | 49.73 | 7.6 - 104.6 | 44.6 | 112 | 42.09 | 88 | 7.40 | 24 | 0.23 |
| | *Total* | *308* | *90.30* | *7.6 - 135.6* | *51.2* | *194* | *82.50* | *90* | *7.56* | *24* | *0.23* |

| | | | | | | | | | | | |
|---|---|---|---|---|---|---|---|---|---|---|---|
| **Plot 161** | PISI | 71 | 64.65 | 23.1 - 162.1 | 90.3 | 68 | 64.44 | 3 | 0.21 | 0 | 0.00 |
| | TSHE | 175 | 50.52 | 7.6 - 126.5 | 50.8 | 95 | 46.94 | 55 | 3.32 | 25 | 0.26 |
| | *Total* | *246* | *115.17* | *7.6 - 162.1* | *64.7* | *163* | *111.38* | *58* | *3.53* | *25* | *0.26* |

**Table S2**. Gap analysis summary statistics for 10 stem mapped plots in southeast Alaska. Gaps were calculated using no plot edge buffer. Height is a fixed value designating canopy tree threshold (i.e., 20, 25, 30 m); S and G indicate gap sampling method: S = shadow length, G = geometric. SEM is standard error of the sampling mean.

| | | | | Number of gaps in size class [proportion of total plot area] ($m^2$) | | | | | | | |
|---|---|---|---|---|---|---|---|---|---|---|---|
| **Plot** | **Height-method** | **Gaps $ha^{-1}$** | **Mean area ± SEM ($m^2$)** | **0-50** | **51-100** | **101-200** | **201-300** | **301-400** | **401-500** | **501-600** | **600+** |
| **Medium density** | | | | | | | | | | | |
| 104 | 20-S | 8 | 242.4 ± 47.1 | 0 [0.00] | 2 [0.01] | 5 [0.06] | 2 [0.04] | 1 [0.02] | 1 [0.03] | 1 [0.04] | 0 [0.00] |
| | 20-G | 13 | 264.7 ± 90.8 | 4 [0.01] | 6 [0.03] | 1 [0.01] | 3 [0.06] | 1 [0.03] | 0 [0.00] | 1 [0.04] | 2 [0.17] |
| | 25-S | 7 | 274.2 ± 58.5 | 0 [0.00] | 2 [0.01] | 2 [0.01] | 2 [0.04] | 0 [0.00] | 4 [0.13] | 0 [0.00] | 0 [0.00] |
| | 25-G | 11 | 302.0 ± 84.4 | 1 [0.0] | 4 [0.02] | 3 [0.03] | 2 [0.03] | 1 [0.03] | 2 [0.06] | 0 [0.00] | 2 [0.14] |
| | 30-S | 5 | 404.7 ± 151.0 | 0 [0.00] | 2 [0.01] | 2 [0.02] | 0 [0.00] | 0 [0.00] | 1 [0.03] | 0 [0.00] | 2 [0.13] |
| | 30-G | 4 | 710.5 ± 461.8 | 0 [0.00] | 2 [0.01] | 1 [0.01] | 0 [0.00] | 1 [0.03] | 1 [0.04] | 0 [0.00] | 1 [0.21] |
| 130 | 20-S | 7 | 251.5 ± 43.0 | 0 [0.00] | 1 [0.01] | 4 [0.05] | 2 [0.04] | 2 [0.05] | 0 [0.00] | 1 [0.04] | 0 [0.00] |
| | 20-G | 15 | 229.3 ± 60.6 | 6 [0.01] | 5 [0.02] | 5 [0.05] | 0 [0.00] | 0 [0.00] | 1 [0.03] | 3 [0.12] | 2 [0.12] |
| | 25-S | 3 | 380.9 ± 68.9 | 0 [0.00] | 0 [0.00] | 0 [0.00] | 1 [0.02] | 1 [0.02] | 1 [0.03] | 1 [0.04] | 0 [0.00] |
| | 25-G | 13 | 271.0 ± 36.4 | 1 [0.00] | 2 [0.01] | 3 [0.03] | 3 [0.10] | 2 [0.05] | 3 [0.09] | 2 [0.08] | 0 [0.00] |
| | 30-S | 4 | 412.9 ± 84.4 | 0 [0.00] | 0 [0.00] | 0 [0.00] | 3 [0.06] | 1 [0.02] | 0 [0.00] | 0 [0.00] | 2 [0.10] |
| | 30-G | 8 | 559.3 ± 214.8 | 0 [0.00] | 1 [0.01] | 0 [0.00] | 6 [0.11] | 0 [0.00] | 1 [0.03] | 0 [0.00] | 3 [0.29] |
| 132 | 20-S | 6 | 201.3 ± 54.9 | 0 [0.00] | 2 [0.01] | 3 [0.03] | 1 [0.01] | 1 [0.02] | 0 [0.00] | 1 [0.04] | 0 [0.00] |
| | 20-G | 15 | 195.8 ± 39.3 | 3 [0.01] | 4 [0.02] | 8 [0.08] | 2 [0.03] | 1 [0.02] | 1 [0.03] | 0 [0.00] | 2 [0.09] |
| | 25-S | 5 | 272.4 ± 67.7 | 0 [0.00] | 0 [0.00] | 3 [0.02] | 1 [0.02] | 1 [0.02] | 1 [0.03] | 1 [0.04] | 0 [0.00] |
| | 25-G | 9 | 376.7 ± 87.0 | 1 [0.00] | 0 [0.00] | 3 [0.03] | 3 [0.05] | 1 [0.02] | 1 [0.03] | 3 [0.12] | 1 [0.09] |
| | 30-S | 5 | 290.4 ± 54.5 | 0 [0.00] | 0 [0.00] | 2 [0.02] | 3 [0.06] | 1 [0.02] | 0 [0.00] | 1 [0.04] | 0 [0.00] |
| | 30-G | 8 | 389.4 ± 100.3 | 0 [0.00] | 1 [0.01] | 2 [0.02] | 4 [0.07] | 2 [0.05] | 0 [0.00] | 1 [0.04] | 2 [0.15] |
| 141 | 20-S | 6 | 186.2 ± 15.6 | 0 [0.00] | 0 [0.00] | 4 [0.04] | 4 [0.06] | 0 [0.00] | 0 [0.00] | 0 [0.00] | 0 [0.00] |
| | 20-G | 17 | 176.2 ± 29.4 | 5 [0.01] | 5 [0.03] | 6 [0.06] | 4 [0.07] | 0 [0.00] | 4 [0.13] | 0 [0.00] | 0 [0.00] |
| | 25-S | 5 | 213.4 ± 28.2 | 0 [0.00] | 0 [0.00] | 4 [0.04] | 2 [0.04] | 1 [0.02] | 0 [0.00] | 0 [0.00] | 0 [0.00] |
| | 25-G | 16 | 209.4 ± 25.9 | 2 [0.01] | 3 [0.02] | 8 [0.09] | 5 [0.09] | 2 [0.05] | 3 [0.09] | 0 [0.00] | 0 [0.00] |
| | 30-S | 3 | 1498.7 ± 784.6 | 0 [0.00] | 0 [0.00] | 1 [0.01] | 0 [0.00] | 0 [0.00] | 0 [0.00] | 0 [0.00] | 3 [0.41] |
| | 30-G | 3 | 2028.0 ± 1298.5 | 0 [0.00] | 0 [0.00] | 1 [0.01] | 0 [0.00] | 0 [0.00] | 0 [0.00] | 0 [0.00] | 3 [0.56] |

| | | | | | | | | | | | |
|---|---|---|---|---|---|---|---|---|---|---|---|
| 220 | 20-S | 5 | 146.1 ± 20.9 | 0 [0.00] | 1 [0.01] | 5 [0.05] | 1 [0.02] | 0 [0.00] | 0 [0.00] | 0 [0.00] | 0 [0.00] |
| | 20-G | 16 | 149.4 ± 21.4 | 4 [0.01] | 6 [0.03] | 7 [0.07] | 4 [0.07] | 1 [0.03] | 1 [0.03] | 0 [0.00] | 0 [0.00] |
| | 25-S | 4 | 281.3 ± 71.8 | 0 [0.00] | 0 [0.00] | 2 [0.01] | 1 [0.02] | 2 [0.05] | 0 [0.00] | 1 [0.04] | 0 [0.00] |
| | 25-G | 13 | 251.5 ± 70.4 | 2 [0.01] | 4 [0.02] | 6 [0.06] | 3 [0.05] | 0 [0.00] | 1 [0.03] | 0 [0.00] | 2 [0.14] |
| | 30-S | 4 | 880.4 ± 509.6 | 0 [0.00] | 0 [0.00] | 1 [0.01] | 2 [0.03] | 1 [0.02] | 0 [0.00] | 0 [0.00] | 2 [0.31] |
| | 30-G | 4 | 1188.2 ± 712.3 | 0 [0.00] | 1 [0.01] | 1 [0.01] | 0 [0.00] | 0 [0.00] | 2 [0.06] | 0 [0.00] | 2 [0.42] |
| **Full density** | | | | | | | | | | | |
| 32 | 20-S | 0 | 0.0 ± 0.0 | 0 [0.00] | 0 [0.00] | 0 [0.00] | 0 [0.00] | 0 [0.00] | 0 [0.00] | 0 [0.00] | 0 [0.00] |
| | 20-G | 1 | 81.6 ± 0.0 | 0 [0.00] | 1 [0.01] | 0 [0.00] | 0 [0.00] | 0 [0.00] | 0 [0.00] | 0 [0.00] | 0 [0.00] |
| | 25-S | 1 | 206.9 ± 0.0 | 0 [0.00] | 0 [0.00] | 0 [0.00] | 1 [0.01] | 0 [0.00] | 0 [0.00] | 0 [0.00] | 0 [0.00] |
| | 25-G | 5 | 96.6 ± 34.7 | 1 [0.00] | 5 [0.02] | 0 [0.00] | 0 [0.00] | 1 [0.02] | 0 [0.00] | 0 [0.00] | 0 [0.00] |
| | 30-S | 2 | 1570.8 ± 647.0 | 0 [0.00] | 0 [0.00] | 0 [0.00] | 1 [0.02] | 0 [0.00] | 0 [0.00] | 0 [0.00] | 2 [0.31] |
| | 30-G | 4 | 1096.7 ± 551.6 | 0 [0.00] | 0 [0.00] | 2 [0.02] | 0 [0.00] | 2 [0.05] | 0 [0.00] | 0 [0.00] | 2 [0.40] |
| 76 | 20-S | 5 | 160.6 ± 25.7 | 0 [0.00] | 2 [0.01] | 3 [0.03] | 2 [0.03] | 0 [0.00] | 0 [0.00] | 0 [0.00] | 0 [0.00] |
| | 20-G | 11 | 135.6 ± 27.5 | 4 [0.01] | 3 [0.01] | 5 [0.04] | 2 [0.03] | 1 [0.02] | 1 [0.03] | 0 [0.00] | 0 [0.00] |
| | 25-S | 4 | 211.2 ± 37.4 | 0 [0.00] | 0 [0.00] | 2 [0.02] | 3 [0.05] | 1 [0.02] | 0 [0.00] | 0 [0.00] | 0 [0.00] |
| | 25-G | 11 | 199.9 ± 48.2 | 3 [0.01] | 4 [0.02] | 3 [0.03] | 3 [0.05] | 1 [0.03] | 1 [0.03] | 0 [0.00] | 1 [0.05] |
| | 30-S | 5 | 412.8 ± 141.8 | 0 [0.00] | 0 [0.00] | 2 [0.02] | 3 [0.05] | 0 [0.00] | 0 [0.00] | 0 [0.00] | 2 [0.13] |
| | 30-G | 6 | 533.3 ± 129.9 | 0 [0.00] | 0 [0.00] | 1 [0.01] | 3 [0.05] | 1 [0.02] | 1 [0.03] | 0 [0.00] | 3 [0.22] |
| 111 | 20-S | 3 | 187.0 ± 61.8 | 0 [0.00] | 2 [0.01] | 0 [0.00] | 1 [0.02] | 1 [0.02] | 0 [0.00] | 0 [0.00] | 0 [0.00] |
| | 20-G | 12 | 126.4 ± 10.8 | 2 [0.01] | 3 [0.02] | 12 [0.13] | 0 [0.00] | 0 [0.00] | 0 [0.00] | 0 [0.00] | 0 [0.00] |
| | 25-S | 1 | 105.4 ± 0.0 | 0 [0.00] | 0 [0.00] | 1 [0.01] | 0 [0.00] | 0 [0.00] | 0 [0.00] | 0 [0.00] | 0 [0.00] |
| | 25-G | 5 | 127.3 ± 26.5 | 0 [0.00] | 4 [0.02] | 1 [0.01] | 2 [0.03] | 0 [0.00] | 0 [0.00] | 0 [0.00] | 0 [0.00] |
| | 30-S | 1 | 106.4 ± 7.0 | 0 [0.00] | 1 [0.01] | 1 [0.01] | 0 [0.00] | 0 [0.00] | 0 [0.00] | 0 [0.00] | 0 [0.00] |
| | 30-G | 8 | 155.1 ± 29.9 | 0 [0.00] | 4 [0.02] | 4 [0.04] | 2 [0.03] | 0 [0.00] | 1 [0.03] | 0 [0.00] | 0 [0.00] |
| 143 | 20-S | 3 | 107.4 ± 17.6 | 0 [0.00] | 2 [0.01] | 2 [0.02] | 0 [0.00] | 0 [0.00] | 0 [0.00] | 0 [0.00] | 0 [0.00] |
| | 20-G | 12 | 126.4 ± 10.8 | 2 [0.01] | 3 [0.02] | 12 [0.13] | 0 [0.00] | 0 [0.00] | 0 [0.00] | 0 [0.00] | 0 [0.00] |

| | | | | | | | | | | | |
|---|---|---|---|---|---|---|---|---|---|---|---|
| | 25-S | 1 | 105.4 ± 0.0 | 0 [0.00] | 0 [0.00] | 1 [0.01] | 0 [0.00] | 0 [0.00] | 0 [0.00] | 0 [0.00] | 0 [0.00] |
| | 25-G | 5 | 127.3 ± 26.5 | 0 [0.00] | 4 [0.02] | 1 [0.01] | 2 [0.03] | 0 [0.00] | 0 [0.00] | 0 [0.00] | 0 [0.00] |
| | 30-S | 1 | 106.4 ± 7.0 | 0 [0.00] | 1 [0.01] | 1 [0.01] | 0 [0.00] | 0 [0.00] | 0 [0.00] | 0 [0.00] | 0 [0.00] |
| | 30-G | 8 | 155.1 ± 29.9 | 0 [0.00] | 4 [0.02] | 4 [0.04] | 2 [0.03] | 0 [0.00] | 1 [0.03] | 0 [0.00] | 0 [0.00] |
| 161 | 20-S | 4 | 167.8 ± 24.6 | 0 [0.00] | 1 [0.01] | 4 [0.05] | 1 [0.02] | 0 [0.00] | 0 [0.00] | 0 [0.00] | 0 [0.00] |
| | 20-G | 17 | 133.0 ± 19.6 | 6 [0.02] | 2 [0.01] | 12 [0.12] | 3 [0.05] | 0 [0.00] | 1 [0.03] | 0 [0.00] | 0 [0.00] |
| | 25-S | 1 | 151.2 ± 12.9 | 0 [0.00] | 0 [0.00] | 2 [0.02] | 0 [0.00] | 0 [0.00] | 0 [0.00] | 0 [0.00] | 0 [0.00] |
| | 25-G | 8 | 140.1 ± 23.0 | 2 [0.01] | 3 [0.02] | 3 [0.04] | 3 [0.05] | 0 [0.00] | 1 [0.03] | 0 [0.00] | 0 [0.00] |
| | 30-S | 1 | 165.6 ± 23.4 | 0 [0.00] | 0 [0.00] | 2 [0.02] | 0 [0.00] | 0 [0.00] | 0 [0.00] | 0 [0.00] | 0 [0.00] |
| | 30-G | 5 | 146.8 ± 22.1 | 0 [0.00] | 2 [0.01] | 4 [0.04] | 1 [0.02] | 0 [0.00] | 0 [0.00] | 0 [0.00] | 0 [0.00] |

**Table S3**. Gap analysis summary statistics for 10 stem mapped plots in southeast Alaska. Gaps were calculated using an edge buffer equal to the lower limit gap size (i.e. threshold distance). Height is a fixed value designating canopy tree threshold (i.e. 20, 25, 30 m); S and G indicate gap sampling method: S = shadow length, G = geometric. SEM is standard error of the sampling mean.

| | | | | Number of gaps in size class [proportion of total plot area] ($m^2$) | | | | | | | |
|---|---|---|---|---|---|---|---|---|---|---|---|
| | **Height-method** | **Gaps $ha^{-1}$** | **Mean area ± SEM ($m^2$)** | **0-50** | **51-100** | **101-200** | **201-300** | **301-400** | **401-500** | **501-600** | **600+** |
| **Medium density** | | | | | | | | | | | |
| 104 | 20-S | 6 | 213.6 ± 34.2 | 0 [0.00] | 1 [0.01] | 5 [0.06] | 1 [0.02] | 2 [0.05] | 0 [0.00] | 0 [0.00] | 0 [0.00] |
| | 20-G | 8 | 332.8 ± 128.0 | 1 [0.00] | 4 [0.02] | 0 [0.00] | 3 [0.05] | 0 [0.00] | 1 [0.03] | 0 [0.00] | 2 [0.16] |
| | 25-S | 3 | 349.8 ± 85.4 | 0 [0.00] | 0 [0.00] | 1 [0.01] | 1 [0.02] | 0 [0.00] | 1 [0.03] | 1 [0.04] | 0 [0.00] |
| | 25-G | 6 | 331.7 ± 113.4 | 0 [0.0] | 2 [0.01] | 2 [0.02] | 3 [0.05] | 0 [0.00] | 0 [0.00] | 0 [0.00] | 2 [0.12] |
| | 30-S | 2 | 505.3 ± 130.9 | 0 [0.00] | 0 [0.00] | 0 [0.00] | 1 [0.02] | 0 [0.00] | 0 [0.00] | 0 [0.00] | 2 [0.09] |
| | 30-G | 1 | 1211.7 ± 1112.7 | 0 [0.00] | 1 [0.01] | 0 [0.00] | 0 [0.00] | 0 [0.00] | 0 [0.00] | 0 [0.00] | 1 [0.16] |
| 130 | 20-S | 5 | 208.5 ± 18.5 | 0 [0.00] | 0 [0.00] | 3 [0.04] | 4 [0.07] | 0 [0.00] | 0 [0.00] | 0 [0.00] | 0 [0.00] |
| | 20-G | 8 | 340.3 ± 64.1 | 0 [0.00] | 2 [0.01] | 2 [0.02] | 2 [0.03] | 1 [0.02] | 1 [0.03] | 2 [0.08] | 2 [0.09] |
| | 25-S | 1 | 220.5 ± 141.6 | 0 [0.00] | 1 [0.01] | 0 [0.00] | 0 [0.00] | 1 [0.03] | 0 [0.00] | 0 [0.00] | 0 [0.00] |
| | 25-G | 10 | 251.5 ± 23.3 | 0 [0.00] | 0 [0.00] | 3 [0.03] | 8 [0.14] | 2 [0.05] | 1 [0.03] | 0 [0.00] | 0 [0.00] |
| | 30-S | 2 | 292.4 ± 43.4 | 0 [0.00] | 0 [0.00] | 0 [0.00] | 2 [0.04] | 1 [0.03] | 0 [0.00] | 0 [0.00] | 0 [0.00] |
| | 30-G | 6 | 404.2 ± 169.7 | 0 [0.00] | 2 [0.01] | 2 [0.02] | 2 [0.03] | 1 [0.02] | 0 [0.00] | 0 [0.00] | 2 [0.16] |

| | | | | | | | | | | | |
|---|---|---|---|---|---|---|---|---|---|---|---|
| 132 | 20-S | 2 | 210.1 ± 56.7 | 0 [0.00] | 0 [0.00] | 1 [0.01] | 1 [0.01] | 1 [0.02] | 0 [0.00] | 0 [0.00] | 0 [0.00] |
| | 20-G | 9 | 215.0 ± 51.8 | 2 [0.00] | 2 [0.01] | 3 [0.03] | 3 [0.05] | 1 [0.03] | 1 [0.03] | 0 [0.00] | 1 [0.05] |
| | 25-S | 2 | 314.7 ± 82.5 | 0 [0.00] | 0 [0.00] | 1 [0.01] | 1 [0.02] | 0 [0.00] | 1 [0.03] | 0 [0.00] | 0 [0.00] |
| | 25-G | 6 | 381.4 ± 105.3 | 0 [0.0] | 0 [0.00] | 4 [0.04] | 1 [0.02] | 0 [0.00] | 1 [0.03] | 2 [0.08] | 1 [0.07] |
| | 30-S | 2 | 347.2 ± 72.9 | 0 [0.00] | 0 [0.00] | 0 [0.00] | 1 [0.02] | 1 [0.02] | 0 [0.00] | 1 [0.04] | 0 [0.00] |
| | 30-G | 5 | 408.7 ± 165.4 | 0 [0.00] | 1 [0.01] | 2 [0.02] | 2 [0.03] | 0 [0.00] | 0 [0.00] | 0 [0.00] | 2 [0.14] |
| 141 | 20-S | 5 | 182.0 ± 12.8 | 0 [0.00] | 0 [0.00] | 5 [0.06] | 2 [0.03] | 0 [0.00] | 0 [0.00] | 0 [0.00] | 0 [0.00] |
| | 20-G | 10 | 235.2 ± 73.7 | 1 [0.00] | 4 [0.02] | 4 [0.04] | 2 [0.03] | 0 [0.00] | 2 [0.06] | 0 [0.00] | 1 [0.08] |
| | 25-S | 1 | 265.7 ± 74.4 | 0 [0.00] | 0 [0.00] | 1 [0.01] | 0[0.00] | 1 [0.02] | 0 [0.00] | 0 [0.00] | 0 [0.00] |
| | 25-G | 9 | 230.2 ± 38.6 | 1 [0.0] | 2 [0.01] | 2 [0.02] | 5 [0.08] | 0 [0.00] | 3 [0.09] | 0 [0.00] | 0 [0.00] |
| | 30-S | 3 | 642.2 ± 60.0 | 0 [0.00] | 0 [0.00] | 0 [0.00] | 0 [0.00] | 0 [0.00] | 0 [0.00] | 2 [0.08] | 2 [0.10] |
| | 30-G | 4 | 924.0 ± 503.4 | 0 [0.00] | 0 [0.00] | 1 [0.01] | 1 [0.02] | 1 [0.03] | 0 [0.00] | 0 [0.00] | 2 [0.27] |
| 220 | 20-S | 3 | 146.1 ± 9.2 | 0 [0.00] | 0 [0.00] | 4 [0.04] | 0 [0.00] | 0 [0.00] | 0 [0.00] | 0 [0.00] | 0 [0.00] |
| | 20-G | 11 | 158.6 ± 28.5 | 3 [0.01] | 2 [0.01] | 6 [0.06] | 2 [0.03] | 1 [0.02] | 1 [0.03] | 0 [0.00] | 0 [0.00] |
| | 25-S | 2 | 318.9 ± 114.0 | 0 [0.00] | 0 [0.00] | 1 [0.01] | 1 [0.02] | 0 [0.00] | 0 [0.00] | 1 [0.04] | 0 [0.00] |
| | 25-G | 6 | 356.2 ± 104.2 | 0 [0.00] | 1 [0.00] | 2 [0.02] | 4 [0.07] | 0 [0.00] | 0 [0.00] | 0 [0.00] | 2 [0.13] |

| | | | | | | | | | | | |
|---|---|---|---|---|---|---|---|---|---|---|---|
| | 30-S | 2 | 914.4 ± 483.3 | 0 [0.00] | 0 [0.00] | 0 [0.00] | 1 [0.02] | 0 [0.00] | 0 [0.00] | 0 [0.00] | 2 [0.18] |
| | 30-G | 3 | 1041.3 ± 606.3 | 0 [0.00] | 0 [0.00] | 1 [0.01] | 1 [0.02] | 0 [0.00] | 0 [0.00] | 0 [0.00] | 2 [0.27] |
| **Full density** | | | | | | | | | | | |
| 32 | 20-S | 0 | 0.0 ± 0.0 | 0 [0.00] | 0 [0.00] | 0 [0.00] | 0 [0.00] | 0 [0.00] | 0 [0.00] | 0 [0.00] | 0 [0.00] |
| | 20-G | 1 | 78.3 ± 0.0 | 0 [0.00] | 1 [0.01] | 0 [0.00] | 0 [0.00] | 0 [0.00] | 0 [0.00] | 0 [0.00] | 0 [0.00] |
| | 25-S | 1 | 206.1 ± 0.0 | 0 [0.00] | 0 [0.00] | 0 [0.00] | 1 [0.01] | 0 [0.00] | 0 [0.00] | 0 [0.00] | 0 [0.00] |
| | 25-G | 1 | 193.3 ± 108.0 | 0 [0.00] | 1 [0.01] | 0 [0.00] | 0 [0.00] | 1 [0.02] | 0 [0.00] | 0 [0.00] | 0 [0.00] |
| | 30-S | 2 | 855.6 ± 641.0 | 0 [0.00] | 1 [0.00] | 0 [0.00] | 0 [0.00] | 1 [0.03] | 0 [0.00] | 0 [0.00] | 1 [0.15] |
| | 30-G | 4 | 833.3 ± 525.7 | 0 [0.00] | 0 [0.00] | 1 [0.01] | 1 [0.02] | 1 [0.02] | 1 [0.03] | 0 [0.00] | 1 [0.21] |
| 76 | 20-S | 1 | 207.8 ± 33.2 | 0 [0.00] | 0 [0.00] | 1 [0.01] | 1 [0.02] | 0 [0.00] | 0 [0.00] | 0 [0.00] | 0 [0.00] |
| | 20-G | 8 | 124.0 ± 38.1 | 1 [0.00] | 6 [0.03] | 2 [0.02] | 0 [0.00] | 1 [0.02] | 1 [0.03] | 0 [0.00] | 0 [0.00] |
| | 25-S | 1 | 334.3 ± 0.0 | 0 [0.00] | 0 [0.00] | 0 [0.00] | 0 [0.00] | 1 [0.02] | 0 [0.00] | 0 [0.00] | 0 [0.00] |
| | 25-G | 6 | 195.5 ± 56.7 | 1 [0.00] | 1 [0.01] | 4 [0.04] | 2 [0.03] | 0 [0.00] | 0 [0.00] | 0 [0.00] | 1 [0.04] |
| | 30-S | 1 | 422.6 ± 58.5 | 0 [0.00] | 0 [0.00] | 0 [0.00] | 0 [0.00] | 1 [0.03] | 1 [0.03] | 0 [0.00] | 0 [0.10] |
| | 30-G | 4 | 414.8 ± 82.8 | 0 [0.00] | 0 [0.00] | 2 [0.03] | 0 [0.00] | 1 [0.02] | 0 [0.00] | 1 [0.04] | 2 [0.09] |
| 111 | 20-S | 0 | 0.0 ± 0.0 | 0 [0.00] | 0 [0.00] | 0 [0.00] | 0 [0.00] | 0 [0.00] | 0 [0.00] | 0 [0.00] | 0 [0.00] |
| | 20-G | 7 | 123.8 ±32.1 | 0 [0.00] | 7 [0.04] | 2 [0.02] | 0[0.00] | 1 [0.03] | 0 [0.00] | 0 [0.00] | 0 [0.00] |

| | | | | | | | | | | | |
|---|---|---|---|---|---|---|---|---|---|---|---|
| | 25-S | 1 | 354.0 ± 0.0 | 0 [0.00] | 0 [0.00] | 0 [0.00] | 0 [0.00] | 1 [0.02] | 0 [0.00] | 0 [0.00] | 0 [0.00] |
| | 25-G | 4 | 161.6 ± 65.6 | 0 [0.0] | 2 [0.01] | 2 [0.02] | 0 [0.00] | 0 [0.00] | 1 [0.03] | 0 [0.00] | 0 [0.00] |
| | 30-S | 1 | 448.8 ± 0.0 | 0 [0.00] | 0 [0.00] | 0 [0.00] | 0 [0.00] | 0 [0.00] | 1 [0.03] | 0 [0.00] | 0 [0.00] |
| | 30-G | 2 | 381.7 ± 227.6 | 0 [0.0] | 0 [0.00] | 2 [0.02] | 0 [0.00] | 0 [0.00] | 0 [0.00] | 0 [0.00] | 1 [0.06] |
| 143 | 20-S | 0 | 0.0 ± 0.0 | 0 [0.00] | 0 [0.00] | 0 [0.00] | 0 [0.00] | 0 [0.00] | 0 [0.00] | 0 [0.00] | 0 [0.00] |
| | 20-G | 9 | 92.2 ± 13.8 | 5 [0.01] | 2 [0.01] | 6 [0.06] | 0 [0.00] | 0 [0.00] | 0 [0.00] | 0 [0.00] | 0 [0.00] |
| | 25-S | 0 | 0.0 ± 0.0 | 0 [0.00] | 0 [0.00] | 0 [0.00] | 0 [0.00] | 0 [0.00] | 0 [0.00] | 0 [0.00] | 0 [0.00] |
| | 25-G | 2 | 135.2 ± 51.4 | 1 [0.00] | 0 [0.00] | 1 [0.01] | 1 [0.02] | 0 [0.00] | 0 [0.00] | 0 [0.00] | 0 [0.00] |
| | 30-S | 0 | 0.0 ± 0.0 | 0 [0.00] | 0 [0.00] | 0 [0.00] | 0 [0.00] | 0 [0.00] | 0 [0.00] | 0 [0.00] | 0 [0.00] |
| | 30-G | 3 | 183.7 ± 14.7 | 0 [0.00] | 0 [0.00] | 2 [0.02] | 2 [0.03] | 0 [0.00] | 0 [0.00] | 0 [0.00] | 0 [0.00] |
| 161 | 20-S | 1 | 199.2 ± 63.4 | 0 [0.00] | 0 [0.00] | 1 [0.01] | 1 [0.02] | 0 [0.00] | 0 [0.00] | 0 [0.00] | 0 [0.00] |
| | 20-G | 12 | 123.6 ±26.4 | 6 [0.02] | 3 [0.02] | 5 [0.05] | 2 [0.03] | 0 [0.00] | 1 [0.03] | 0 [0.00] | 0 [0.00] |
| | 25-S | 0 | 0.0 ± 0.0 | 0 [0.00] | 0 [0.00] | 0 [0.00] | 0 [0.00] | 0 [0.00] | 0 [0.00] | 0 [0.00] | 0 [0.00] |
| | 25-G | 4 | 180.2 ± 68.2 | 0 [0.00] | 3 [0.02] | 0 [0.00] | 1 [0.01] | 0 [0.00] | 1 [0.03] | 0 [0.00] | 0 [0.00] |
| | 30-S | 0 | 0.0 ± 0.0 | 0 [0.00] | 0 [0.00] | 0 [0.00] | 0 [0.00] | 0 [0.00] | 0 [0.00] | 0 [0.00] | 0 [0.00] |
| | 30-G | 1 | 145.2 ± 9.4 | 0 [0.00] | 0 [0.00] | 2 [0.02] | 0 [0.00] | 0 [0.00] | 0 [0.00] | 0 [0.00] | 0 [0.00] |

**Table S4.** Summary of within stand level spatial patterns of widely spaced individuals (i.e. patch size = 1) and patches of overstory trees for 10 Sitka spruce-western hemlock forests in SE Alaska. BA is basal area in meters squared and total density is per plot.

| | | *Patch size (number of trees)* | | | | | |
|---|---|---|---|---|---|---|---|
| **Plot** | | **1** | **2-4** | **5-7** | **8-10** | **11-15** | **16+** |
| **Medium density** | | | | | | | |
| **104** | *# Patches ha$^{-1}$* | 7 | 6 | 4 | 1 | 1 | 2 |
| | *% Total density* | 6.1 | 14.6 | 18.3 | 4.9 | 15.2 | 40.9 |
| | *%Total BA* | 6.5 | 16.6 | 15.1 | 4.9 | 15.2 | 41.4 |
| **130** | *# Patches ha$^{-1}$* | 14 | 14 | 3 | 1 | 1 | 1 |
| | *% Total density* | 14.5 | 38.9 | 16.8 | 6.1 | 10.7 | 13.0 |
| | *%Total BA* | 16.2 | 39.4 | 16.7 | 6.1 | 10.7 | 11.9 |
| **132** | *# Patches ha$^{-1}$* | 13 | 6 | 2 | 1 | 2 | 1 |
| | *% Total density* | 12.4 | 15.9 | 11.7 | 5.5 | 24.8 | 29.7 |
| | *%Total BA* | 14.0 | 16.5 | 10.7 | 5.5 | 24.8 | 24.0 |
| **141** | *# Patches ha$^{-1}$* | 12 | 12 | 3 | 2 | 1 | 1 |
| | *% Total density* | 11.6 | 29.0 | 17.4 | 19.6 | 10.9 | 11.6 |
| | *%Total BA* | 12.5 | 35.1 | 17.4 | 19.6 | 10.9 | 9.8 |
| **220** | *# Patches ha$^{-1}$* | 4 | 8 | 4 | 3 | 1 | 1 |
| | *% Total density* | 3.6 | 16.8 | 21.6 | 21.6 | 15.0 | 21.6 |
| | *%Total BA* | 3.2 | 12.8 | 23.4 | 21.6 | 15.0 | 18.5 |
| **Full density** | | | | | | | |
| **32** | *# Patches ha$^{-1}$* | 2 | 4 | 0 | 0 | 0 | 1 |
| | *% Total density* | 1.0 | 5.4 | 0.0 | 0.0 | 0.0 | 93.6 |
| | *%Total BA* | 1.4 | 5.8 | 0.0 | 0.0 | 0.0 | 92.8 |
| **76** | *# Patches ha$^{-1}$* | 4 | 4 | 2 | 1 | 0 | 2 |
| | *% Total density* | 3.0 | 7.5 | 8.0 | 4.5 | 0.0 | 77.0 |
| | *%Total BA* | 3.2 | 7.7 | 5.9 | 4.5 | 0.0 | 78.7 |
| **111** | *# Patches ha$^{-1}$* | 1 | 3 | 1 | 0 | 1 | 2 |
| | *% Total density* | 0.8 | 4.2 | 2.7 | 0.0 | 9.3 | 83.0 |
| | *%Total BA* | 0.4 | 4.9 | 5.2 | 0.0 | 9.3 | 77.9 |
| **143** | *# Patches ha$^{-1}$* | 6 | 3 | 1 | 0 | 0 | 3 |
| | *% Total density* | 2.9 | 3.3 | 4.0 | 0.0 | 0.0 | 89.9 |
| | *%Total BA* | 3.4 | 5.2 | 3.7 | 0.0 | 0.0 | 87.7 |
| **161** | *# Patches ha$^{-1}$* | 4 | 5 | 2 | 0 | 0 | 3 |
| | *% Total density* | 2.6 | 9.9 | 7.8 | 0.0 | 0.0 | 79.7 |
| | *%Total BA* | 1.8 | 9.8 | 9.4 | 0.0 | 0.0 | 79.0 |

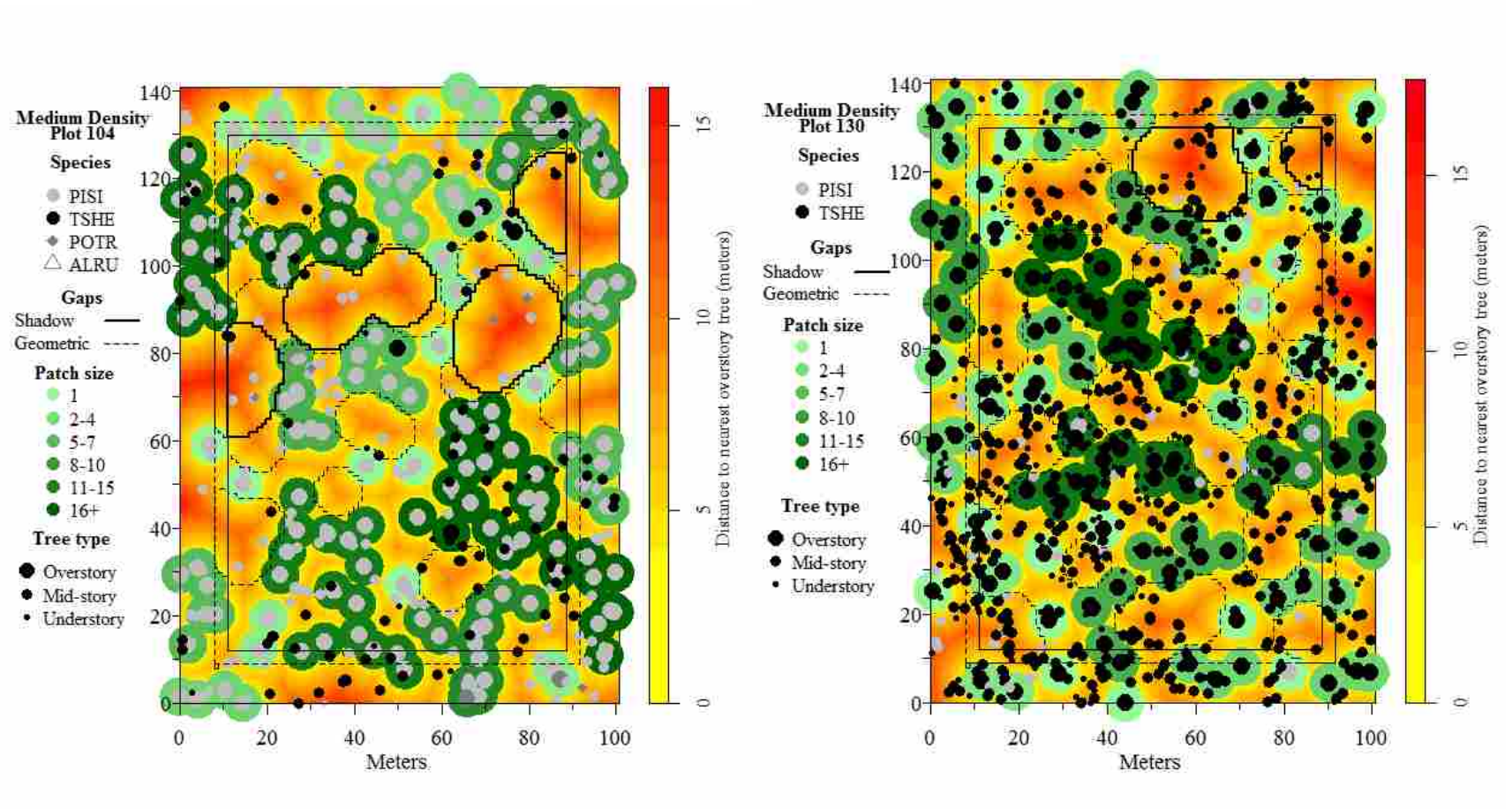
Medium Density
Plot 104
Species
PISI
TSHE
POTR
ALRU
Gaps
Shadow
Geometric
Patch size
1
2-4
5-7
8-10
11-15
16+
Tree type
Overstory
Mid-story
Understory
Meters
Distance to nearest overstory tree (meters)
Medium Density
Plot 130
Species
PISI
TSHE
Gaps
Shadow
Geometric
Patch size
1
2-4
5-7
8-10
11-15
16+
Tree type
Overstory
Mid-story
Understory
Meters
Distance to nearest overstory tree (meters)

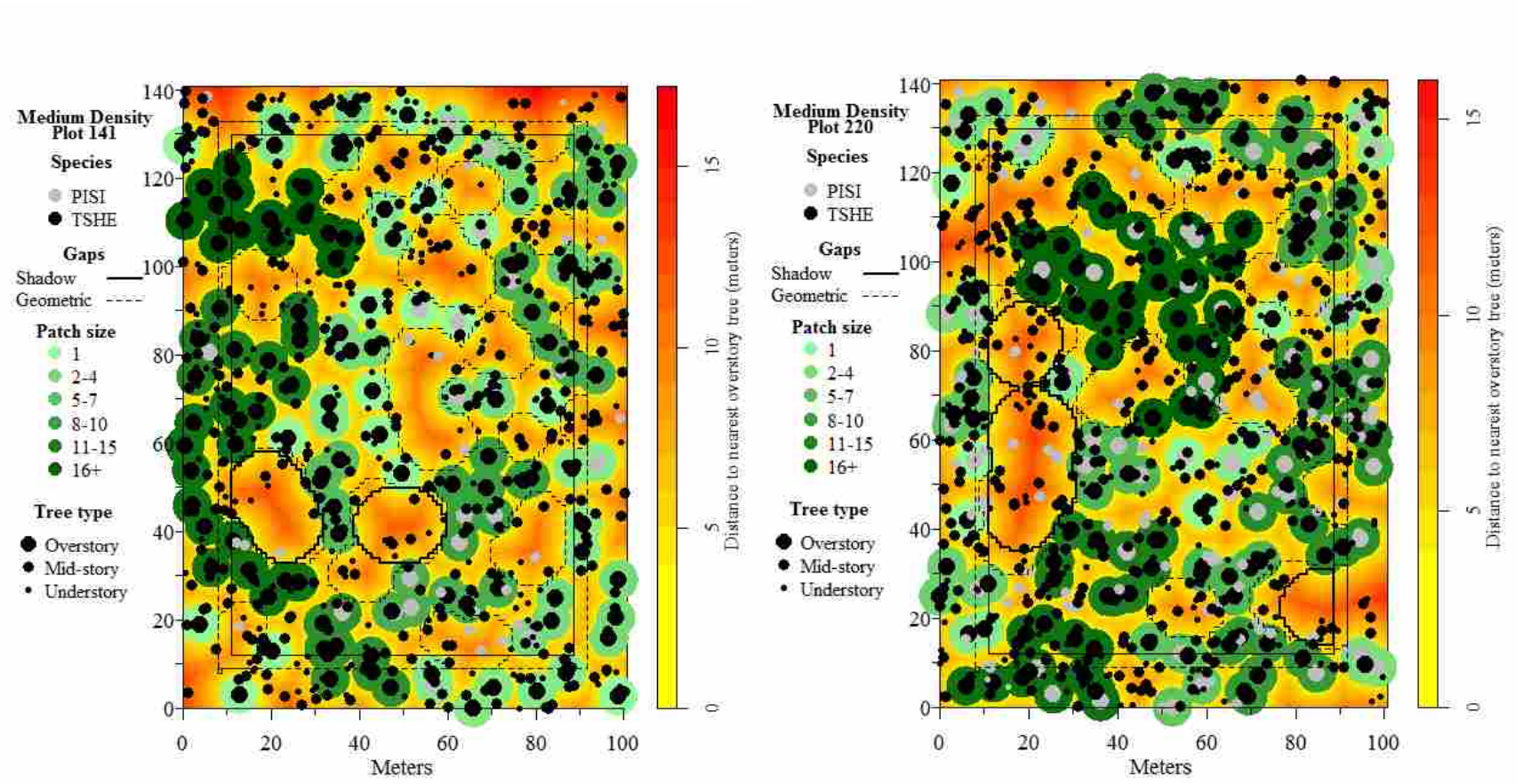


**Figure S1.** Stem maps by plot for medium density Sitka spruce western hemlock forests in southeast Alaska. Tree boles are colored by species and size represents overstory, mid-story, and understory positions. A 4.44 m radius was used to project tree crowns on overstory trees to show patches at a fixed distance of 8.88 m. Patch size is the number of trees in a patch. Gaps and associated plot buffer distances are shown with a solid or dashed line. Background coloration is a graphical display of open area where colors indicate the distance to the nearest overstory trees in meters.

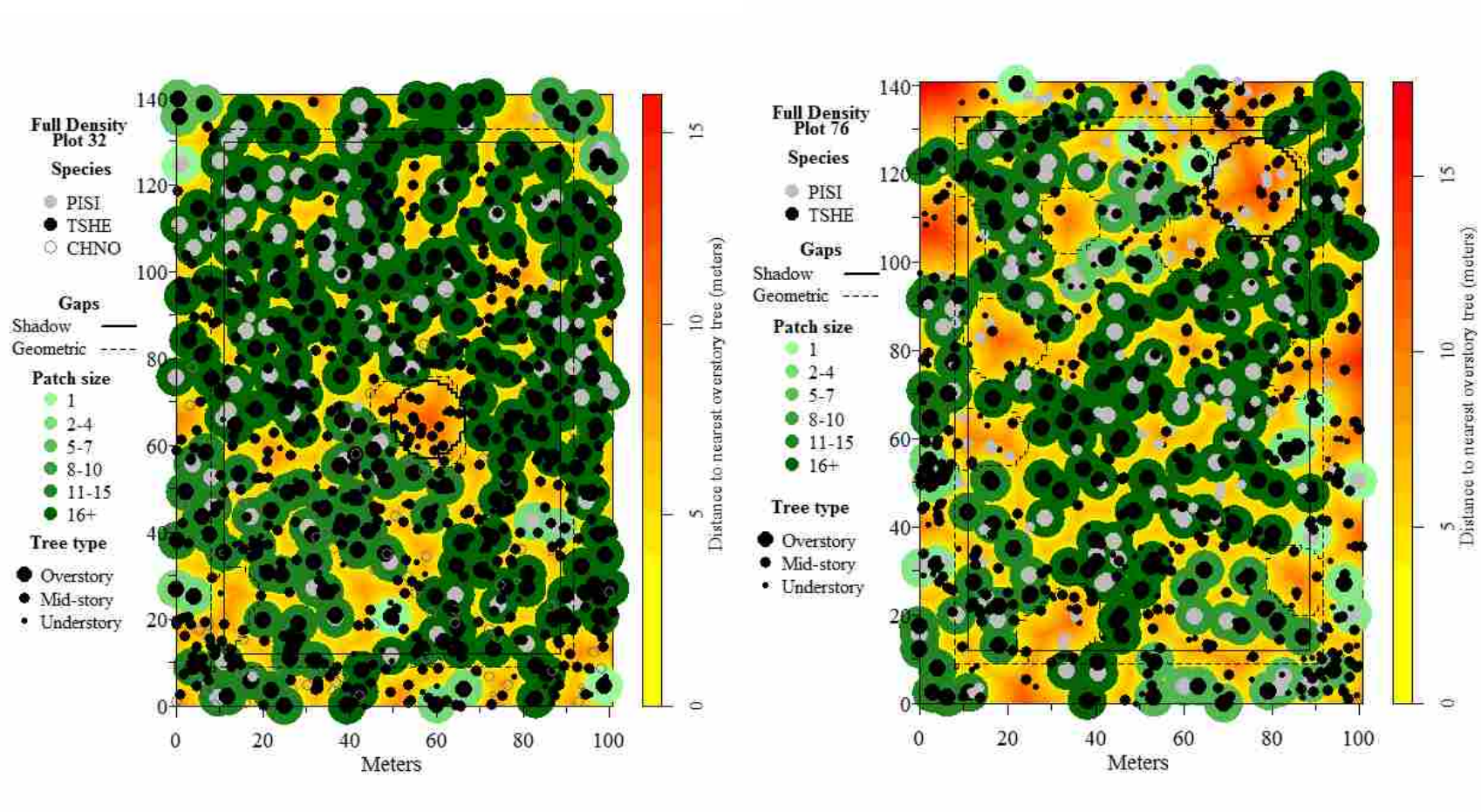
Full Density
Plot 32
Species
PISI
TSHE
CHNO
Gaps
Shadow
Geometric
Patch size
1
2-4
5-7
8-10
11-15
16+
Tree type
Overstory
Mid-story
Understory
Meters
Distance to nearest overstory tree (meters)
Full Density
Plot 76
Species
PISI
TSHE
Gaps
Shadow
Geometric
Patch size
1
2-4
5-7
8-10
11-15
16+
Tree type
Overstory
Mid-story
Understory
Meters
Distance to nearest overstory tree (meters)

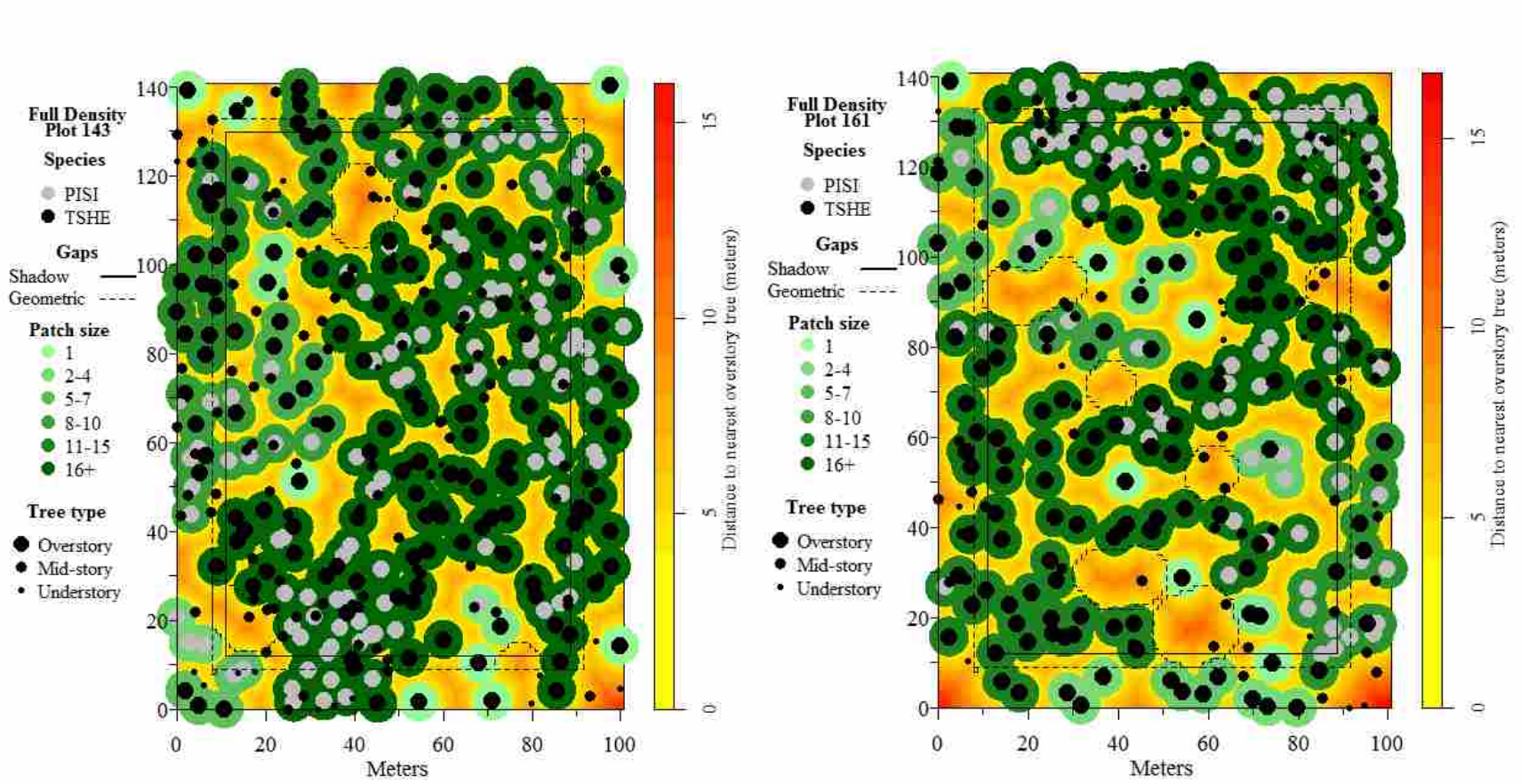


**Figure S2.** Stem maps by plot for full density Sitka spruce western hemlock forests in southeast Alaska. Tree boles are colored by species and size represents overstory, mid-story, and understory position. A 4.44 m radius was used to project tree crowns on overstory trees to show patches at a fixed distance of 8.88 m. Patch size is the number of trees in a patch. Gaps and associated plot buffer distances are shown with a solid or dashed line. Background coloration is a graphical display of open area where colors indicate the distance to the nearest overstory trees in meters.

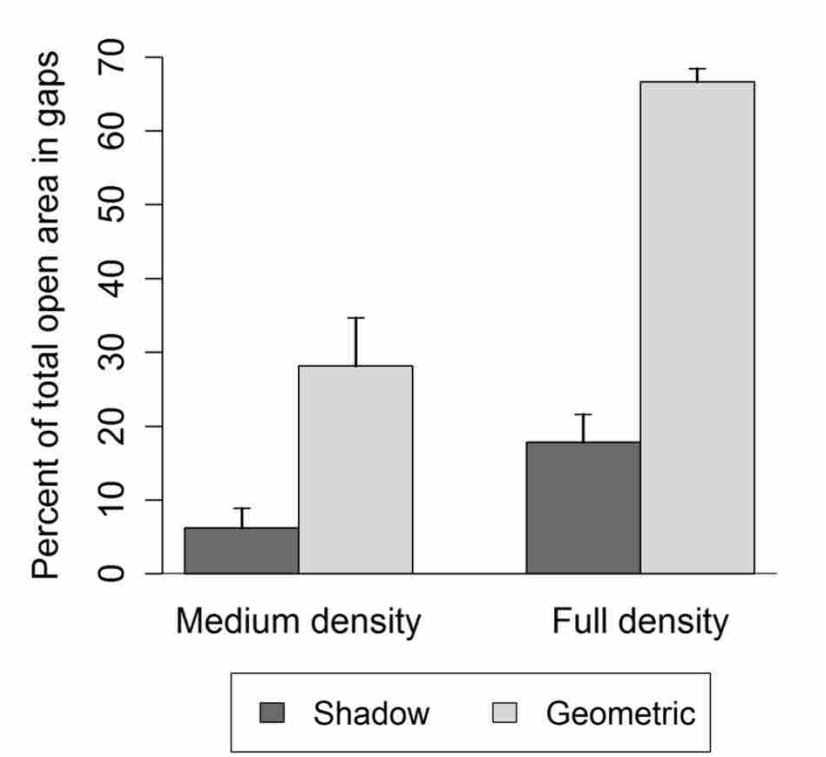


**Figure S3.** Percent of total plot are in openings categorized as a shadow or geometric gap pooled by overstory density for old-growth Sitka-spruce western hemlock forest in southeast Alaska. Open area has no overstory canopy.

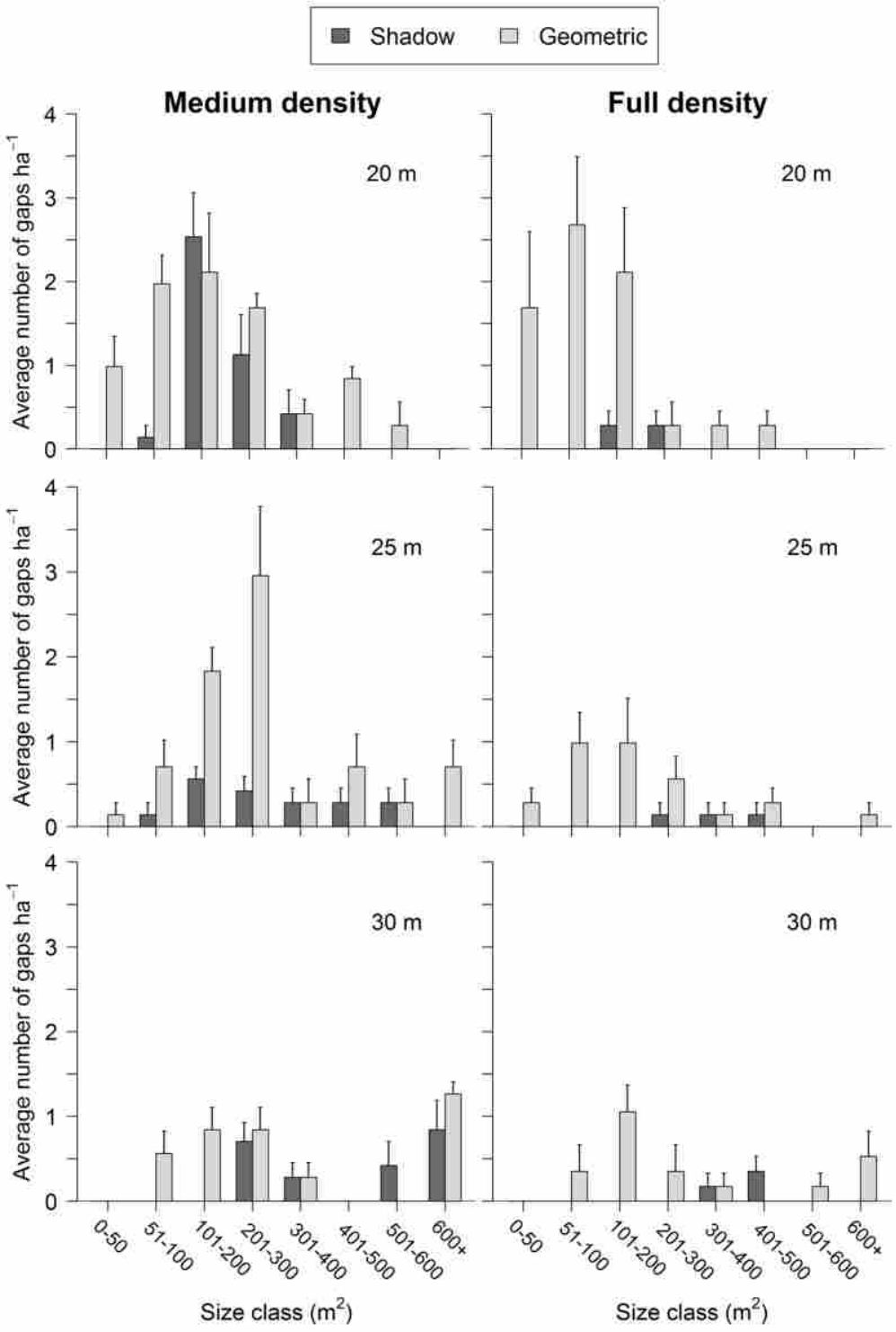


**Figure S4.** Average number of edge buffered gaps on a per hectare basis by size class for 10 old-growth Sitka spruce-western hemlock forest in southeast Alaska pooled by canopy density. An edge buffer with a distance equal to the minimum gap distance was applied to the gap calculations. Error bars are one standard error of the mean. Shadow and geometric are the methods used to define a functional gap for the analysis. Minimum functional gap size is 42.3 $m^2$ and 15.5 $m^2$ for shadow and geometric gaps respectively.

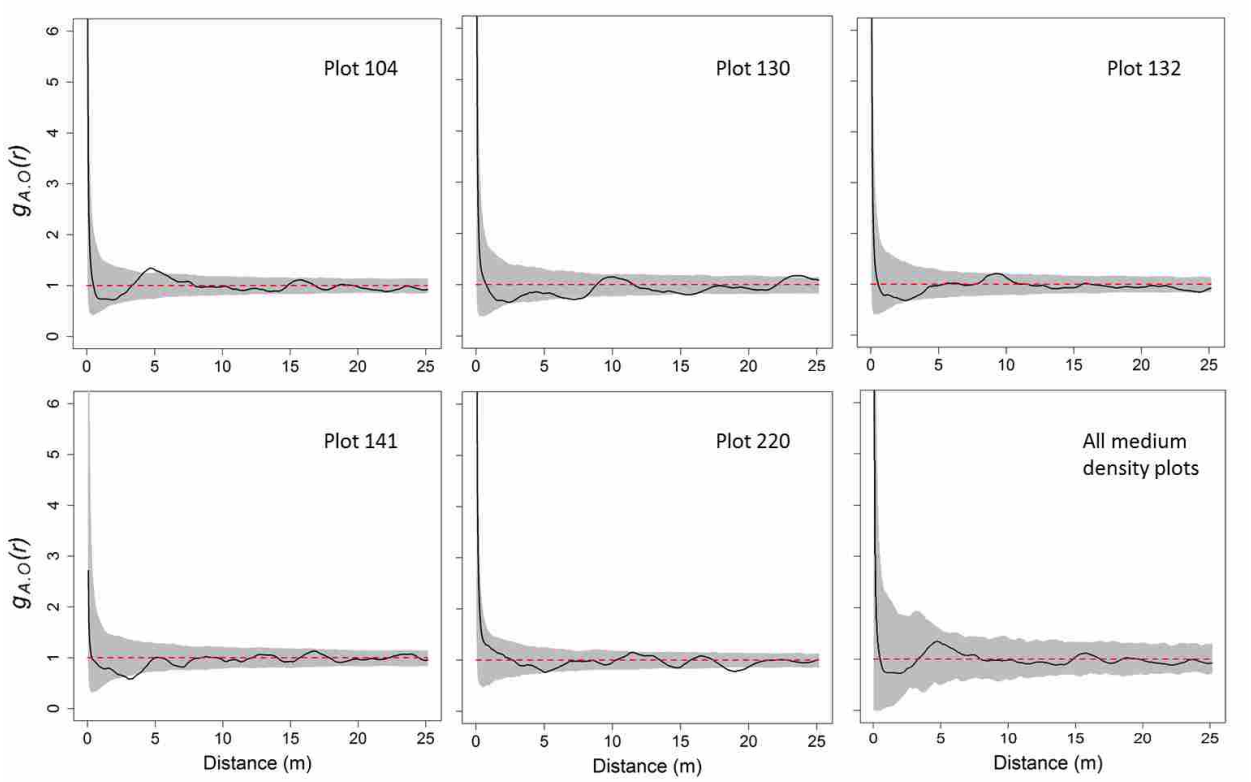


**Figure S5.** Pair correlation function for all overstory trees (≥ 25 m tall) in medium density plots and for all plots pooled.

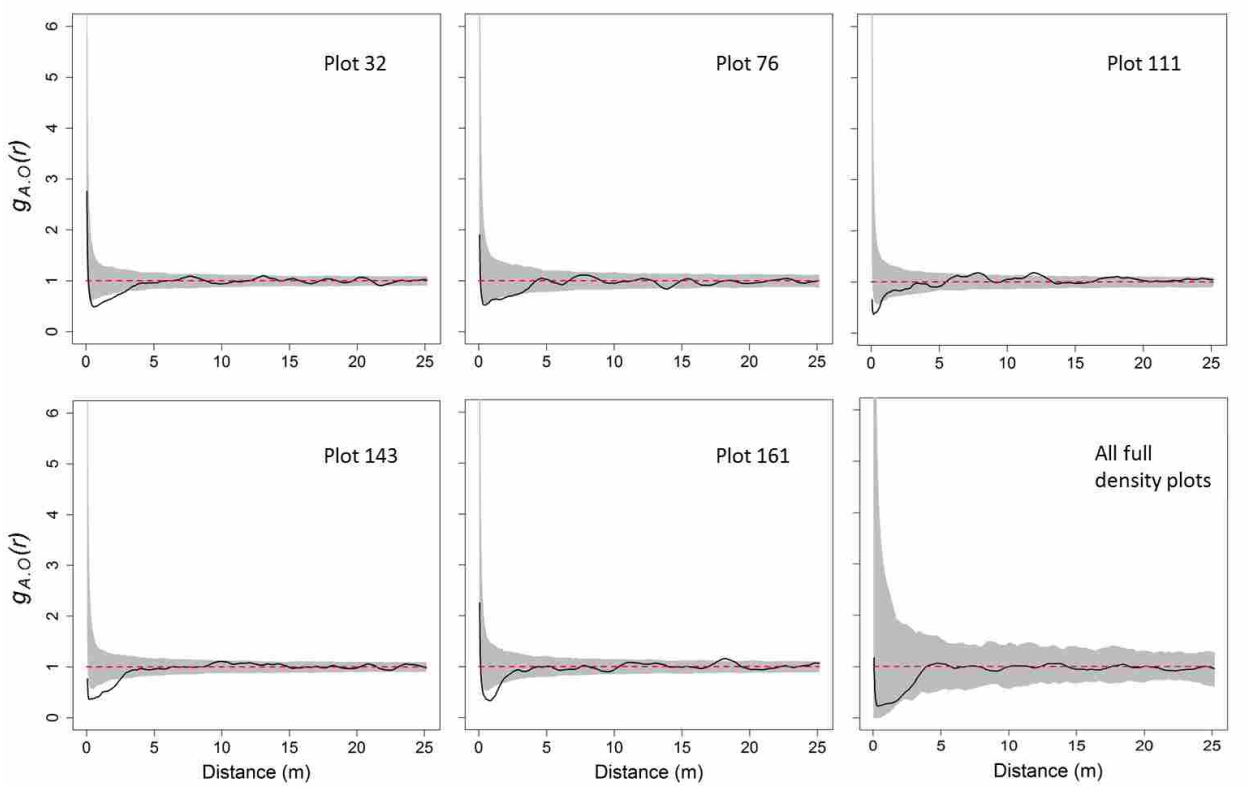


**Figure S6.** Pair correlation function for all overstory trees (≥ 25 m tall) in full density plots and for all plots pooled.

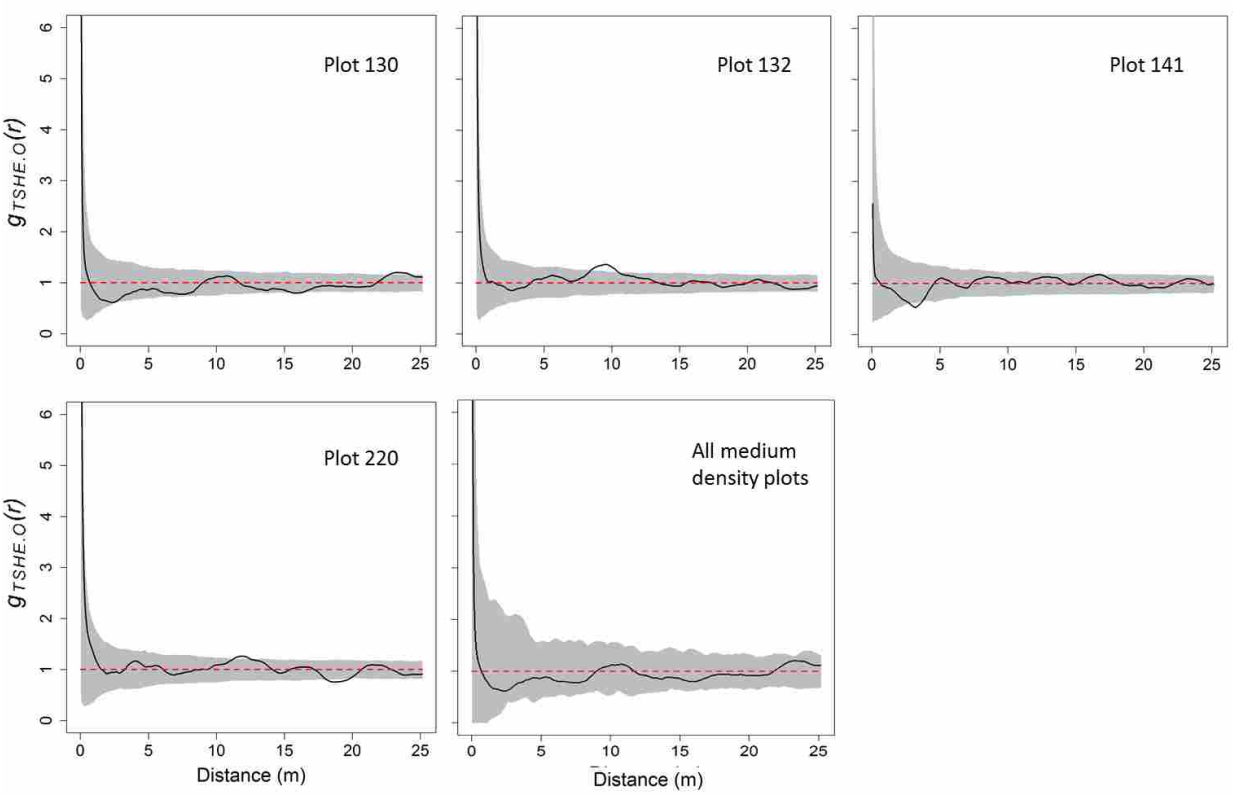


**Figure S7.** Pair correlation function for overstory western hemlock (TSHE) trees (≥ 25 m tall) in medium density plots and for all plots pooled. Plot 104 was eliminated from the analysis due to insufficient sample size of overstory hemlock.

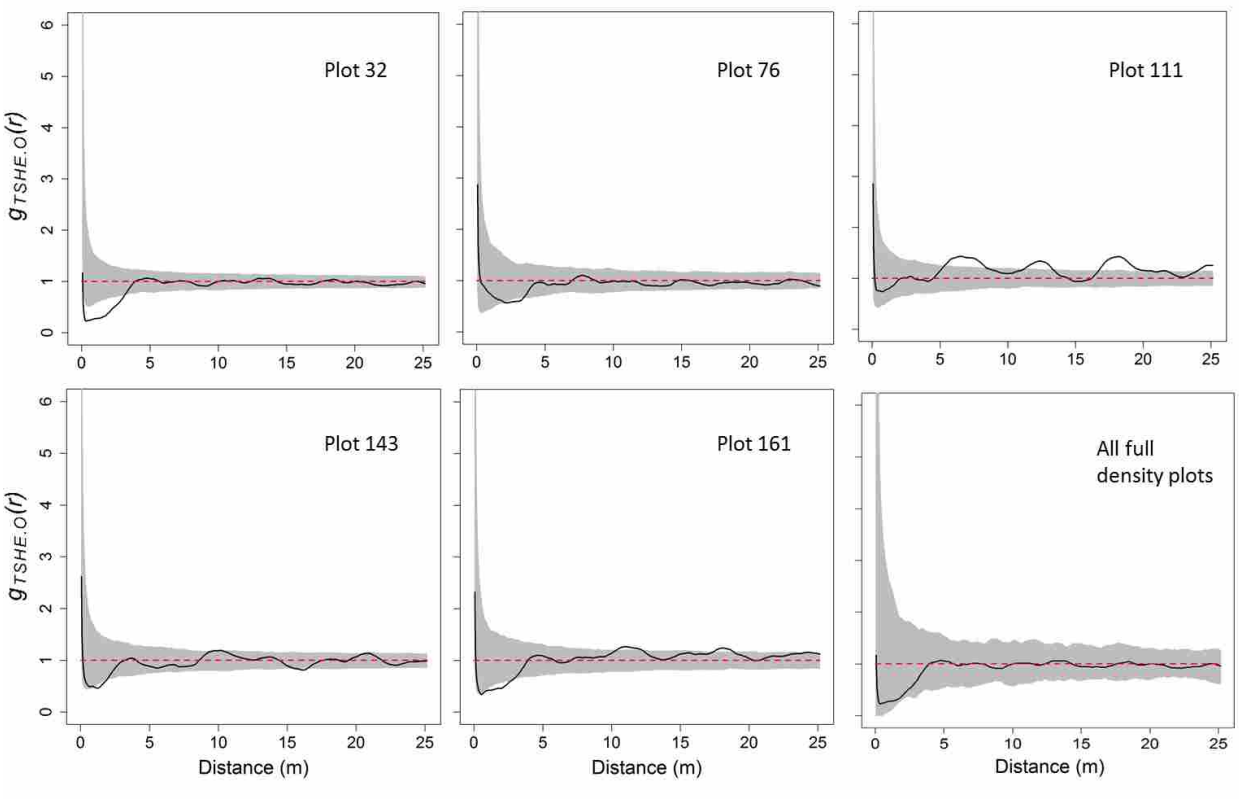


**Figure S8.** Pair correlation function for overstory hemlock (TSHE) trees (≥ 25 m tall) in full density plots and for all plots pooled.

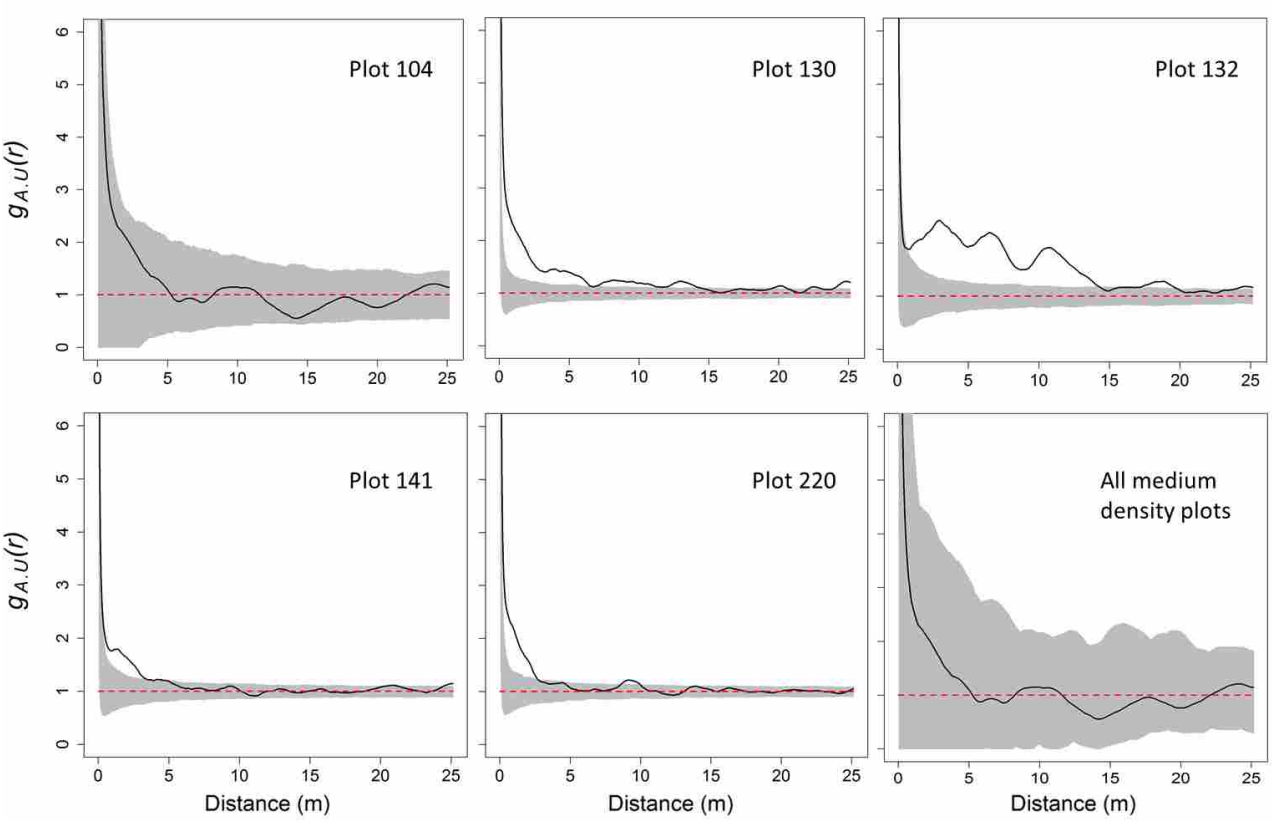


**Figure S9**. Pair correlation function for all understory trees (≤ 10 m tall) in medium density plots and for all plots pooled.

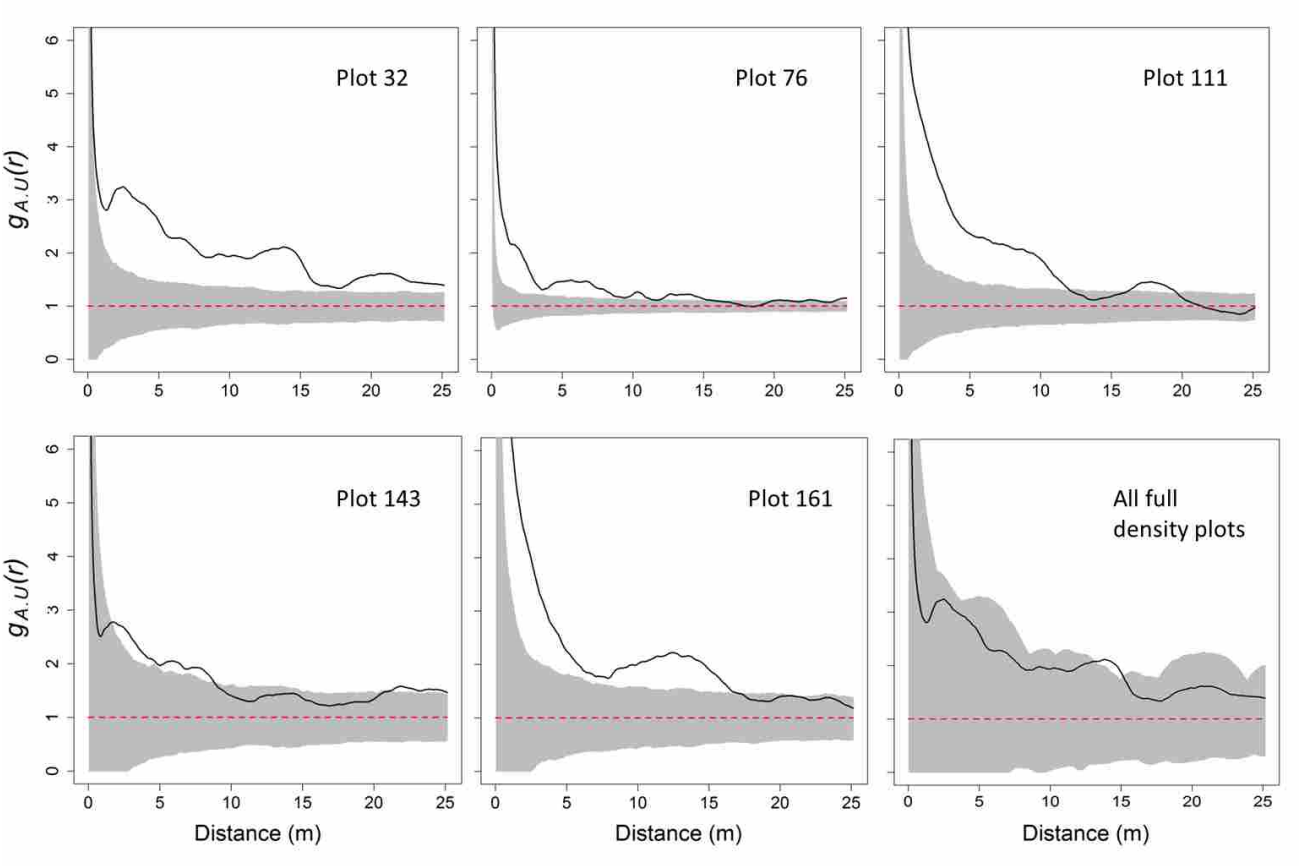


**Figure S10.** Pair correlation function for all understory trees (≤ 10 m tall) in full density plots and for all plots pooled.

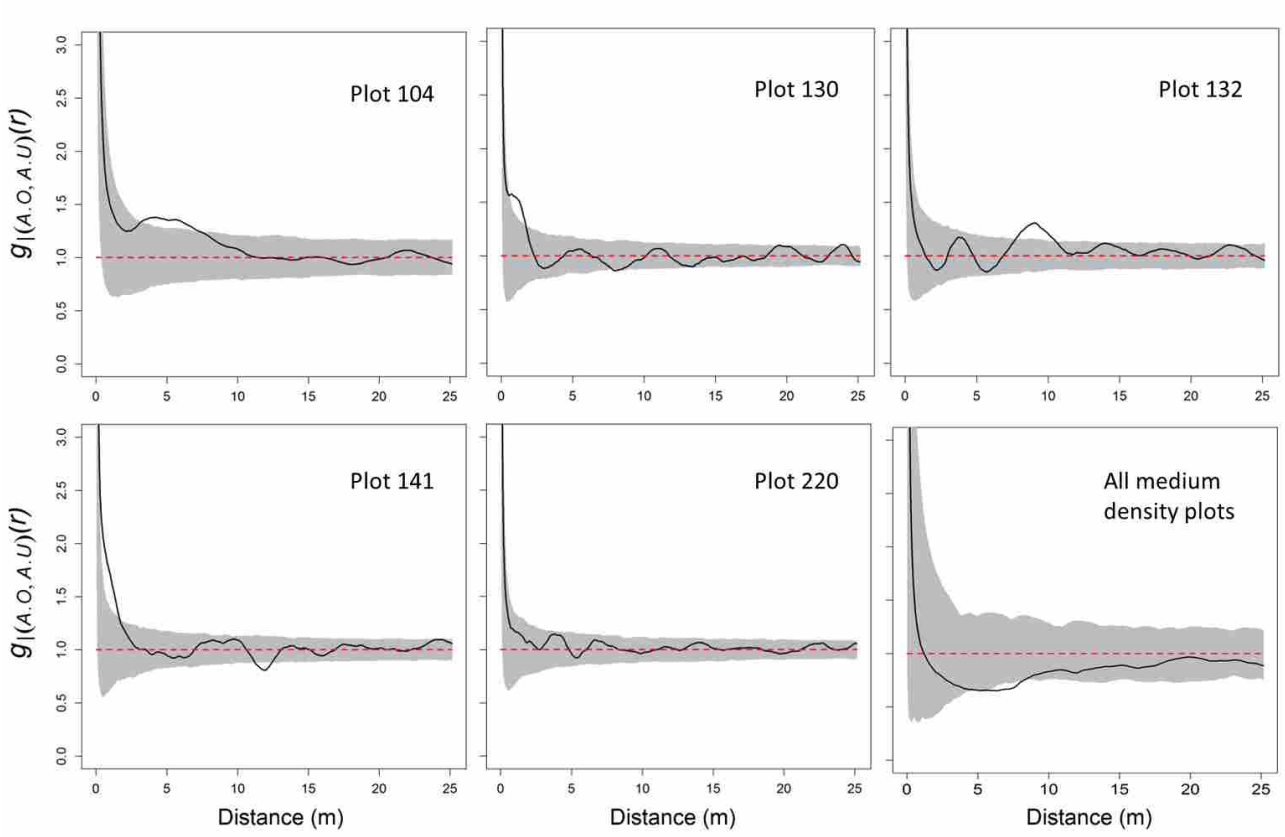


**Figure S11**. Bivariate pair correlation function for medium density plots and for all plots pooled for all understory trees in relation to all overstory trees.

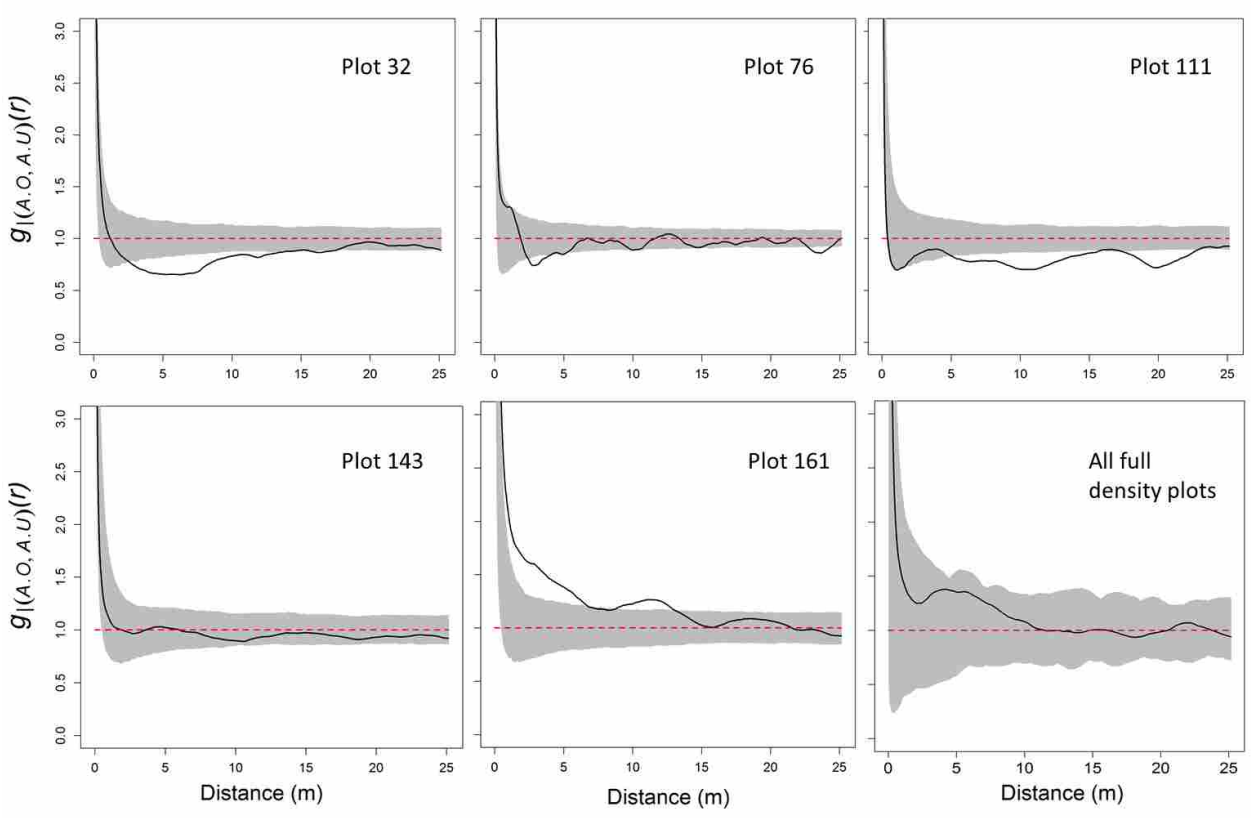


**Figure S12**. Bivariate pair correlation function for full density plots and for all plots pooled for all understory trees in relation to all overstory trees.

## CHAPTER 2 Supplementary Material

**Table S1.** Summary of attributes for sampled neighborhoods within the site. $n = 6$ for each neighborhood type. Immediate neighborhood is the trees directly influencing the snow in these plots calculated as the number of trees within 10 m of plot center. Tree height to open width ratio uses average overstory tree height at the study site to the average opening diameter. Value following ± is standard deviation.

| Neighborhood | Size range | Mean Size | Traits |
|---|---|---|---|
| **Individuals (dbh)** | | | *Total Crown Biomass (kg)* |
| ponderosa pine | 42.3 - 70.2 | 54.1 ± 10.2 | 417.01 ± 176.61 |
| western larch | 21.5 - 35.9 | 29.3 ± 4.7 | 43.15 ± 11.22 |
| Douglas-fir | 31.7 - 61.9 | 43.9 ± 10.2 | 204.75 ± 115.02 |
| | | | *Immediate Neighborhood* |
| **Clumps (# trees)** | 18 - 99 | 52.5 ± 35.7 | 14 ± 5 |
| | | | *OpenWidth:TreeHeight* |
| **Openings ($m^2$)** | 234 - 930 | 446.5 ± 275.1 | 1.07 ± 0.32 |

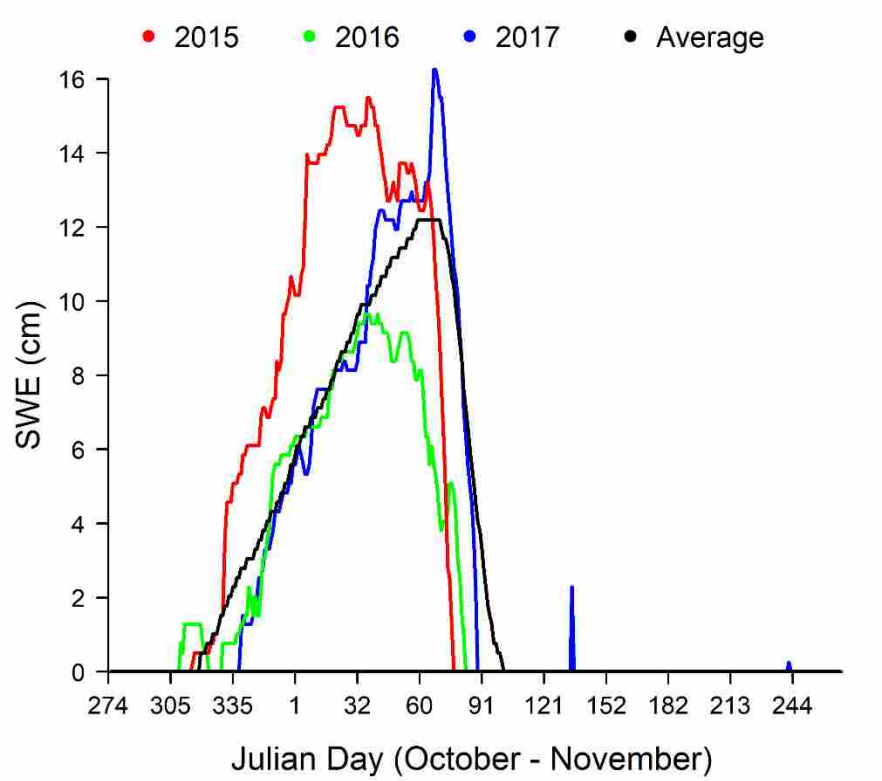


**Figure S1**. Water year snow water equivalent recorded at Lubrecht Flume SNOTEL station (October 1-September 30). Lubrecht Flume is located at 1425 m, 175 m above and 11.38 km southeast of the study site. Long term station average is from 1980-2010. Peak SWE in 2017 = 16.3 cm, 2016 =9.7 cm, 2015 = 15.5 cm, Average = 12.2 cm.

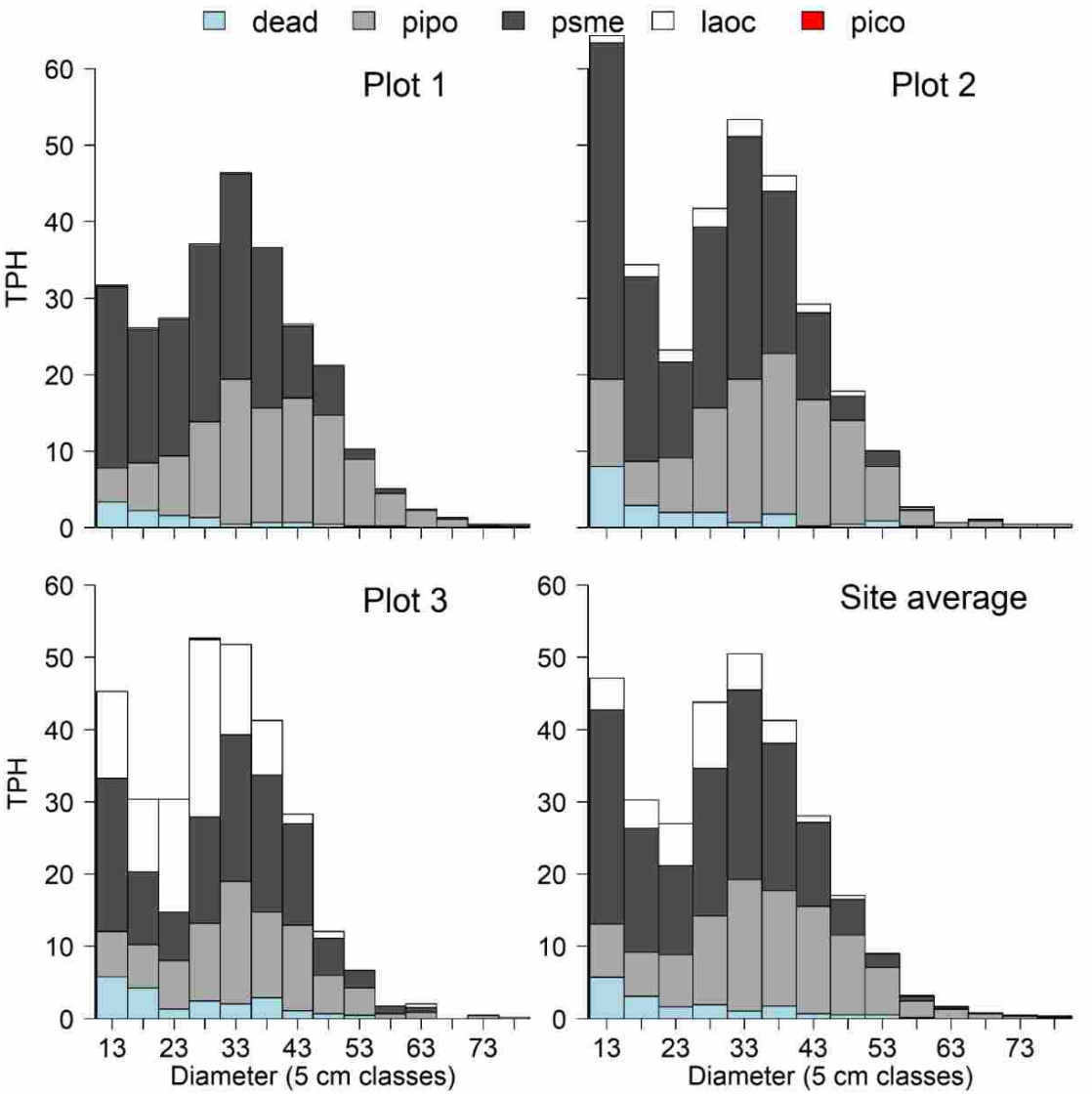


**Figure S2**. Distribution of tree density by size and species for a mixed-conifer forest. Tree size is presented in 5 cm diameter classes for trees >10.0 cm dbh and stacked by species, with the first tier representing tree snags ("dead"). The bottom right figure is average across all plots. PIPO is ponderosa pine, PSME is Douglas-fir, LAOC is western larch, and PICO is lodgepole pine. There is only 1 lodgepole in the entire site, in plot 3.

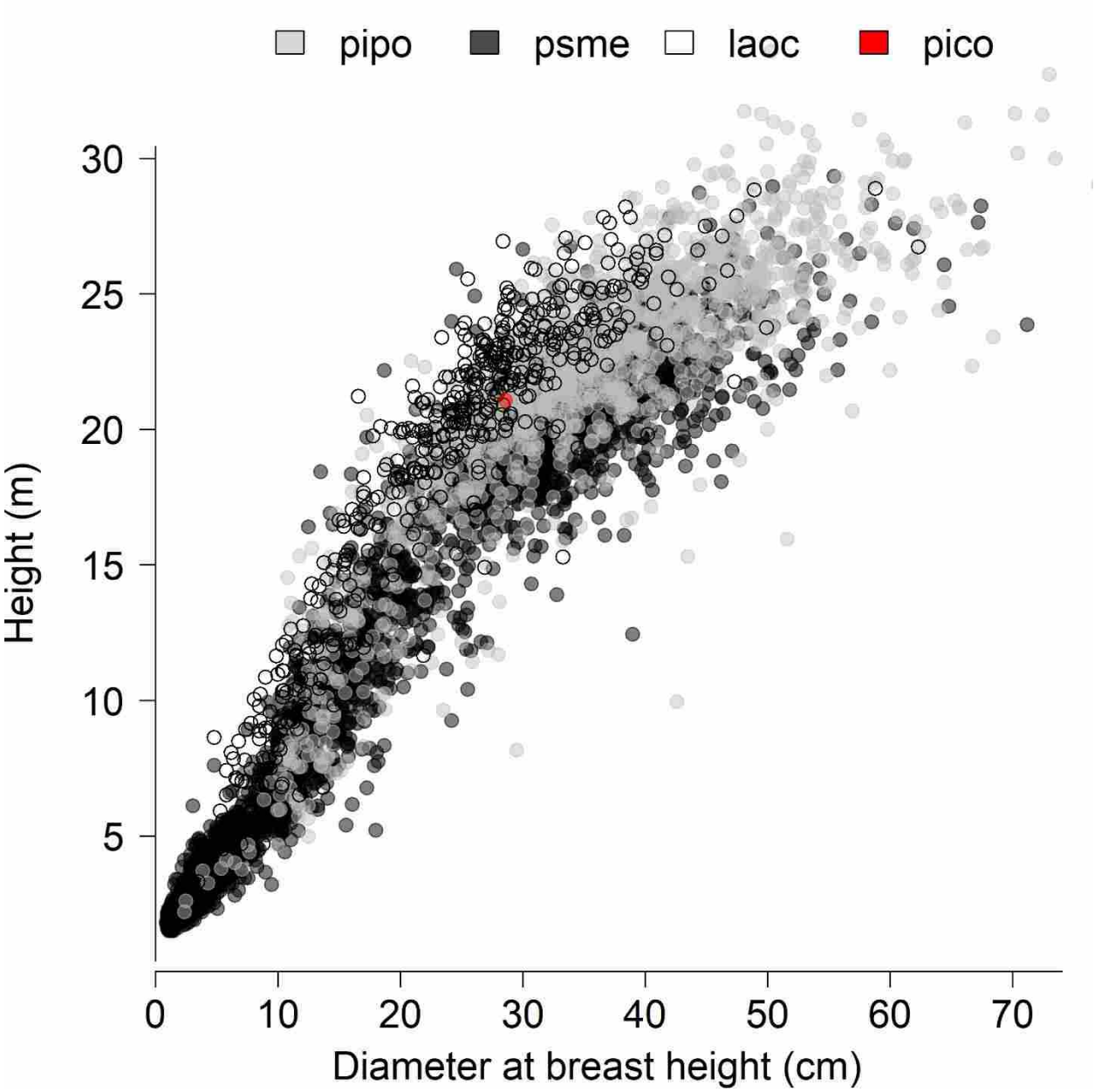


**Figure S3.** Height to diameter relationship for species in a western U.S. mixed conifer forest. *n*=1416 for PIPO, *n*=3435 for PSME, *n*=492 for LAOC, and *n*=1 for PICO. Included diameters range from 0.9 – 79.5 cm with a minimum height of 1.37 m and maximum height of 33.94 m.

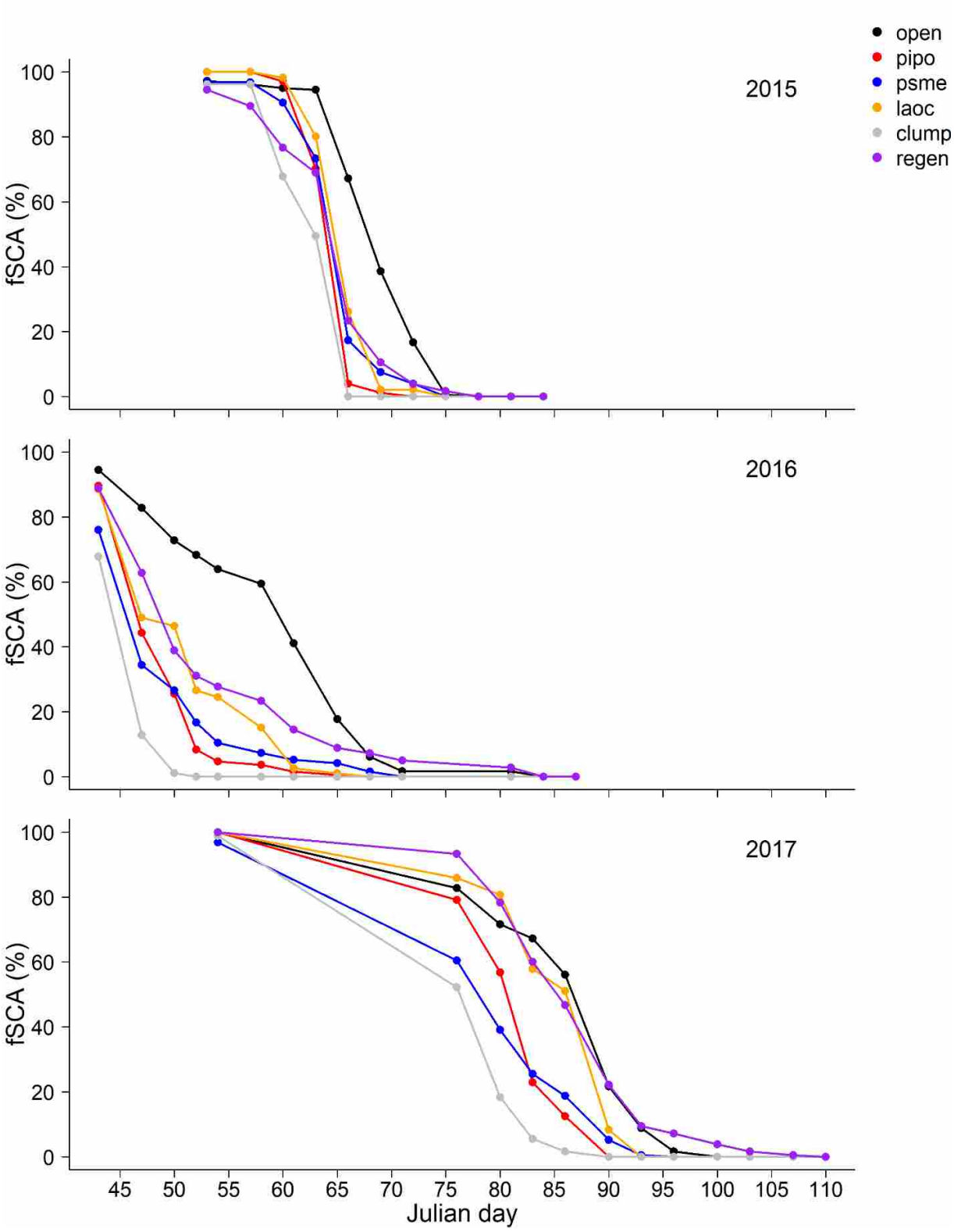


**Figure S4**. Fractional snow cover melt curves for all neighborhoods from 2015-2017. Snow cover is presented as percent of sample points with snow remaining over time given in Julian days instead of days since peak melt.

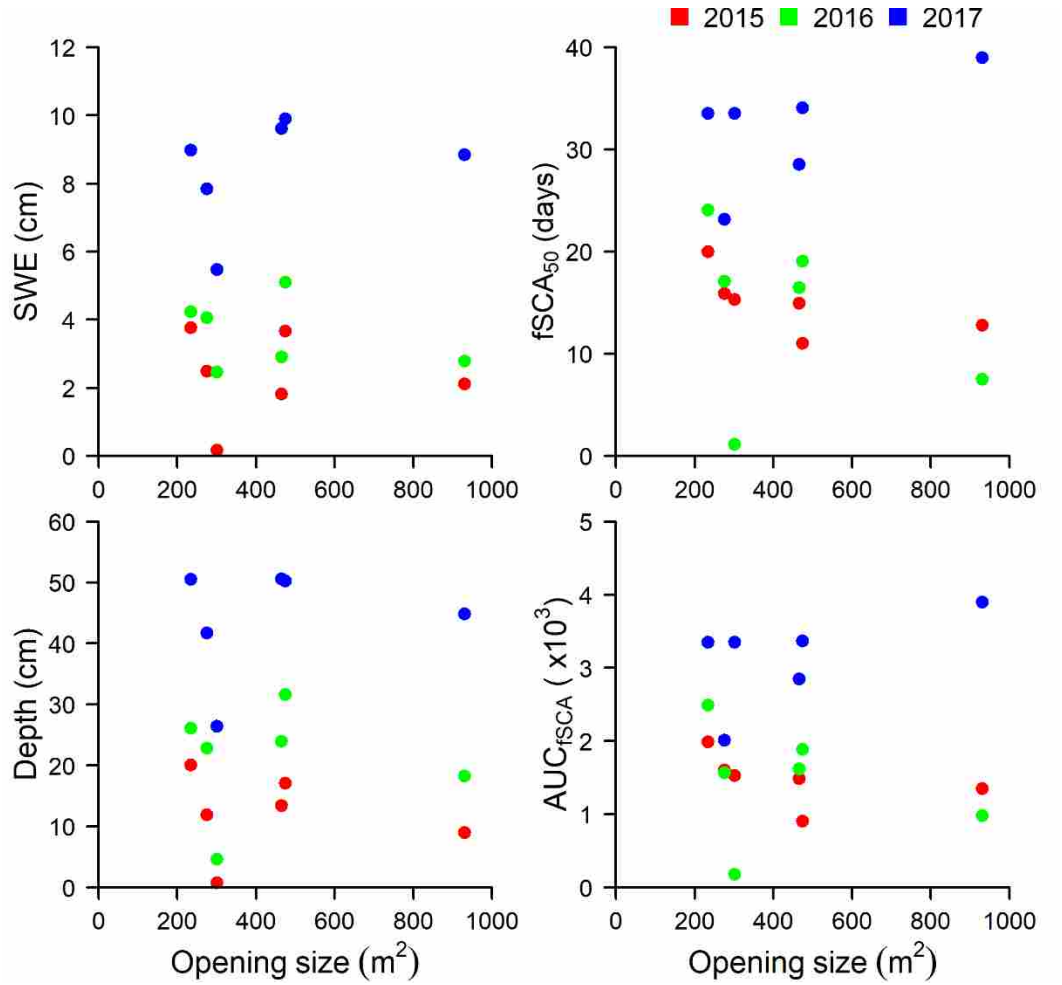


**Figure S5**. Snow accumulation and melt characteristics across opening size. Dotted line is a 1:1 relationship where openings of increasing size would have increasing values of snow characteristics.

## CHAPTER 3 Supplementary Material

**Table S1**. Radial distance selection model fitting criteria (AIC) for predictive ground variables for snow water equivalent (SWE), snow density, and snow disappearance date (SDD). Distances ranged from 1-15m. Bolded values correspond minimal AIC values and indicated the selected radius.

| Radius | 1 | 2 | 3 | 4 | 5 | 6 | 7 | 8 | 9 | 10 | 11 | 12 | 13 | 14 | 15 |
|---|---|---|---|---|---|---|---|---|---|---|---|---|---|---|---|
| **Variables** | | | | | | | **Snow water equivalent (SWE)** | | | | | | | | |
| *tree.den* | 31956.73 | 31157.14 | 30670.58 | 30301.34 | 29854.76 | 29434.57 | 29025.15 | 28635.89 | 28167.89 | 27832.49 | 27578.05 | 27205.72 | 26821.76 | 26388.06 | **25979.40** |
| *Abs.LAOC* | 32071.12 | 31346.86 | 30921.14 | 30514.96 | 30038.82 | 29593.25 | 29158.08 | 28741.99 | 28247.62 | 27890.82 | 27632.74 | 27250.29 | 26861.47 | 26423.08 | **26005.63** |
| *Abs.intermed* | 32067.33 | 31311.66 | 30875.20 | 30469.01 | 29992.88 | 29553.72 | 29133.30 | 28724.44 | 28246.78 | 27901.26 | 27644.02 | 27265.38 | 26880.49 | 26446.24 | **26036.33** |
| *Abs.codom* | 32047.32 | 31290.06 | 30846.48 | 30441.66 | 29965.63 | 29536.85 | 29110.67 | 28712.48 | 28223.62 | 27885.75 | 27622.54 | 27249.79 | 26867.62 | 26438.82 | **26030.51** |
| *Abs.dom* | 31993.34 | 31176.21 | 30682.20 | 30316.06 | 29863.96 | 29442.84 | 29009.33 | 28631.99 | 28173.85 | 27837.09 | 27609.73 | 27244.55 | 26871.18 | 26447.78 | **26035.11** |
| *Hegyi* | 31961.13 | 31172.65 | 30693.38 | 30274.59 | 29783.75 | 29336.65 | 28892.77 | 28484.05 | 28000.83 | 27650.82 | 27395.98 | 27025.58 | 26645.84 | 26213.71 | **25798.73** |
| *SumNN* | 31759.45 | 31152.32 | 30810.84 | 30456.91 | 30008.62 | 29588.57 | 29164.32 | 28765.27 | 28287.99 | 27943.38 | 27687.37 | 27309.42 | 26928.31 | 26497.98 | **26085.11** |
| | | | | | | | **Snow density** | | | | | | | | |
| *tree.den* | -5854.41 | -5725.89 | -5616.19 | **-6157.33** | -6076.32 | -5997.74 | -5940.11 | -5875.97 | -5785.92 | -5694.64 | -5625.52 | -5595.74 | -5547.05 | -5479.71 | -5504.59 |
| *Abs.LAOC* | -5854.17 | -5723.25 | -5606.11 | **-6136.31** | -6047.87 | -5975.78 | -5916.67 | -5853.29 | -5765.71 | -5678.37 | -5614.95 | -5587.23 | -5539.89 | -5473.99 | -5498.58 |
| *Abs.intermed* | -5854.34 | -5724.10 | -5608.86 | **-6138.32** | -6056.08 | -5978.08 | -5921.40 | -5856.57 | -5768.90 | -5681.86 | -5617.20 | -5589.74 | -5540.93 | -5474.37 | -5498.10 |
| *Abs.codom* | -5854.83 | -5725.09 | -5609.59 | **-6142.29** | -6059.36 | -5985.93 | -5927.20 | -5863.04 | -5773.74 | -5686.89 | -5620.79 | -5591.37 | -5544.22 | -5476.94 | -5501.55 |
| *Abs.dom* | -5855.11 | -5724.78 | -5616.27 | **-6165.67** | -6082.25 | -6005.27 | -5950.12 | -5884.38 | -5790.87 | -5692.67 | -5623.44 | -5594.43 | -5545.28 | -5479.09 | -5504.35 |
| *Hegyi* | -5854.68 | -5723.71 | -5607.69 | **-6143.87** | -6061.07 | -5989.81 | -5934.03 | -5871.61 | -5784.40 | -5695.95 | -5631.54 | -5600.45 | -5553.40 | -5488.65 | -5515.20 |
| *SumNN* | -5870.37 | -5739.01 | -5621.27 | **-6149.42** | -6061.97 | -5986.22 | -5927.37 | -5862.15 | -5773.21 | -5685.87 | -5622.24 | -5594.16 | -5546.54 | -5480.09 | -5504.22 |
| | | | | | | | **Snow disappearance date (SDD)** | | | | | | | | |
| *tree.den* | 190807.57 | 187892.88 | 185455.16 | 183175.80 | 180772.33 | 178449.32 | 176151.68 | 173873.43 | 171370.33 | 168897.03 | 166451.59 | 163999.37 | 161540.16 | 158995.95 | **156527.42** |
| *Abs.LAOC* | 190954.96 | 188136.09 | 185691.29 | 183370.42 | 180916.89 | 178512.37 | 176151.90 | 173812.66 | 171273.34 | 168769.87 | 166303.97 | 163830.61 | 161365.98 | 158810.12 | **156334.69** |
| *Abs.intermed* | 190938.05 | 188119.34 | 185700.82 | 183419.63 | 181002.19 | 178643.42 | 176324.10 | 174023.51 | 171504.36 | 169012.70 | 166555.91 | 164087.54 | 161626.76 | 159082.94 | **156612.59** |
| *Abs.codom* | 190899.82 | 188045.34 | 185611.21 | 183308.70 | 180875.07 | 178523.67 | 176217.15 | 173920.44 | 171400.87 | 168924.31 | 166471.88 | 164011.19 | 161548.19 | 159001.35 | **156532.95** |
| *Abs.dom* | 190874.25 | 187940.92 | 185482.30 | 183160.79 | 180728.43 | 178389.82 | 176057.14 | 173783.79 | 171279.96 | 168794.21 | 166345.93 | 163892.11 | 161426.08 | 158877.04 | **156405.58** |
| *Hegyi* | 190783.19 | 187855.10 | 185356.27 | 183014.48 | 180553.83 | 178179.28 | 175843.14 | 173536.12 | 171014.49 | 168528.97 | 166078.05 | 163622.41 | 161164.64 | 158617.51 | **156146.76** |
| *SumNN* | 190645.78 | 187921.17 | 185603.78 | 183374.91 | 180978.12 | 178627.23 | 176312.52 | 174014.42 | 171497.58 | 169008.14 | 166552.70 | 164085.80 | 161625.92 | 159082.43 | **156611.81** |

**Table S2**. Radial distance selection model fitting criteria (AIC) for predictive LiDAR variables for snow water equivalent (SWE), snow density, and snow disappearance date (SDD). Distances ranged from 1-8m. L-skewness and L-kurtosis were fit with a model containing only fixed effects, others utilized a mixed effects model. Bolded values correspond minimal AIC values and indicated the selected radius.

| Radius | 1 m | 2 m | 3 m | 4 m | 5 m | 6 m | 7 m | 8 m |
|---|---|---|---|---|---|---|---|---|
| **Variable** | **Snow water equivalent (SWE)** | | | | | | | |
| *Elev.mean* | 36357.5 | 29015.3 | **29008.4** | 29039.4 | 29101.7 | 29176.7 | 29263.7 | 29343.1 |
| *Elev.L2* | 36494.2 | **29305.6** | 29378.6 | 29443.8 | 29490.1 | 29533.1 | 29576.3 | 29614.1 |
| *Elev.L.CV* | 36589.4 | 29137.9 | 28982.7 | **28918.0** | 28948.7 | 29003.0 | 29069.9 | 29144.2 |
| *Elev.L.skewness* | 38655.4 | 36416.0 | 36363.3 | **36361.9** | 36399.6 | 36447.3 | 36485.8 | 36528.3 |
| *Elev.L.kurtosis* | 38649.5 | **36774.2** | 36780.6 | 36811.4 | 36820.1 | 36821.3 | 36827.2 | 36839.9 |
| *Elev.P95* | 36388.1 | **29189.2** | 29281.9 | 29351.3 | 29415.6 | 29498.4 | 29571.2 | 29613.9 |
| *Elev.P99* | 36388.5 | **29187.8** | 29280.8 | 29365.4 | 29446.1 | 29528.2 | 29578.0 | 29635.7 |
| *Crown.cover* | 36261.9 | 28686.5 | **28614.2** | 28627.2 | 28702.7 | 28810.5 | 28929.1 | 29033.2 |
| | **Snow density** | | | | | | | |
| *Elev.mean* | -7564.8 | -7713.6 | **-7721.0** | -7719.7 | -7716.6 | -7713.6 | -7707.6 | -7700.3 |
| *Elev.L2* | -7554.2 | -7699.4 | **-7702.5** | -7695.9 | -7688.4 | -7683.5 | -7677.3 | -7669.5 |
| *Elev.L.CV* | -7546.6 | -7683.2 | -7705.6 | -7717.2 | -7725.6 | **-7734.6** | -7724.3 | -7716.6 |
| *Elev.L.skewness* | -6657.7 | -7682.1 | -7699.4 | **-7705.0** | -7703.1 | -7700.6 | -7690.0 | -7683.4 |
| *Elev.L.kurtosis* | -6659.3 | -7659.0 | -7676.9 | **-7679.6** | -7677.6 | -7677.0 | -7665.1 | -7660.4 |
| *Elev.P95* | -7558.0 | **-7710.5** | -7710.3 | -7692.1 | -7684.6 | -7676.8 | -7670.8 | -7664.0 |
| *Elev.P99* | -7557.6 | **-7713.3** | -7700.6 | -7694.6 | -7682.1 | -7674.4 | -7668.8 | -7658.0 |
| *Crown.cover* | -7554.0 | -7715.5 | -7728.4 | -7732.8 | **-7733.9** | -7732.2 | -7724.6 | -7716.3 |
| | **Snow disappearance date (SDD)** | | | | | | | |
| *Elev.mean* | 218883.2 | 157333.9 | 157088.7 | **157026.7** | 157170.2 | 157446.0 | 157799.6 | 158164.5 |
| *Elev.L2* | 219192.4 | **158672.6** | 158776.3 | 158955.3 | 159190.9 | 159456.7 | 159749.5 | 160016.9 |
| *Elev.L.CV* | 219289.6 | 158778.3 | 157871.7 | 157224.5 | 156928.7 | **156875.0** | 157052.9 | 157388.6 |
| *Elev.L.skewness* | 228597.2 | 165593.5 | 164333.3 | 163497.0 | 163263.2 | 163495.8 | 164024.4 | 164743.6 |
| *Elev.L.kurtosis* | 228596.7 | 169713.0 | 169342.4 | 169256.5 | **169296.1** | 169430.6 | 169665.8 | 169926.8 |
| *Elev.P95* | 219003.3 | **158146.2** | 158338.1 | 158728.6 | 159158.8 | 159591.3 | 159984.3 | 160263.2 |

| | | | | | | | | |
|---|---|---|---|---|---|---|---|---|
| *Elev.P99* | 219002.5 | **158164.1** | 158467.3 | 158919.0 | 159389.4 | 159838.7 | 160239.8 | 160520.4 |
| *Crown.cover* | 218862.0 | 156963.0 | 156607.0 | **156517.6** | 156682.5 | 157031.3 | 157456.3 | 157879.8 |

**Table S3.** Snow disappearance metrics for four consecutive snow years in western Montana. 25, 50, 75 and 90% melt indicate the progression through the melt season based on length of time from peak accumulation until final melt (melt length). Melt values are presented as fSCA (fractional snow covered area) associated with the given periods of the melt season. n is sample size. ± standard deviation.

| Year | | SITE | PLOT 3 | PLOT 2 | PLOT 1 |
|---|---|---|---|---|---|
| **2014** | *n* | 5296 | 2652 | 2644 | NA |
| | *melt length* | 49 | 46 | 49 | NA |
| | *25% melt* | 88.5 ± 3.0 | 86.3 | 90.6 | NA |
| | *50% melt* | 59.4 ± 5.6 | 63.3 | 55.4 | NA |
| | *75% melt* | 6.1 ± 6.2 | 1.77 | 10.5 | NA |
| | *90% melt* | 0.4 ± 0.4 | 0.1 | 0.6 | NA |
| **2015** | *n* | 6013 | 3079 | 2934 | NA |
| | *melt length* | 31 | 31 | 31 | NA |
| | *25% melt* | 85.6 ± 19.8 | 99.6 | 71.5 | NA |
| | *50% melt* | 19.9 ± 2.5 | 18.1 | 21.6 | NA |
| | *75% melt* | 6.2 ± 3.1 | 4 | 8.4 | NA |
| | *90% melt* | 0.6 ± 0.4 | 0.3 | 0.8 | NA |
| **2016** | *n* | 8987 | 3083 | 2952 | 2952 |
| | *melt length* | 43 | 41 | 43 | 43 |
| | *25% melt* | 19.3 ± 4.2 | 19.4 | 23.5 | 15.1 |
| | *50% melt* | 5.1 ± 3.7 | 1.8 | 9.1 | 4.4 |
| | *75% melt* | 1.1 ± 0.5 | 0.7 | 1.6 | 1.1 |
| | *90% melt* | 0.3 ± 0.3 | 0.03 | 0.2 | 0.7 |
| **2017** | *n* | 6033 | 3083 | 2950 | NA |
| | *melt length* | 59 | 59 | 55 | NA |
| | *25% melt* | 88.5 ± 2.8 | 87 | 90 | NA |
| | *50% melt* | 66.8 ± 5.9 | 62.6 | 71 | NA |
| | *75% melt* | 2.5 ± 2.3 | 0.8 | 4.1 | NA |
| | *90% melt* | 0.06 ± 0.02 | 0.04 | 0.07 | NA |

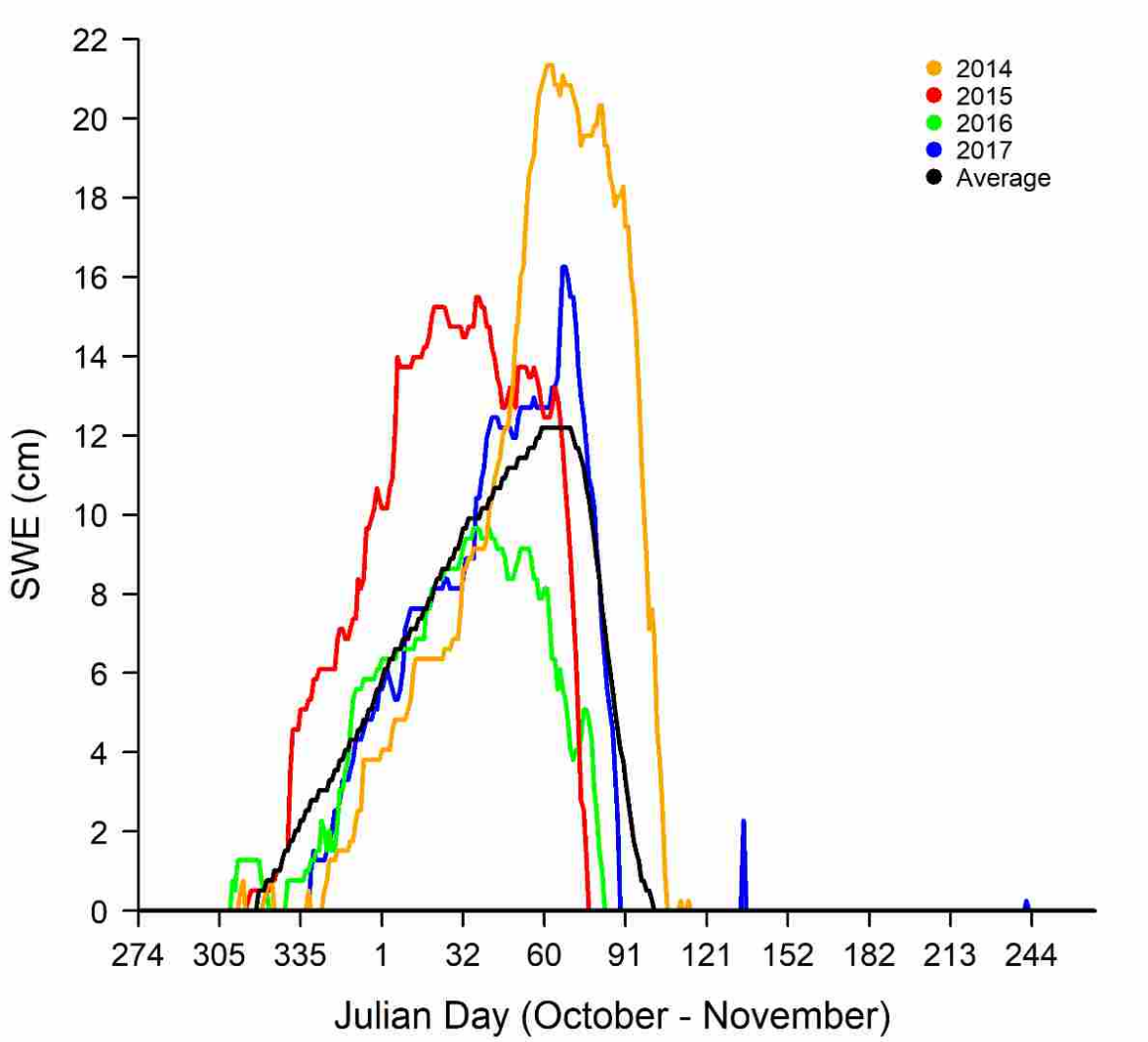


**Figure S1.** Lubrecht Flume SNOTEL snow water equivalent for 2014 – 2017. The dark line is the long term average.

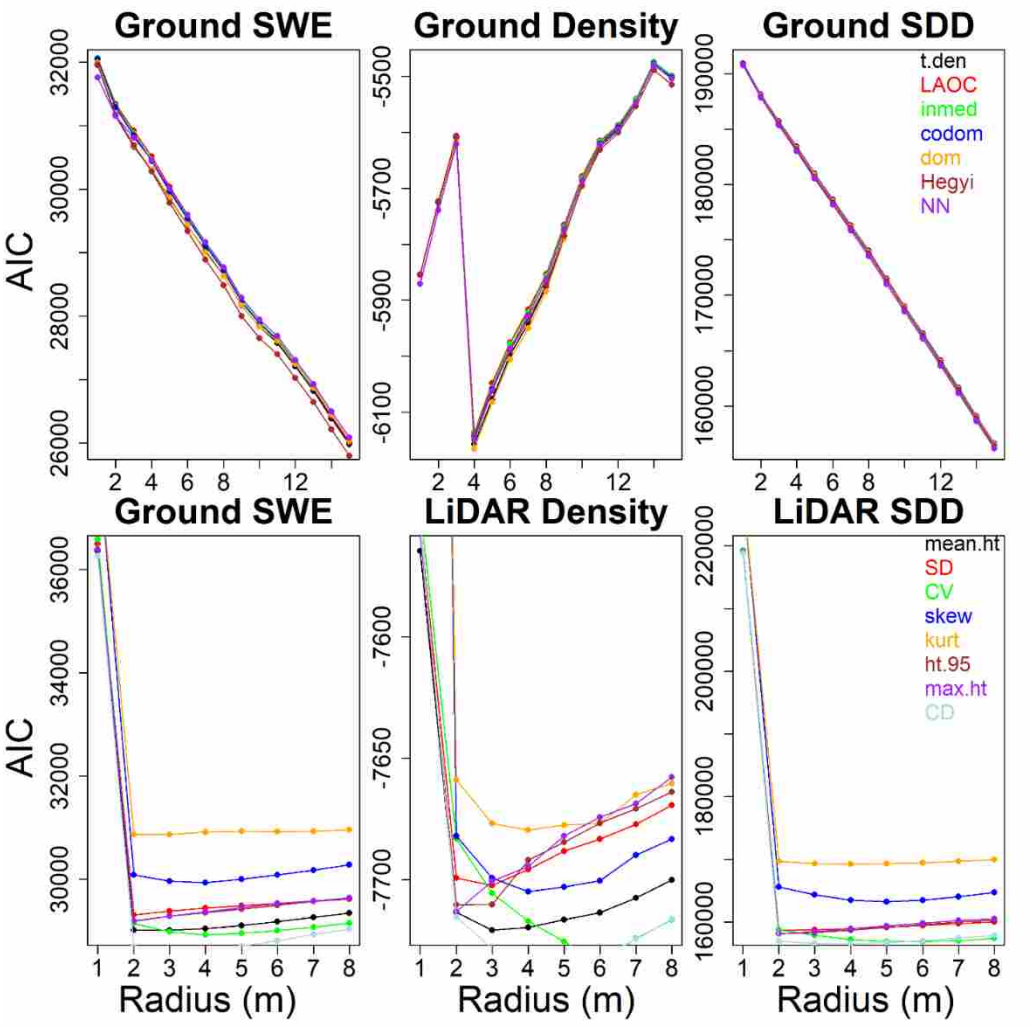


**Figure S2.** Forest canopy metric subplot radius selection using a linear mixed effects model. Ground metrics were calculated over subplots with radii ranging from 1-15 m and LiDAR derived metrics from 1-8 m. Optimal radii were chosen based on minimized AIC.

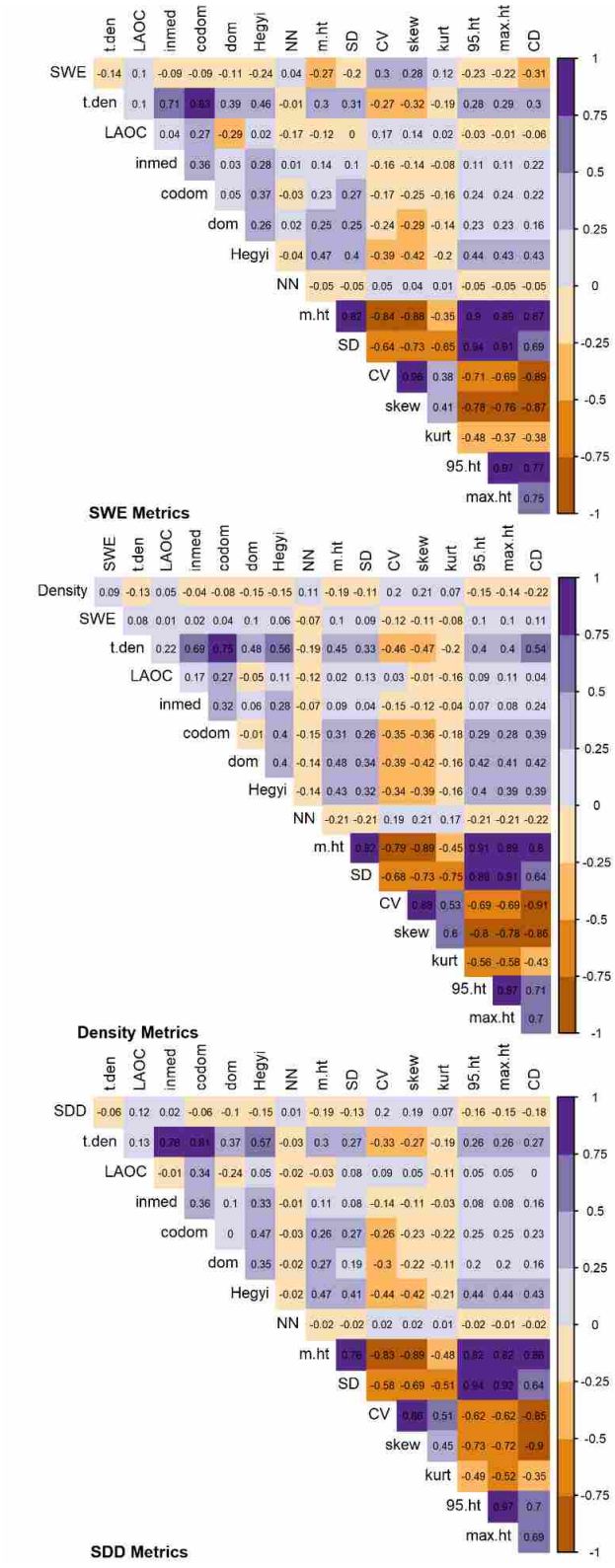


**Figure S3**. Pearson's correlation coefficients for SWE, density, and SDD for ground and LiDAR based predictor variables. Individual plots for response variables are given to reflect the variation in optimal radial distances used to select predictor variable inclusion.